NTNU – Trondheim
Norwegian University of
Science and Technology

Active and passive measures to maintain pressure in LNG fuel systems for ships

Hugo Eugen Hernes

Master of Energy and Environmental Engineering
Submission date: June 2015
Supervisor: Petter Nekså, EPT
Co-supervisor: Kjell Kolsaker, EPT

Norwegian University of Science and Technology
Department of Energy and Process Engineering

NTNU

Norwegian University
of Science and Technology

Department of Energy
and Process Engineering

EPT-M-2015-33

MASTER THESIS

for

Student Hugo Eugen Hernes

Spring 2015

Active and passive measures to maintain pressure in LNG fuel systems for ships

Aktive og passive tiltak for å opprettholde trykk i LNG drivstoffsystemer for skip

Background and objective

LNG is being introduced as fuel for both land based and marine transport applications. For use in marine applications, some of the drivers for the introduction are:

- To comply with new emission regulations related to NOx and other gases in new emission control areas (ECAs)
- Reduced fuel costs due to cost difference between LNG and maritime bunker oil
- Environmental aspects related to reduced CO_2 emissions by utilizing LNG

Several vessels that use LNG as their primary source of fuel have been put into operation and more are planned. These as well as other LNG fuelled ships has experienced situations where a drop in fuel tank pressure has led to motor power outage.

The aim of this Master's project is to perform theoretical, modelling and simulation efforts in order to understand and investigate concepts to mitigate drop of pressure in LNG fuel systems

The following tasks are to be considered:

1. Perform a literature survey relevant for active and passive pressurization of LNG tanks during ship movement
2. Further development of the model for prediction of pressure holding in the fuel tank
3. Establish an understanding of required pressure build up capacity under different conditions
4. Select a limited number of passive and/or active concepts for further detailed modelling and simulation
5. Investigate possible implementation of these and practical implications to be considered
6. Propose a plan for further work

-- " --

Within 14 days of receiving the written text on the master thesis, the candidate shall submit a research plan for his project to the department.

When the thesis is evaluated, emphasis is put on processing of the results, and that they are presented in tabular and/or graphic form in a clear manner, and that they are analyzed carefully.

The thesis should be formulated as a research report with summary both in English and Norwegian, conclusion, literature references, table of contents etc. During the preparation of the text, the candidate should make an effort to produce a well-structured and easily readable report. In order to ease the evaluation of the thesis, it is important that the cross-references are correct. In the making of the report, strong emphasis should be placed on both a thorough discussion of the results and an orderly presentation.

The candidate is requested to initiate and keep close contact with his/her academic supervisor(s) throughout the working period. The candidate must follow the rules and regulations of NTNU as well as passive directions given by the Department of Energy and Process Engineering.

Risk assessment of the candidate's work shall be carried out according to the department's procedures. The risk assessment must be documented and included as part of the final report. Events related to the candidate's work adversely affecting the health, safety or security, must be documented and included as part of the final report. If the documentation on risk assessment represents a large number of pages, the full version is to be submitted electronically to the supervisor and an excerpt is included in the report.

Pursuant to "Regulations concerning the supplementary provisions to the technology study program/Master of Science" at NTNU §20, the Department reserves the permission to utilize all the results and data for teaching and research purposes as well as in future publications.

The final report is to be submitted digitally in DAIM. An executive summary of the thesis including title, student's name, supervisor's name, year, department name, and NTNU's logo and name, shall be submitted to the department as a separate pdf file. Based on an agreement with the supervisor, the final report and other material and documents may be given to the supervisor in digital format.

☐ Work to be done in lab (Water power lab, Fluids engineering lab, Thermal engineering lab)
☐ Field work

Department of Energy and Process Engineering, 14. January 2015

Olav Bolland
Department Head

Petter Nekså
Academic Supervisor

Research Advisor:
Kjell Kolsaker, NTNU EPT

Preface

This master thesis was carried out at the Department of Energy and Process Engineering at the Norwegian University of Science and Technology (NTNU). The work was done in the second semester of the Academic Year 2014/2015 and comprises 30 ECTS credits.

As no field work or laboratory experiments have been conducted as a part of the master thesis, no risk assessment document was needed.

I would like to acknowledge and thank Petter Nekså for supervising me through my master thesis. I am also grateful for the help provided by my co-supervisor Kjell Kolsaker, in particular his advice on the design of the simulation models.

Trondheim, Norway

June 2015

Hugo Eugen Hernes

Abstract

The purpose of this master thesis is to investigate the effects of active and passive measures to maintain the pressure in LNG fuel systems for ships. The background was two de-loading events that occurred on the gas engines on KV Bergen, a Norwegian Coast Guard vessel, in 2012 and 2013. The events triggered research, both on why a sudden large drop in the fuel tank pressure can occur, and how they could be prevented in the future.

The task required development of two models or simulation tools. One model was needed to assess the capacity of the Pressure Build-up Unit (PBU) on KV Bergen, another to analyse different aspects relevant for the pressure development of a fuel tank. Thus, the models had to quantify the drop in pressure, assess the contribution from various parameters decisive for the development of the tank pressure, such as relevant tank, LNG system and sea conditions. An inert gas for rapid pressurization of the fuel tank was additionally including in the model. The models are scripted in Matlab and utilize the thermodynamic properties provided by the software REFPROP NIST. The models draw on accessible data for KV Bergen and another LNG fueled vessel, the car-ferry MF Korsfjord.

In the capacity model for the PBU, the principles of the thermosyphon effect are used for calculating the mass flow rate and the return temperature of the LNG. A sensitivity analysis was carried out to evaluate the importance of different parameters on the design geometry and the system configurations of the PBU onboard KV Bergen.

The fuel tank pressure development model consists of the internal energy and the mass balance of the vapor and the liquid sections of the fuel tank. Departing from the basic pressurization capacity with evaporation through the PBU and condensation at the liquid-vapor interface, the model add in-tank waves representing the impact of rough sea, injection of gaseous Nitrogen to achieve additional pressurization capacity, and the use of warmer LNG to reduce the condensation rate.

The results obtained in this master thesis strongly suggest that an LNG fueled vessel should be capable of ensuring that the bulk LNG in the fuel tank keeps a temperature with a liquid saturation pressure higher than the designed minimum pressure for the gas engines. According to the thermodynamics, it will then no longer be possible for the tank pressure to fall so low that it will cause a de-loading of the gas engines. For KV Bergen, warm LNG at minimum -143.15 °C (130 K) with a liquid saturation pressure of 3.75 bar, is sufficient. The de-loading pressure limit is stated to be 3.6 bar for the gas engines on KV Bergen (DiRenzo 2014a). To obtain warm enough LNG, the fuel can either be heated during the bunkering process or later in the fuel tank by the PBU. The increase for the first approach is negligible compared to the time the PBU needs for heating up a full tank with cold LNG.

A thermal governed PID-controller should be installed in the PBU, ensuring that the LNG is completely evaporated and sufficiently superheated before returned to the fuel tank.

Finally, Nitrogen can be injected into the LNG tank if the PBU for any reason is not capable of maintaining the pressure. As an inert gas, the added Nitrogen does hardly impact the material quality of the LNG, and is thus well suited as a pressurant.

Sammendrag

Formålet med masteroppgaven er å undersøke aktive og passive tiltak for å opprettholde trykk i drivstoffsystemer for LNG om bord på skip. Bakgrunnen for arbeidet er to hendelser i 2012 og 2013 der kystvaktskipet KV Bergen mistet all effekt på naturgassmotorene grunnet fall i trykket i skipets drivstofftank. Disse hendelsene har igangsatt forskning, både for å finne ut hvorfor tanktrykket plutselig kan falle kraftig, men også hvordan dette kan unngås.

Oppgaven krevde utviklingen av to modeller eller simuleringsverktøy. Den første modellerer kapasiteten til dagens trykkoppbyggingsenhet (PBU) på KV Bergen, den andre analyserer relevante forhold som påvirker utviklingen av trykket i drivstofftanken. Modellene måå kunne kvantifisere fall i trykk samt bidragene til de enkelte parametre som påvirker trykkutviklingen, slik som fyllingsgrad og tanktrykk, konfigurasjonen av LNG-systemet og sjøgang. Modellene er skrevet i Matlab og nyttiggjør seg av programvaren REFPROP NIST for verdier for termodynamiske parametre.

Kapasitetsmodellen for PBU'en anvender prinsippene for en termosyfon til å beregne massestrømmen og returtemperaturen til gassen. En sensitivitetsanalyse er utført for å kunne anslå betydningen av designgeometri og systemkonfigurasjoner for PBU'en ombord på KV Bergen.

Trykkutviklingsmodellen er basert på både indre energi- og massebalanser for både væske- og gassfasene i drivstofftanken. Utover den generelle trykkutviklingen som følge av fordampning gjennom PBU'en og kondensering ved væskeoverflaten, modelleres bølgebevegelser inne i tanken for å simulere røff sjø, injeksjon av nitrogen for å oppnå ekstra trykkoppbygging, og bruk av varmere LNG for å redusere kondensasjonsraten.

Resultatene fra masteroppgaven fastslår at LNG-drevne farkoster er i stand til å påse at væskefasen i drivstofftanken holder en minimumstemperatur med et væskemetningstrykk høyere enn minimums designtrykk til naturgassmotorene. For KV Bergen er det tilstrekkelig med varm LNG på minimum -143 °C (130 K) med et væskemetningstrykk på 3.75 bar. Minimumstrykket for å unngå å miste motoreffekten på KV Bergen er oppgitt å være 3.6 bar (DiRenzo 2014a). For å oppnå varm nok LNG kan drivstoffet enten bli varmet opp under bunkringsprosessen, eller det kan bli varmet av PBU'en i etterkant. Den ekstra tiden som er nødvendig ved bunkringen, er mye korter enn de mer enn 16 timene det tar å varme opp en tank fylt med kald LNG ved bruk av trykkoppbyggeren.

En termostyrt PID-regulator som kan senke massestrømmen gjennom PBU'en om returtemperaturen er lavere enn ønsket, og dermed sikre full fordampning bør implementeres i trykkoppbyggeren.

Nitrogen kan også injisers inn i drivstofftanken dersom PBU'en av en eller annen grunn ikke klarer å opprettholde trykket i tanken. Som en inert gass, påvirker ikke nitrogenet den materielle kvaliteten til LNG'en nevneverdig, og er derfor velegnet som trykksetter. LNG-fartøy har allerede en infrastruktur for nitrogen om bord, da nitrogen brukes til å rense LNG-systemet. Derfor er bare mindre modifikasjoner nødvendige for denne muligheten.

Table of Contents

List of figures

List of tables

Abbreviation

BL	Boundary Layer
CO_2	Carbon dioxide
ECA	Emission Control Area
EIA	U.S. Energy Information Administartion
EU	European Union
GRU	Gas Ramp Unit
HFO	Heavy Fuel Oil
IEA	International Energy Agency
KV	"Kystvakten" - Ship type abbreviation for the Norwegian Coast Guard
LNG	Liquefied Natural Gas
MDO	Marine Diesel Oil
MF	Motor Ferry - Ship type abbreviation
NIST	National Institute of Standards and Technology
NG	Natural Gas
NO_x	Nitrogen oxide
PBU	Pressure Build-up Unit
PID	Proportional-integral-derivative (PID controller)
PM	Particulate Matter
PVU	Product Vaporizer Unit
REFPROP	A Thermodynamic database from NIST
S	Sulfur
SO_x	Sulfur oxide
WG	Water-glycol or "water-ethylene glycol mixture"

Nomenclature

Parameter	Description	Units
A	Area	m^2
Cp	Specific heat capacity	J/(kgK)
d	Diameter	m
DR	Destruction ratio	-
e	Tube roughness	m
E	Energy	J
g	Gravity constant	m/s^2
G	Mass flow flux	$kg/(sm^2)$
h	Heat transfer coefficient	J/(kgK)
h	Specific enthalpy	J/kg
k	Thermal conductivity	W(mK)
l	Length	m
m	Mass	kg
$\dot{m}$	Mass flow rate	kg/s
N	Number of turns per coil	-
n	Number of coils in PBU	-
P	Pressure	Pa
Pr	Prandtl number	-
r	Radius	m
Re	Reynolds number	-
ρ	Density	kg/m^3
SF	Sloshing factor (for motions inside the tank)	-
T	Temperature	°C or K
U & u	Internal energy, specific internal energy	J & J/kg
v	Velocity	m/s
V	Volume	m^3
$\dot{V}$	Volume flow rate	m^3/s
$\dot{Q}$	Heat rate	W
$\dot{W}$	Work	W
X	Thickness of boundary layer	m
x	Vapor mass fraction	kg/kg
z	Vertical height	m

Sub-script	Description
BL	Boundary layer, liquid top layer in tank
bulk	Bulk LNG condition in tank
bunkering	Conditions for the LNG bunkered.
calm	Under calm conditions, no motions
con	Condensation
conduction	Conduction
critical	Critical
eff	Effective, e.g. diameter or length
freeze	Freezing point
GRU	Inlet conditions of GRU
ht	Heat transferring, used for describing area for condensation
in	Inlet conditions
intermediate	Intermediate
liq	Liquid
max	Maximum
min	Minimum
out	Outlet conditions
PBU	Through the PBU cycle
pitch	Vertical distance from center to center of the pipe in the coils
PVU	Through the PVU cycle
recommended	Recommended value
return	Conditions for flow returning to the fuel tank
sat	Saturation condition
tank	Condition inside tank, geometry of tank
target	Targeted temperature
fuel	Condition of fuel outlet of the tank
universal	Universal
vap	Vapour
WG	Water-glycol mixture

1. Introduction

Natural gas is increasingly used as fuel for marine transportation. Often quoted advantages are lower emissions to air, less noise from the engine and lower fuel costs. The latter depends on relative fuel prices, taxation and investments, and this is probably most important for the ship-owners. Disadvantages are both higher investment costs and technical and operational challenges. In (Hernes 2014) the benefits and disadvantages of NG were discussed in more detail, only the main issues are presented below. A description of the LNG fuel system and the experiences from the de-loading events of the NG engines on the Norwegian Coast Guard vessel KV Bergen are given in the following sub-chapters.

1.1 Why NG is used as fuel in the marine sector

The two main drivers for use of NG as fuel in the marine sector are improved economics and stricter legislation, frequently related to emissions of pollutants to air. These are outlined in two sub-chapters on environment and economy.

1.1.1 Environment

As governments across the world are implementing new emission regulations areas (ECA) for coastal water, harbors and in inland waterways, and stricter requirements are expected to be implemented in the years to come, ship owners are required to take action. Figure 1 shows the gradual tightening of Sulphur content allowed used in marine fuels globally and for selected regions. From 2016, ECA will also include restrictions on NO_x emissions from new ships (Acciaro 2014), and thereby better reflecting the negative health and environmental effects from marine activity.

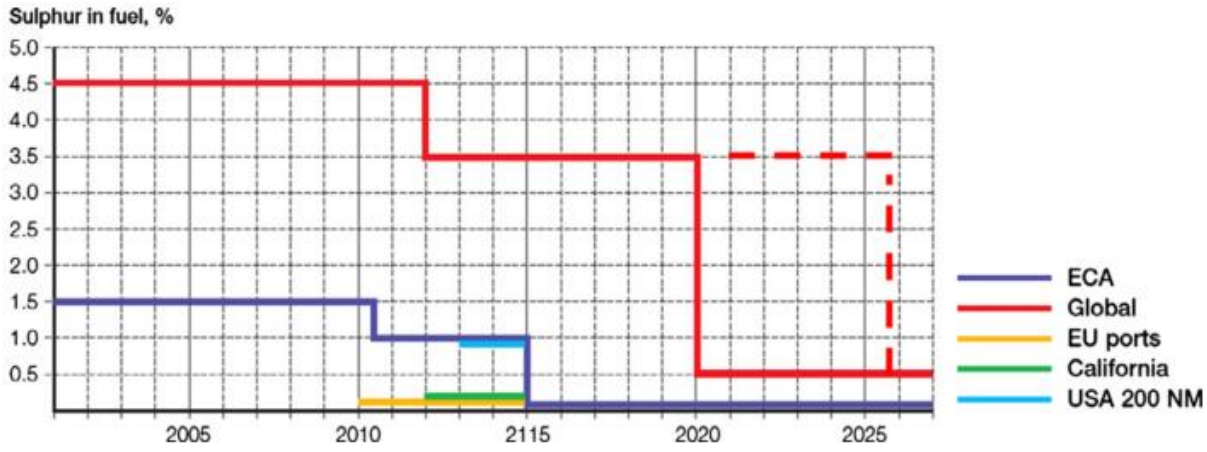

Figure 1 - The evolution of global and local sulphur legislation - (Cullinane and Bergqvist 2014)

A ship-owner has several option to comply with the stricter regulation. He can continue burning standard heavy fuel oil (HFO) by installing scrubbers to clean the exhaust gas,

use the more expensive marine diesel oil (MDO) in existing system when sailing inside ECA's, or similar regions, or switch to NG. The latter can be accomplished by either using NG in combination with HFO in a dual fuel engine, or using only NG in specified NG Engines. Table 1 shows the effects of different solutions compared to standard operations using HFO as fuel. From an environmental aspect, it is evident that LNG is the preferred fuel. Of course there may be some variations in these numbers for the different fuels and abatement technologies when including the whole value chain in well-to-wake life cycle analysis.

Abatement technology/measure	Emission reduction (%)			
	SO_x	NO_x	PM	CO_2
Basic internal engine modifications for 2 strokes, slow speed only	0	−20	0	0
Advanced internal engine modifications	0	−30	0	0
Direct water injection	0	−50	0	0
Humid air motors	0	−70	0	0
Exhaust gas recirculation + scrubbing	−93	−35	−63	0
Selective catalytic reduction (2.7% S residual oil fuel)	0	−90	0	0
Sea water scrubbing	−75	0	−25	0
Fuel switching (from 2.7% S to 1.5% S HFO)	−44	0	−18	0
Fuel switching (from 2.7% > 0.5% S HFO)	−81	0	−20	0
Low S marine diesel (from 0.5 to >0.1% S)	−80	0	0	0
Liquefied Natural Gas (LNG)	−90	−80	−100	−20

Table 1 - Gas emission reduction for different technologies and solutions, compared to standard operations using HFO - (Burel, Taccani et al. 2013)

1.1.2 Economy

Ship owners will typically choose the least costly way to comply with new legislations, but the actual chosen method will depend on type of vessel, sailing routes, availability of different fuels in harbors and not the least if it is a new-build or an existing ship.

Even if the capital expenditures are larger for a natural gas drive system, lower operational costs may still make it profitable to use NG. As more and more vessels are equipped with gas drive systems, the difference in investment costs compared to diesel systems should decline. Relative fuel prices expressed in calorific terms are important, and so are taxes and economic incentives, if any. IEA and EIA data suggest lower LNG than MDO prices in the future (Acciaro 2014). With the drop in oil prices in 2014, the cost benefit of NG compared to diesel have been somewhat reduced, but this can change again.

Due to large investments, LNG is an option for new-builds, and only to a small extent for retrofitting of existing fuel systems. One reason that ship owners may discard LNG for both new-builds and retrofitting, is the use of the discounted cash flow method when taking investment decisions. Embracing the opportunities for a favorable fuel price development by

using real options instead, more NG-propulsion projects may seem profitable for the ship owner. Using the fuel price forecasts in (Acciaro 2014) for real options, LNG systems become profitable in all cases shown Table 2.

Alternative	CapEx	2020	
		Fuel costs	Savings
(0) Base line	$0	$19,242,062	$0
(1) LNG now	$18,000,000	$14,198,639	$5,043,423
(2) LNG in 2014	$19,080,000	$14,960,328	$4,281,734
(3) LNG in 2015	$20,224,800	$15,633,297	$3,608,765
(4) LNG in 2016	$21,438,288	$16,268,492	$2,973,570
(5) LNG in 2017	$22,724,585	$16,846,815	$2,395,246
(6) LNG in 2018	$24,088,060	$17,550,111	$1,691,951
(7) LNG in 2019	$25,533,344	$18,180,640	$1,061,422

Table 2 – Capital Expenditures, expected total fuel costs and expected savings for the various investment alternatives, using real options - (Acciaro 2014)

Finally, access to LNG is related to significant uncertainty for the ship-owner. Whereas HFO and MDO are available in all harbors, LNG has a less developed infrastructure for delivery. Ship-owners face the risk of LNG delivery problems due to the lack of or only immature infrastructure. LNG may not be available at all, or a delivery may not be on time, and thus delaying the ship's departure. This may potentially cause large profit losses if relying only on LNG. Today, LNG is usually transported to a harbor by truck, but purpose-built vessels for LNG distribution are being developed.

1.2 The Ships and their LNG fuel system

This sub-chapter describes the essential data for the ships KV Bergen and MF Korsfjord. The objective is to provide an introduction to the ships and the design of its LNG fuel system, to facilitate further reading and understanding of the de-loading events presented in the next sub-chapter and the rest of this thesis.

MF Korsfjord, a car ferry operating for the time being in Trondheimsfjorden by Fjord1, uses the same of NG Engines as KV Bergen. Information found in the technical brochures for MF Korsfjord can therefore shed light on the de-loading case on KV Bergen. Some of the data used in this thesis are measurement performed on MF Korsfjord (DiRenzo 2014a).

1.2.1 KV Bergen

KV Bergen is a patrol vessel of the Barents class operated by the Norwegian Coast Guard, built in 2010. In order to fulfill its tasks, often in rough seas, KV Bergen needs to have

a reliable propulsion system, good acceleration and top speed, as well as great maneuverability. The ship operates with a diesel-/gas-electric hybrid propulsion system, details given in Table 3. The NG Engines powering the electrical motor are three Mitsubishi GS16R and one GS12R. The electrical motor is combined with the diesel engine on a common reduction gear (The Norwegian Coast Guard 2013).

Parameter	Effect
3 x NG Engine – GS16R	2580 kW (3 á 860 kW)
1 NG Engine – GS12R	635 kW
Diesel engine	4000 kW
Electrical motor	2500 kW

Table 3 - KV Bergen propulsion system - (The Norwegian Coast Guard 2013)

More details on size of the ship and the fuel tank are provided in Table 4 below. The tank is cylindrical with bended ends, lying horizontally and orientated in parallel with the ships length (The Norwegian Coast Guard 2013). There are different methods of calculating the volume of the fuel tank, for warm and cold volume. This thesis uses the gross volume, both for calculations regarding the NG vapor in the fuel tank and for the evaporation capacity simulations. The effective length is the average length of the tank when the end sections are assumed straight and not bended. The effective length is calculated by the cross sectional area of the fuel tank and the gross volume.

Parameters	Values
Ship	
- Length	93 m
- Width	16.6 m
- Depth	8.6 m
- Gross tonnage	4025 ton
Fuel tank	
- Pressure - max	9 barg
- Volume - gross	234 m^3
- Inner diameter	4.9 m
- Length	13.5 m
- Length - effective	12.41 m

Table 4 - Geometric details for KV Bergen (Norwegian Maritime Authority 2013) and (Cryo AB 2012)

The NG Engines require a certain pressure to operate. In order to monitor and control both pressure and gas flow to the engines, a Gas Ramp Unit (GRU) is installed between the

fuel tank and the engines. The GRU reduces the pressure from the fuel stream from the LNG tank down to the desired engine pressure. Table 5 indicates pressure level upstream the GRU that the Mitsubishi engines can handle.

Location	Pressure
Engine entrance	120 kPa (200 mbarg)
Fuel gas, min	350 kPa
Fuel gas, max	800 kPa

Table 5 – Pressure rates for Mitsubishi GS16R - PTK - (Mitsubishi Heavy Industries 2014)

Since the fuel is stored as LNG, it is necessary to heat and evaporate it in the Vaporizer before it enters the engines as NG. The NG needs to be fully evaporated and superheated to above 21°C (Cryo AB - KV Bergen 2009). The desired tank pressure is kept by a vapor cushion consisting of NG. The heat utilized for evaporation and heating of the fuel and for the fuel tank pressurization, is delivered by a water-glycol mixture in the Vaporizer. Figure 2 shows this with a simple not-to-scale sketch. A more detailed description of the system is provided in Chapter 2.

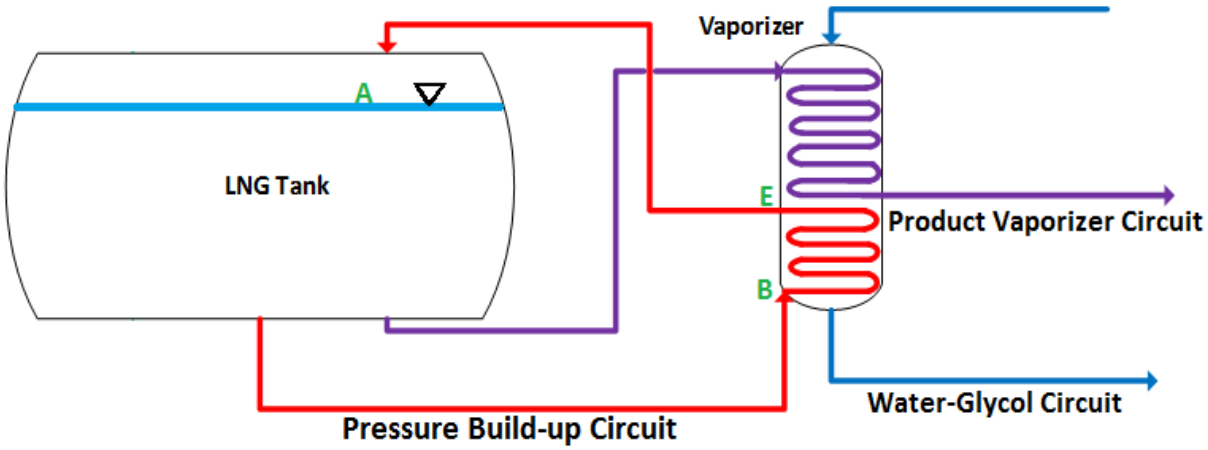

Figure 2 – Sketch of the LNG fuel system on KV Bergen – modified from (DiRenzo, Nekså et al. 2014b)

1.2.2 MF Korsfjord

MF Korsfjord is a car ferry operating in sheltered waters, in Trondheimsfjorden, thus there are not the same requirements for ship-design and construction as for KV Bergen. MF Korsfjord is a longer but lighter vessel than KV Bergen. Some technical data are listed in Table 6.

Parameters	Values
Ship	
- Length	122.7 m
- Width	16.2 m
- Depth	5.1 m
- Gross tonnage	2971 ton
Fuel tank	
- Pressure, max	10 barg
- Volume - gross	125 m^3
- Inner diameter	3.6 m
- Length	13.3 m
- Length - effective	12.28 m

Table 6 - Geometric details for MF Korsfjord – (Linde Cryo AB 2008) , (Cryo AB 2007) and (Norwegian Maritime Authority 2013)

The same assumptions and calculation methods are used to find the effective fuel tank length of MF Korsfjord as for KV Bergen.

1.3 De-loading events on KV Bergen

This thesis is based on two de-loading events on KV Bergen. The first event happened on 18th of October 2012, and the second in November 2013. This chapter outlines how the events are presented by (DiRenzo 2014a) and in the black-out report from the events (Espeland 2012).

In the black-out report for the first de-loading on 18th of October 2012, Chief Engineer Espeland describes two separate de-loading events. The report gives no clear indications on why the drop in pressure could be so large, and why it happened so fast that the NG Engines lost all power. In the first event the NG Engines load where producing 2200 kW, corresponding to 88 % of full load. No explanation for the first de-loading was provided in the report. After resetting the whole LNG system, a second trial with all four engines was conducted. When the NG Engines reached 92% off full load, the system de-loaded again. It was observed that the pressure in the fuel tank dropped by more than one bar, from 4.6 bar to below 3.6 bar. In a third trial, no de-loading occurred. According to Espeland, there were

only small waves (0.1-0.5 m), little current (0-3 knots) and light air (1-3 knots), nothing that independently should trigger sloshing inside the fuel tank.

The October 2012 report does not state any conditions of the tank prior to the de-loading. The ship bunkered LNG in the morning and the de-loading happened in the afternoon, thus it can be assumed that the fuel tank was almost full. Therefore there was only a small vapor cushion keeping the tank pressure at desired level. The liquid bulk temperature differs little from the temperature at bunkering, and the temperature in the vapor phase is given by the PBU exit temperature and the bulk temperature. This leaves the tank pressure before the two events as the key initial parameter for the de-loading events. Although it is not stated in the report, it was most likely a sudden drop in tank pressure that caused the first de-loading event, as well as for the second event. In addition, it should be logical to assume that the PBU circuit was operating under both incidents, though not capable to prevent the fall in pressure. The PBU, or Pressure Build-up Unit, is increasing the tank pressure by evaporating part of the LNG.

Also the second event in November 2013 occurred shortly after bunkering. This time 101 m^3 was bunkered and the tank pressure was increased to 4.6 bar. After one hour of producing 1400 kW from two NG Engines while the PBU circuit was operating, the tank pressure started to decrease. When the pressure reached 3.9 bar, the Chief Engineer switched to the diesel engine to avoid a de-loading of the NG Engines. Not until the vessel entered sheltered waters, it was possible to increase the tank pressure. Espeland reports that the waves were around three meters.

The information on the two de-loading events states that the drop in pressure is larger than what the PBU was capable to compensate, even when the NG Engines did not run at full load. In other words, with a condensation rate larger than the evaporation rate, $\dot{m}_{con} > \dot{m}_{PBU}$, the vapor density decreases and causes the pressure reduction. It is logically to assume that at normal circumstances the PBU is designed to be able to build up the tank pressure faster than the tank pressure is reduced by fuel consumption and condensation. Thus, there must be external sources disturbing the system and leading to the rapid drop in pressure. The most plausible explanation is that the condensation rate increases extensively for some reason. If the PBU operates as designed, there are only relative small variations in the evaporated mass flow for pressure build-up process. It is a possibility that the PBU controller did not work as intended, resulting in a decrease in the evaporation rate. In the event in November 2013, it was reported up to three meter high waves. In October 2012, there were only small waves, but the speed can be assumed to be high due to the high engine load, compensating for the smaller wave amplitude in terms of in-tank motions.

In the literature study, two measures to maintain pressure in the LNG fuel systems are studied, covering both a concept for reducing the condensation rate and an additional concept for pressurization of the fuel tank. First, a detailed description of the LNG fuel system on KV Bergen is provided.

2. LNG fuel system on KV Bergen

This chapter reviews the details of the LNG fuel system on KV Bergen, and is thus the foundation for the pressure development, evaporation and condensation models designed for this master thesis, presented in Chapter 4. The main source for information about the fuel tank and the Vaporizer unit, is the operational manual regarding the natural gas propulsion system on KV Bergen, provided by (Cryo AB 2010).

2.1 Fuel tank

The fuel tank has a perlite insulation between the outer and the inner tank shell. Vacuum is maintained between the tanks to reduce heat in-leakages. In this thesis, the heat in-leakages are assumed to be negligible, and thus not included. The physical constraints on the tank are minimum -196 °C (77 K) and maximum 9 barg. If the pressure exceeds 8.3 bar, the excess vapor is vented from the tank to the atmosphere via a vent mast. Cryo AB, the manufacture of the LNG fuel system, recommends operating pressures for the fuel tank as given in Table 7.

Pressure	**bar**
$P_{recommended,\ min}$	4.2
$P_{recommended}$	4.6
$P_{recommended,\ max}$	7.5

Table 7 - Recommended fuel tank pressures for KV Bergen - (Cryo AB 2012)

The LNG is bunkered sub-cooled compared to the operation tank pressure. During bunkering LNG flows into the tank either from the top or from the bottom, dependent on the pressure. If the tank pressure P_{tank} is larger than the pressure of the LNG bunkered, $P_{bunkering}$, LNG is bunkered from the top through valve HV 102, and the tank is de-pressurized by the liquid sprayed over the remaining vapor cushion. The location of the different valves described are shown in - Schematic of the valves in the LNG fuel system on KV Bergen - (DiRenzo 2014a) The vapor will then quickly condense. If $P_{tank} \leq P_{bunkering}$, the liquid will be filled through the valve HV 101 from the bottom until the desired filling ratio is reached. The valves mentioned are shown in Figure 3. In general, filling from the bottom will increase P_{tank}, while bunkering from the top will decrease the pressure. There is a 2 inch gas return line from the tank to the bunker station, which secures that P_{tank} does not increase too much when bunkering. If part of the vapor is not removed, P_{tank} would have increased corresponding to the reduced vapor volume as the liquid fills the tank. As the LNG bulk temperature is lower than the saturation temperature and there is space above the LNG, there will be some evaporation after bunkering until equilibrium is established.

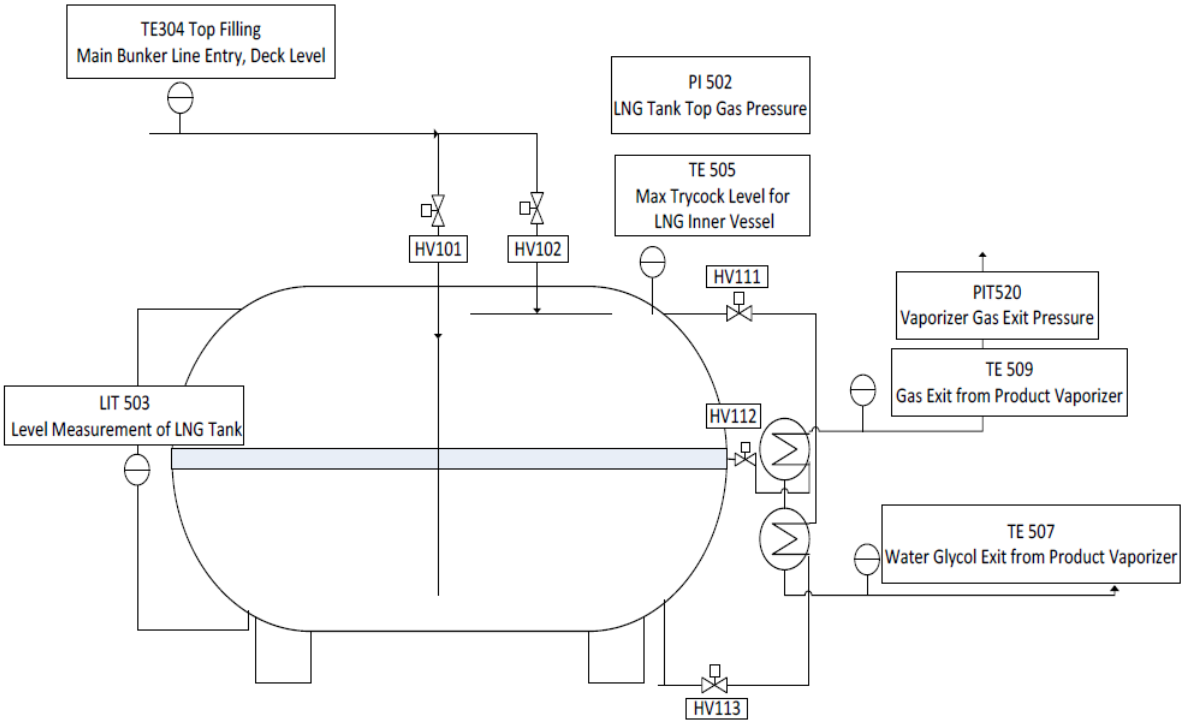

Figure 3 - Schematic of the valves in the LNG fuel system on KV Bergen - (DiRenzo 2014a)

The liquid level inside the fuel tank is determined by measuring the pressure at the top and at the bottom. The difference is converted into liquid height with the help of an estimated liquid density. Given the tank geometry, the liquid height is converted into a liquid volume and the amount of fuel left. The amount of LNG in the fuel tank is in this document referred to as the filling ratio corresponding to the liquid height, and not directly the gross volume of the fuel tank.

$$\text{filling ratio} = \frac{\text{liquid height}}{\text{tank diameter}} \tag{2.1}$$

A filling ratio of 0.9 is thus not the same as that the fuel tank is 90 % full with LNG. When the filling ratio drops below 0.3, the monitors will indicate that it is time for a new bunkering of LNG. Normally the filling ratio after a bunkering is 0.9 (Cryomar 2015).

As long as the average temperature of the vapor section is higher than the LNG bulk temperature T_{bulk}, there will be a slightly warmer liquid top layer above the bulk LNG. This is the normal operating situation. The top layer is the boundary layer between the liquid and the vapor, and is in this paper denoted BL. Due to phase transition occurring in the BL and in the vapor cushion, T_{BL} is on the saturation line and both vapor and liquid are saturated. The pressure at the BL is thus the saturation pressure for T_{BL}. As mentioned above, P_{tank} is measured at the top of the tank, which gives the possibility to calculate P_{BL} by including the static

pressure difference between the interface and the measure instrument. In this document, the static pressure of the vapor is neglected due to the low density of NG vapor compared to the liquid density. Thus, $P_{tank} = P_{BL}$ and is valid for the whole vapor section of the tank, regardless of filling rate, temperature and pressure. Since LNG consists of several components with different boiling points, liquid and vapor will co-exist in the tank with different compositions, even if temperatures are equal.

For a given tank condition, the minimum possible pressure will occur if there is a complete mixing of liquid and vapor (Hernes 2014). The fuel tank will afterwards be in an equilibrium state. All vapor which needs to condensate in order to achieve equilibrium, has condensed. Thus, all vapor is at the dew point and all the liquid at the boiling point. Due to the large mass ratio between the liquid and the vapor, the bubble point temperature will decrease to a temperature slightly above T_{bulk} prior the mixing. Thus, the minimum possible P_{tank} can be assumed to be the bubble point pressure for the given T_{bulk}.

The fuel entering the Gas Ramp Unit needs to have a pressure of at least $P_{GRU, min}$ = 3.5 bar in order to avoid de-loading of the NG Engines. Due to friction losses in the pipes, valves and the vaporizer between the tank and the GRU, P_{tank} needs to be somewhat higher to avoid de-loading. The hydrostatic effect may contribute in the opposite direction, but this depends on how the equipment is located relative to each other and the height difference between the liquid surface in the tank and at which height the evaporation takes place in the PVU, the Product Vaporizer Unit.

If ΔP_{static} is the net pressure gain from the static pressure from the liquid surface in the tank to the GRU inlet, and $\Delta P_{friction}$ is the total pressure loss due to friction between the tank and the GRU, the de-loading tank pressure can be expressed as:

$$P_{\text{de-loading}} = P_{\text{GRU, min}} + \Delta P_{\text{fuel}} = 3.5 \text{ bar} + \Delta P_{\text{friction}} - \Delta P_{\text{static}} \tag{2.2}$$

where ΔP_{fuel} will vary for changing filling ratios and mass flow rates due to different NG Engine loads. The location of evaporation in the PVU will therefore vary, and it is thus difficult to give a precise value or equation for $P_{de\text{-}loading}$. In any case, the drop in pressure in the tank will in a de-loading event be more severe than the difference between P_{tank} and P_{GRU}. DiRenzo used a de-loading limit of $P_{de\text{-}loading}$ = 3.6 bar for the fuel tank in his master thesis in 2014. Due to the arguments above, the same pressure for the de-loading limitation is used as a basis in this thesis.

2.2 Vaporizer - Principles

The Vaporizer is a heat exchanger and consists of two parts in one container, placed inside the Cold Box, connected to the fuel tank. The container is made out of an outer and one inner cylindrical shell, with an arrangement of helically coiled tubes in a ring between them, as in Figure 4 showing the Vaporizer on KV Bergen.

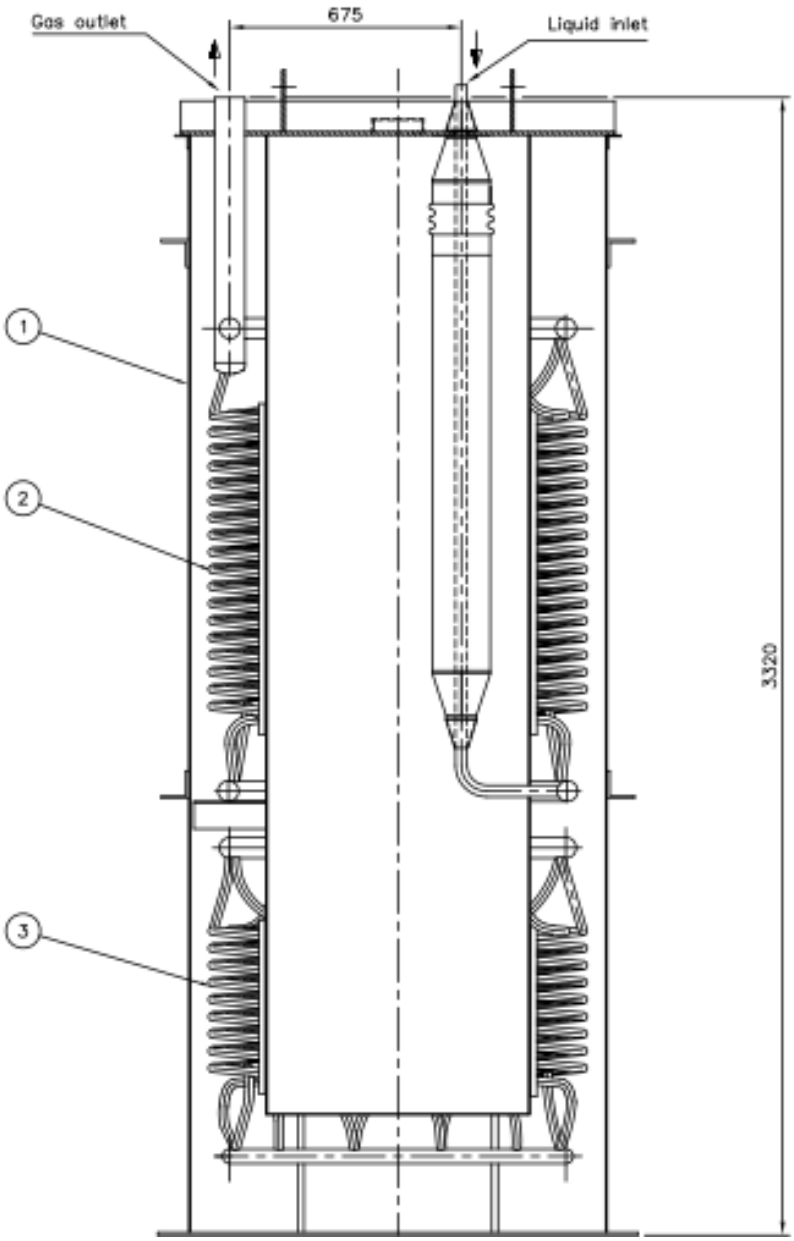

Figure 4 - System drawing of the Vaporizer on the KV Bergen - (Linde Cryo AB 2006)

The PBU, the Pressure Build-up Unit, is located at the bottom and the PVU, the Product Vaporizer Unit for the fuel leaving to the NG Engines, in the upper part. In both units the LNG flows upwards in the helically coiled tubes and the water-glycol mixture flows downwards on the outside of the tubes. The water-glycol mixture flow is driven by two designated circulation pumps, and has a listed flow rate of $\dot{V}_{\mathrm{WG}} = 60\ \mathrm{m}^3/\mathrm{h}$ (Cryo AB - KV Bergen 2009). The Chief Engineer on MF Korsfjord indicated a 50-50 water-ethylene glycol mixture (DiRenzo 2014a), which is the mixing ratio used in this paper. Table 8 gives the recommended temperatures for the water-glycol flow through the Vaporizer, as presented in the operation manual (Cryo AB 2012).

Parameter	Recommended value	Description
$T_{WG,\ in}$	30 °C	Inlet of Vaporizer, PVU inlet
$T_{WG,\ intermediate}$	26 °C	PVU outlet, PBU inlet
$T_{WG,\ out}$	22 °C	Outlet of Vaporizer, PBU outlet

Table 8 - Recommended water-glycol mixture temperatures on KV Bergen - (Cryo AB 2012)

The design value of $T_{WG,\ out}$, 22 °C, is the lowest permitted temperature for the water-glycol mixture in order to ensure no problems with ice formations blocking the flow path. Under normal operations this value for $T_{WG,\ out}$ should not be reached; both $T_{WG,\ in}$ and $T_{WG,\ out}$ should be are well above these limits.

On KV Bergen they have increased the circulation flow rate, where an average of $\dot{V}_{\mathrm{WG}} = 72.44\ \mathrm{m}^3/\mathrm{h}$ was measured together with an average water-glycol mixture temperature $T_{WG,\ avg}$ of 32.85 °C (306 K) (DiRenzo 2014a). Before starting the NG Engines, the water-glycol circuit needs to be operating and be able to evaporate the fuel and further superheating the NG to the required temperature.

The glycol used in the mixture is most likely ethylene glycol (Cryo AB - Components 2005). The freezing point of a 50-50 water-ethylene glycol mixture is $T_{WG,\ freezing}$ = -33.97 °C (239.18 K) (M. Conde Engineering 2011), (Code Consultants Inc 2010). As $T_{WG,\ freezing}$ is much higher than the LNG temperatures, some freeze out of water-glycol could take place on the tubes. As long as the ice is melting again, this should be no larger problem, although it is not desired as it reduces the heat transfer capacity. A real problem occurs if the amount of ice becomes so large that it blocks the hot side of the Vaporizer, or reduces the heat transfer significantly. The consequence may be that the fuel going to the NG Engines is not completely evaporated or necessary superheated. For the PBU, the consequence of an incomplete evaporation is a reduction in the pressure build-up capacity, due to cold droplets falling down over the existing warmer vapor. These droplets will contribute to enhanced condensation and must be avoided. Partial evaporation lowers the hydrostatic “driving force” of the hydrosyphon, but actual increases the mass flow rate through the PBU, due to lower friction induced pressure losses in the return pipe between the PBU and the fuel tank.

In order to prevent ice to form inside the Vaporizer, the outlet temperature of the water-glycol mixture ($T_{WG,\ out}$) and the NG outlet temperature from the PVU ($T_{PVU,\ out}$) are monitored. If the temperature of the NG out of the PVU or the temperature of the water-glycol out of the PBU decreases below the set points of 21 °C and 22 °C, respectively, the LNG streams are stopped by global valves. Even though these temperatures are much higher than the freezing point of the water-glycol mixture, a lowered $T_{PVU,\ out}$ indicates insufficient heat transfer and thus possible icing on the tubes. Since it is difficult to know how the ice forms and melts on the coils inside the Vaporizer, these safety values for the temperatures are set. For lower outflow temperatures, a risk for complete freezing of the Vaporizer is assumed plausible.

If the Vaporizer needs to be warmed up due to severe icing on the tubes or complete blockage of the Vaporizer, the NG Engines can not be used. The explaination is that the system is not able to deliver the fuel as vapor at the specified temperature to the NG Engines. Thus, the vessel needs either to have a parallel system for propulsion power, as diesel engines, or to use Duel Fuel Engines. Neither solution is desired. In a critical situation with possibility for de-loading but the PBU needs to operate, the danger of a complete bloackage of the Vaporizer is unacceptable. The same applies to normal operation conditions if the initial tank pressure is high and the condensation rate is relatively low. Consequently, the design of the water-glycol system needs to be of a scale that prevents severe flow blockage caused by ice on the tubes.

The temperature of the water-glycol mixture will after a long stand still reach ambient temperature, normally around 10-15 °C. Nevertheless, there is still much heat that is transferable to the LNG, even if the temperature is below the minimum value set by (Cryo AB 2012). If the temperature controller for $T_{WG,\,out}$ is overridden at the start-up, where the LNG flow is small, the chance of getting problems with severe ice formations is small. Thus, extra heat added by starting the diesel engine is not needed. If the tank pressure needs to be increased before starting the NG Engines, the same reasoning and procedure can be used.

2.2.1 PBU - the Pressure Build-up Unit

In the pressure build-up process, cold LNG is drained from the tank bottom to the PBU. The flow is controlled by the on/off- globe valve HV 111, located after the PBU on Figure 3. Thus, the flow through the PBU is either at its maximum for the given P_{tank}, filling ratio and heat transfer capacity, or zero. On KV Bergen, the operation pressure is set to the range between 4.5 bar and 4.95 bar. When the pressure drops below 4.5 bar, the PBU is activated and it is de-activated when the tank pressure increases above 4.95 bar.

As shown in Figure 5, the LNG enters the PBU at the bottom in point B and leaves at the top, which is on the side of the Vaporizer, marked with E in Figure 5. The figure is a sketch only of the principles of the PBU-circuit, thus not correctly scaled. In the PBU, the LNG flowing tube consists of five different sections. At the bottom there is a horizontal ring distributing the LNG to the different coils. At the top there is a similar ring collecting all the LNG streams together before leaving the PBU. Between the coils and the rings, there is a straight section at both sides of the coil. All the dimensions are presented later in Table 11 (in Chapter 4.2). Some locations in the PBU circuit are for this work named with letters for increased readability, as A at the liquid-vapor interface, B at the PBU inlet and E at the PBU exit.

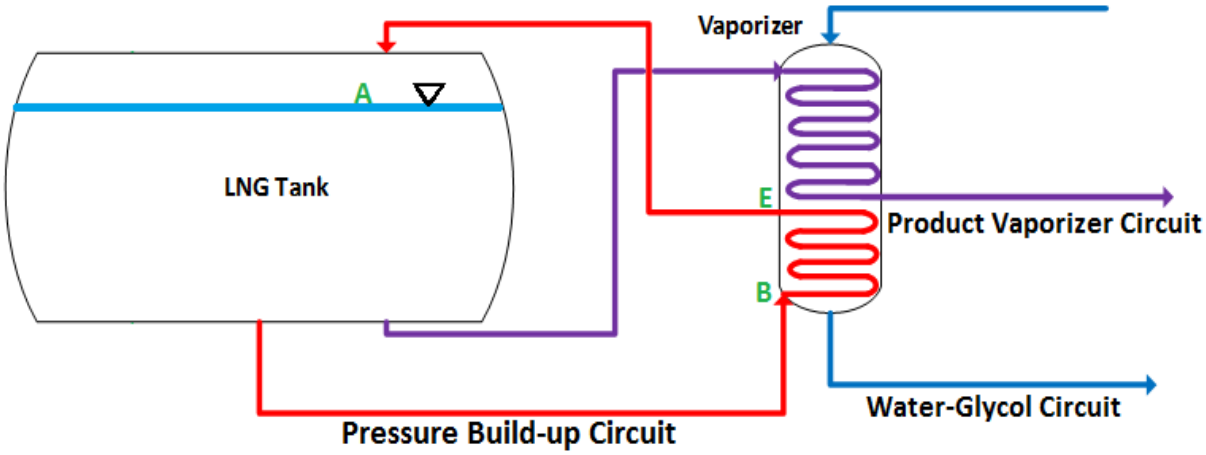

Figure 5 - Sketch of the LNG fuel system on KV Bergen – modified from (DiRenzo, Nekså et al. 2014b)

On KV Bergen the PBU cycle is driven by the thermosyphon effect: the flow through the PBU is not driven mechanically by a pump or similar, but by the heat transferred into the circuit in the PBU. The added heat reduces the density of the LNG, first by sensible heating and then by evaporation (Naterer 2003). The difference in density between LNG and NG gives a difference in the static pressure between the section from the liquid surface in the tank to the bottom of the PBU and the section from the bottom of the PBU through the PBU and back to the liquid surface. This enables the fluid to flow around in the circuit. For a thermosyphon cycle the pressure losses due to the flow through the cycle, equalize the net hydrostatic pressure difference. The maximum flow rate is thus coupled to the filling ratio, tank pressure and the heat transfer rate of the PBU, resulting in a pressure balance throughout the circuit, ΔP_{PBU}. ΔP_{PBU} is the sum of the friction induced pressure loss through the piping and abnormalities, the pressure loss due to the turbulence and acceleration introduced by the evaporation in the PBU and the pressure gain due to the hydrostatic pressure difference. The different contributions of the pressure changes are derived in detail in Chapter 4.5, whereas the pressure balance for the circuit is expressed below:

$$\Delta P_{PBU} = \left(P_B - P_A\right) + \sum_j \Delta P_j + \left(P_A - P_E\right) = 0 \tag{2.3}$$

where the first term represents the difference between the liquid-vapor interface and the inlet of the PBU, the second the sum of changes for each spatial step of the piping inside the PBU and the latter represents the pressure change in the return pipe between the PBU outlet and the fuel tank.

A principle sketch for the thermosyphon effect is shown in Figure 6. The vapor is superheated in the reboiler section. The “Point E” used in the models in this work, would be located at the exit of the reboiler.

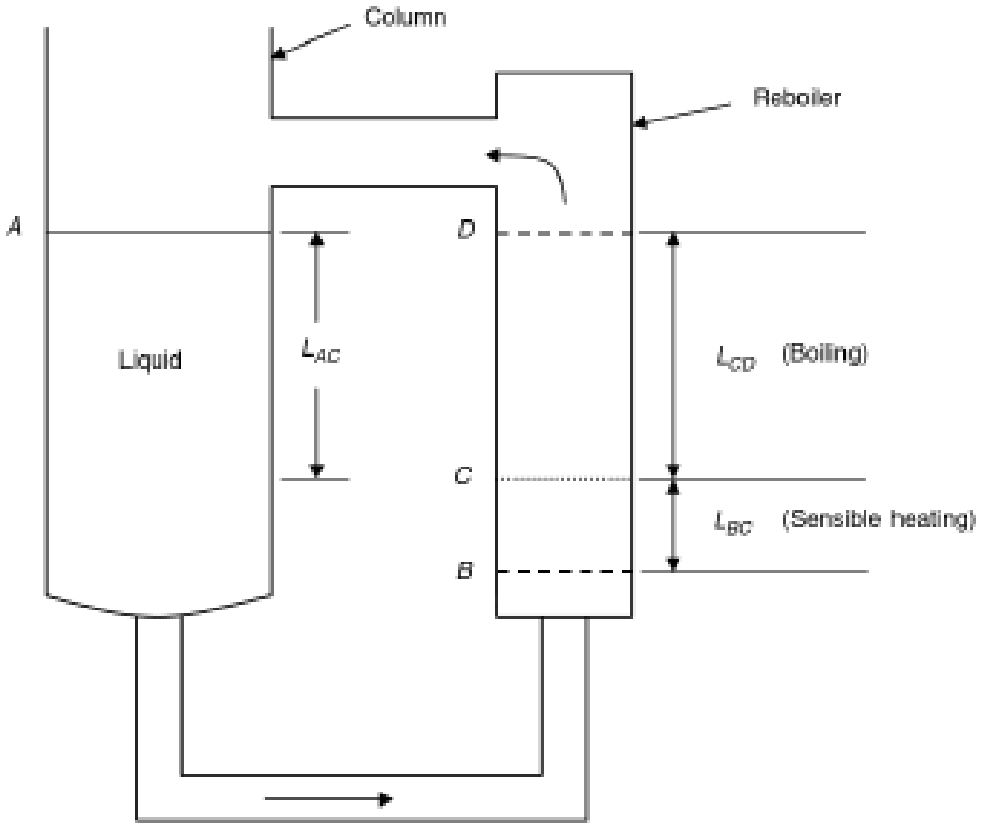

Figure 6 - Simple sketch of the thermosyphon effect - modified from (Serth 2007)

2.2.2 PVU - Vaporization and heating of the fuel upfront the NG Engines

The liquid extracted from the tank for fuel consumption is directed through the upper part of the Vaporizer in Figure 4. The amount of liquid to the engines is governed by the globe valve HV 112, shown in Figure 3. The PVU functions similar as the PBU, only that the size of the unit is larger. This is due to the strict requirement for the gas entering the NG Engines, which needs to be superheated to minimum 21°C (294K) (Cryo AB - KV Bergen 2009). The same source states that the maximal capacity for the PVU is 0.45 kg/s.

If there is no fuel consumption, the valves in the GRU are closed. The liquid stream to the product vaporizer will cease and the remaining liquid in the pipe will evaporate. Due to the expansion of liquid to vapor, the pressure in the pipeline will increase, and the NG vapor will flow back into the fuel tank. With no fuel consumption, P_{tank} will increase and HV 111 will therefore close.

2.3 GRU - Gas Ramp Unit

The GRU is out of the scope of this thesis since it does not affect the fuel tank pressure, and it will only be discussed briefly in order to understand the minimum pressure at the GRU to avoid de-loading. The schematic of the GRU is provided in Figure 7. Vaporized and superheated NG enters the GRU at the bottom and leaves at low pressure at the top right hand corner. The GRU consists of a serie of regulating valves, both for pressure and for flow control purposes, as shown in the figure. The minimum inlet pressure, $P_{GRU,\,min}$ is set to 3.5 bar, while the exit pressure of the GRU, or the engine pressure, is set to be 200 mbarg, 1.2 bar (Cryo AB 2012).

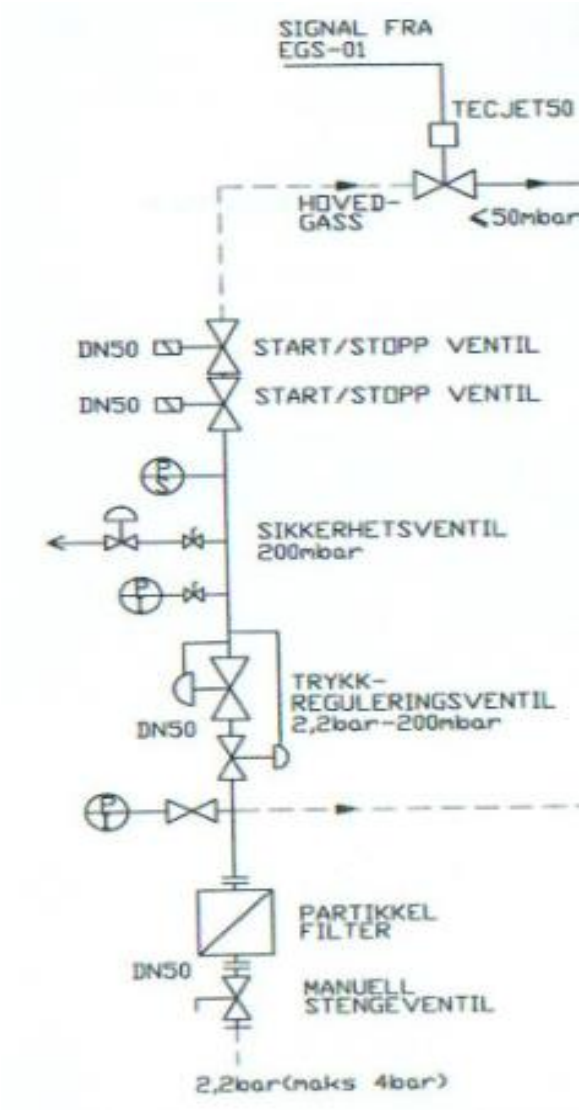

Figure 7 - Gas Ramp Unit at KV Bergen - (Myklebust Verft AS B49/B52 2009)

3. Literature study

The purpose of the literature study is to gather information on how sloshing may affect the condensation rate in an LNG fuel tank on a marine vessel, and how the pressure can be increased rapidly with an inert gas.

3.1 Nitrogen injection for rapid pressurization

For all liquid gas storage tanks, including LNG tanks, condensation and evaporation at the liquid-vapor interface can cause considerable pressure changes. With sloshing, these tanks may be exposed to rapid enhancement of the condensation rate and thus drop in pressure. In order to mitigate this challenge, Nitrogen gas (GN2) can be injected into the tank. As an inert gas, the Nitrogen will increase the pressure due to higher density in the vapor section of the tank. In (Ludwig, Dreyer et al. 2013), an experiment with cold liquid Nitrogen (LN2) pressurized with warm GN2 was conducted. The ambient temperature GN2 was injected at the top of a vertical orientated cylindrical container, and according to (Ludwig, Dreyer et al. 2013), not interfering with the cold liquid due to the fast injection. The negligible interference between a liquid and a pressurant consisting of a different gas, was confirmed by (Flachbart, Hastings et al. 2008) in an experiment with subcooled liquid methane and gaseous helium. As shown in a) in Figure 8 for the Nitrogen experiment, pressurizing the container from 100 kPa to 300 kPa takes 55 seconds, indicated with the dotted line. The increasing temperature during the pressurization for the different vapor layers is presented in part c) of the figure, with the measurement closest to the liquid bulk named T5, and the top measurement named T14.

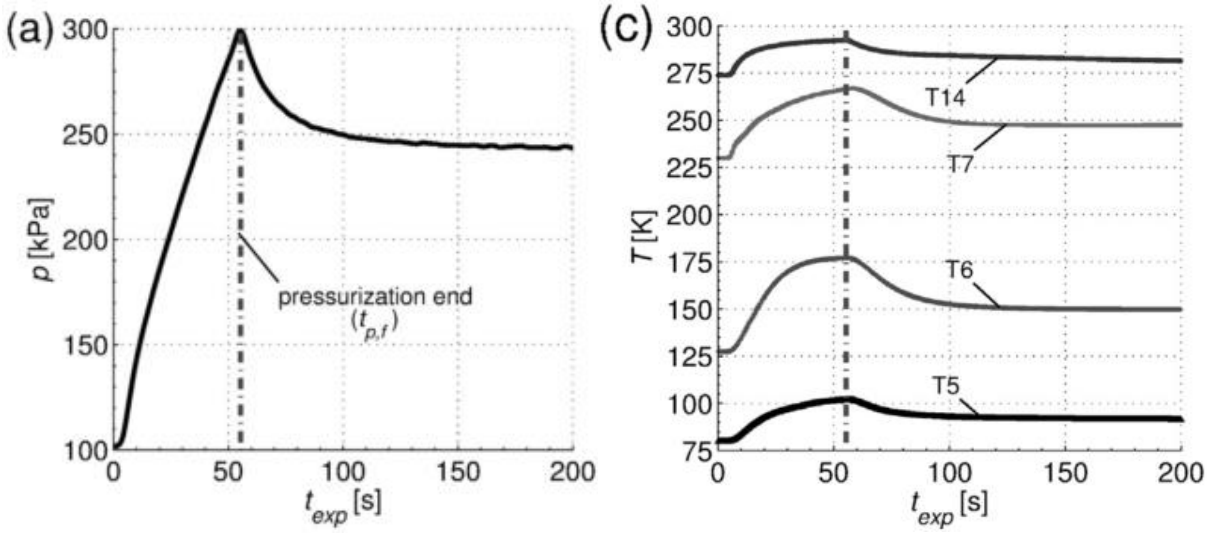

Figure 8 – a) Pressure development when pressurizing liquid N2 with gaseous N2. c) Temperature development in vapor section under pressurization with gaseous N2 - (Ludwig, Dreyer et al. 2013)

(Ludwig, Dreyer et al. 2013) used a small tank of $43 \cdot 10^{-3}$ m^3 with a filling ratio of 0.69, resulting in a vapor volume of $13.33 \cdot 10^{-3}$ m^3. Relating this to the much larger fuel tank on KV Bergen, a serial arrangement of nozzles inside the fuel tank is required to inject the Nitrogen, compared to a single nozzle in the study. Multiple nozzles may ensure sufficiently low outlet velocities and thus reduce the enhanced mixing of warm GN2 with the colder NG. Therefore, it should be possible to increase the pressure of the fuel tank on KV Bergen with at least the same speed as in the experiment, 3.64 kPa/s. It is difficult to predict the necessary pressurization time for vessels like KV Bergen, but several technologies enable a reduction of the gas velocities for the a given mass flow rate into a tank (Transport Canada 1984) and (Dorao 2012). The resulting increase in the mass flow rate from each nozzle should significantly improve the speed of the Nitrogen pressurization.

3.2 Drop in tank pressure due to sloshing of a cryogenic fluid

As extensively discussed in the project work (Hernes 2014), in-tank waves and especially sloshing contribute strongly to enhanced condensation of gaseous NG. The consequence is a severe, rapid drop in pressure. The question is: does the pressure fall to the liquid saturation pressure for the given liquid bulk temperature, or does it stabilize before? In the experiment conducted by (Ludwig, Dreyer et al. 2013) above, the container with liquid and gaseous N2 was allowed to evolve towards equilibrium after the pressurization, indicated in Figure 9 with a red circle. When the pressure was stabilized at approximately 250 kPa, different sloshing experiments where induced on the fluid. Independent of the sloshing violence and the sloshing regime, all results revealed the same pattern, pictured for one of the experiments with the green circle in Figure 9. The results only differ by the size of the drop in pressure and the time length before the pressure was stabilized. The mechanics causing the sloshing was de-activated when the pressure had stabilized. Since the tank was not sufficiently insulated, the heat in-leakages caused a small pressure increase after the sloshing ended ($t_{S,f}$ to $t_{S,f+td}$).

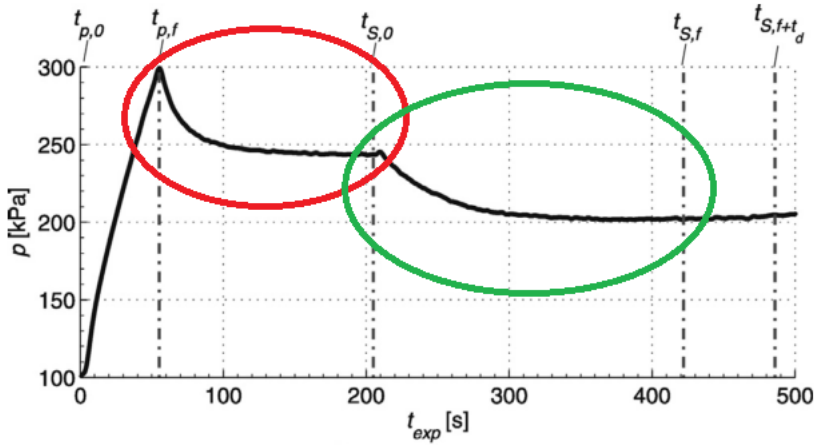

Figure 9 - Pressure development in a tank with LN2 and GN2, when evolving towards equilibrium (red circle) and inducing sloshing (green circle) - modified from (Ludwig, Dreyer et al. 2013)

(Ludwig, Dreyer et al. 2013) found that the pressure fell to somewhere right above the liquid saturation pressure of the liquid N2. For the same sloshing regime, the green circle in Figure 10 shows the temperatures of the top layers of the liquid N2. With a top layer temperature of 83.6 K, the liquid saturation pressure for Nitrogen is 199 kPa. Figure 9 shows that the tank pressure stabilized less than 10 kPa above the calculated liquid saturation pressure.

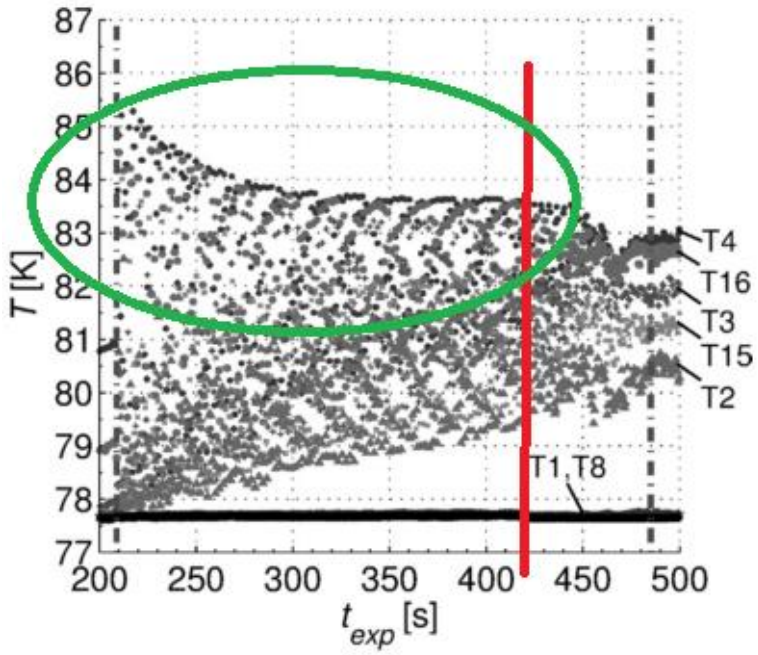

Figure 10 - Temperature development in the top layer of the liquid N2 under sloshing (left side of red line) – modified from (Ludwig, Dreyer et al. 2013)

Based on (Ludwig, Dreyer et al. 2013), the following working theory can be developed. When warm vapor is condensed into the liquid, the creation of a warmer top layer of the liquid, causes an enhanced thermal barrier preventing further large scale condensation, and correspondingly a larger drop in pressure. Applying this working theory on the case of KV Bergen, a warmer top layer of the LNG would decrease the potential drop in pressure when exposed to sloshing. The temperature lift of the top layer can be managed in two ways, either through extensive use of the PBU or by bunkering warmer LNG. The first will transfer heat from the water-glycol mixture via the evaporation and superheating of the LNG to the bulk LNG through condensation, and would thus require operation for a long periode of time before the top layer of the liquid LNG is sufficiently heated. The second approach would guarantee the required temperature immediately after bunkering. Bunkering warm LNG is further discussed in Chapter 6.2.

4 Simulation model development

In order to quantify the pressure build-up capacity of the PBU and thereby the compensation ability for NG condensation inside the fuel tank, the mass flow rate through the PBU needs to be modeled. The knowledge about the internal PBU design of KV Bergen is limited due to business secrets, thus several assumption have been made regarding the design and geometry of the LNG vaporizer system, showed in Figure 11. For the same reasons, the models developed for this thesis have been designed specifically to overcome these uncertainties and minimize the implications of them. Non of the models presented in this thesis consider the inertia of the system, thus the reaction time for all units and developments are set to zero, primarily affecting the activation and de-activation of the PBU.

Compared of the models used in my project work (Hernes 2014), which built on the work by (DiRenzo 2014a), the models used for this master thesis have been completely renewed. Not only were numerous errors of different significance corrected and the level of details increased several times, also the entire iterative process developed to find the temperature and pressure profile throughout the PBU has been fully redone alongside the design. In short, the models are no longer comparable.

Figure 11 shows the five sections of the PBU, used in the models designed. The LNG enters at the bottom in the lower distribution ring, where the LNG is distributed to the different tubes. The first and the last part of the tubes are called lower and upper straight sections. The sections are not completely straight, but in comparison to the coiled section in-between, they can for simplicity assumed to be straight. At the end of the tubes, the NG is gathered in the upper NG collection ring. It is assumed that the LNG is equally distributed between all the coils, and thus have equal temperature and pressure profile developments.

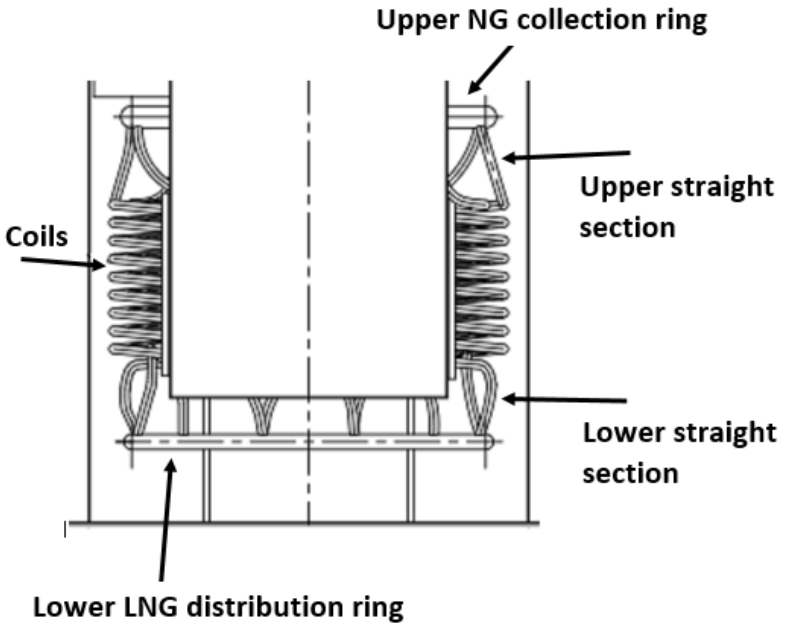

Figure 11 - PBU overview - modified from (Cryo AB - KV Bergen 2009)

In Chapter 4.2, all the necessary parameters for the initial design of the PBU and thermosyphon are presented.

The LNG flowing tubes inside the PBU were for modeling purpose divided into small tube sections. For these spatial steps of 2 cm, the inlet conditions for temperature and pressure were known. Assuming uniformity inside any of these small sections, the heat transferred to the LNG from the water-glycol mixture was modeled. Further, both temperature and pressure as well as the vapor fraction were calculated for the outlet conditions of a spatial step. A more detailed description of the model is presented in later sub-chapters. Reducing the step length from 2 cm to 1 cm did not significantly alter the calculations and the simulated return conditions of the NG from the PBU. Thus, step length of 2 cm was kept for all simulations performed for this thesis, also to save simulation time.

The thermodynamics and fluid mechanics behind the balancing of the thermosyphon effect were studied together with the condensation models. Both regarding the heat transfer from the water-glycol mixture to the LNG and the pressure changes through the entire PBU circuit due to the mass flow rate. The books and journals by (Serth 2007), (Incropera, Dewitt et al. 2013), (Fernández-Seara 2013) and (Kern 1950) have been helpful.

All calculations conducted in this chapter are based on the assumption that the bulk LNG composition of the tank is equal to the LNG shipment bunkered onto KV Bergen on 18 October 2012, the day of the first de-loading event. The note of delivery from (Gassnor 2012), shown in Table 9 as "Eksport 42-AI-2001", has a mismatch regarding the composition. Adding the various molar percentages gives a sum of 100.27 mole %.

Date: 18-Oct-12 Time: 10:39:36

Komponent	Kode	Eksport 42-AI-2001	Produksjon 42-AE-2002
Nitrogen	N2	0.50 %-mol	1.70 %-mol
Metan	C1	95.0 %-mol	93.6 %-mol
Karbondioksyd	CO2	0.00 %-mol	0.00 %-mol
Etan	C2	3.83 %-mol	3.50 %-mol
Propan	C3	0.55 %-mol	0.51 %-mol
Iso-Butan	IC4	0.25 %-mol	0.26 %-mol
Normal-Butan	NC4	0.07 %-mol	0.06 %-mol
Tunge komponenter	Sum C5+	0.07 %-mol	0.08 %-mol

Table 9 - Composition of LNG delivered to KV Bergen 18th October 2012 - (Gassnor 2012)

The LNG composition used in this thesis has been adjusted from the one presented in Table 9, to one which adds up to 100.00 mole %. This has been achieved by reducing the methane component to 94.73 mole %, which gives a total of 100.00 mole %. The reason for only reducing the methane fraction, is that the relative difference between the compositions is small. Applying the adjusted LNG composition as the initial composition in all later calculations, implies that the tank is drained and evacuated before start of bunkering. In reality this would not be the case. The vapor cushion would be destroyed and the bunkered LNG would be added to the rest of the old LNG, as described in Chapter 2. The old LNG is slightly warmer than the new LNG. Even though two layers of LNG could have been observed immediately after bunkering, they would quickly have been mixed. The problem of finding the combined composition after bunkering when old LNG is present, and thus the equilibrium of the LNG, is not discussed in this thesis.

The initial molar composition of the combined LNG and NG in the tank is assumed to be as shown in Table 10 alongside the mass fractions. All Matlab calculations using REFPROP-calls in the simulations are performed on a mass fraction basis. The bulk composition, and thus the LNG drained to both the PBU and to the NG Engines, is assumed to be homogenous and equal to the initial bulk composition.

Component	mole %	mass %
Nitrogen	0.50	0.82
Methane	94.73	89.56
Ethane	3.83	6.79
Propane	0.55	1.43
Isobutane	0.25	0.86
Butane	0.07	0.24
Pentane	0.07	0.30

Table 10 – Initial LNG composition used in the models

The tank modeled in this work is similar to the one on KV Bergen, a cylindrical horizontal tank. The curved end surfaces are for simplicity assumed straight, giving a fixed effective length of the tank for the entire inner diameter. This effective length is between the actual tank length and the length of only the straight cylindrical shell, without the curved ends. This influences only the area of the liquid-vapor interface and little else. Consequently, the condensation rate is slightly higher at high and low filling ratios and lower at intermediate filling ratios, when applying straight end walls compared to curved ones. This is due to the small error in the liquid-vapor interface area used for the condensation rate calculations, the error is assumed negligible. The tank parameters were presented earlier in Table 4.

It is evident that the results obtained in this thesis will differ with varying LNG composition. This theme is not covered in this master thesis, as the principles presented would be similar.

4.1 Amount of heat transferred to the LNG in the PBU

The heat transferred from the hot to the cold side in the PBU varies from one of the earlier mentioned defined small spatial steps of the tube to the next. The conditions on the water-glycol side are assumed to be constant throughout the PBU; thus the outer heat transfer coefficient is fixed for a given geometry. However, the conditions on the inside of the tubes vary with increasing temperature and decreasing pressure through the PBU. Thus, since the overall heat transfer coefficient and the difference in temperature between the hot and the cold side vary, the heat transferred for each section will differ and needs to be calculated for each spatial step.

The heat that can be transferred in the PBU from the water-glycol to the LNG, is determined by the parameters of the heat exchanger. The overall heat transfer coefficient is a product of the parameters of the hot and cold streams, the PBU design and the conditions of the fuel tank. On the other hand, the required $\dot{Q}_{PBU,tot}$ relate to the heat needed for the enthalpy increase through the PBU to reach the targeted exit temperature of the NG T_{target}, depends both on tank pressure and LNG bulk temperature, as shown in Figure 12. This subchapter therefore aims to study and establish the equations regarding the possible heat transfer both for the different sections and in total for the entire PBU.

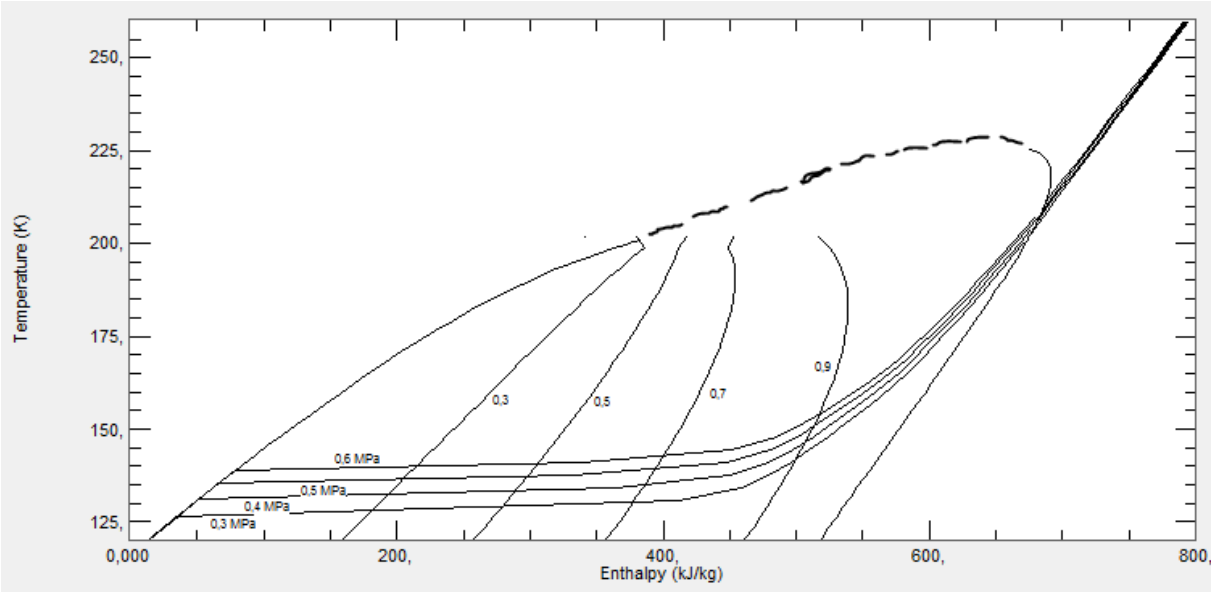

Figure 12 – Enthalpy-temperature diagram for the LNG, including relevant isobars from 3 bar to 6 bar and vapor quality lines - generated in REFPROP, added saturation line (dashed) through critical region

The heat transfer for both one spatial step of the tube and the entire PBU are expressed in the equations below, where subscript "j" indicates one of the small spatial steps. The parameters inside the parenthesis in the first equation are some of the parameters used to derive the overall heat transfer coefficient UA_j.

$$\dot{Q}_{PBU,\,j} = UA_j\ (\dot{m}_{PBU},\ T_j,\ P_j,\ k_j,\ d_{tube,\,i,\,j},\ l_j,\ \dot{V}_{WG},\ T_{WG,\,avg},\ t_{ice},\ k_{WG,\,ice})\ \Delta T_j \tag{4.1}$$

$$\dot{Q}_{PBU,\,tot} = \sum_j \dot{Q}_{PBU,\,j} \tag{4.2}$$

An arithmetic temperature difference for each step is used, where the temperatures on both sides of the tube wall are assumed to be constant for any small section. Whereas the LNG/NG temperature at the section inlet is used as the temperature on the cold side, the averaged water-glycol temperature for the whole Vaporizer is used on the hot side.

$$\Delta T_j = T_{WG,\,avg} - T_{LNG,\,j} \tag{4.3}$$

The inside of the tube is marked with the subscript "i", the outside with "o". The heat transferring area of a section is different between the inside of the tube $A_{i,\,j}$, and the outside area $A_{o,\,j}$, due to the tube wall thickness and the potential ice formation. Thus, it is necessary to use both the areas and include them in the overall heat transfer coefficient U_j found in (Incropera, Dewitt et al. 2013), resulting in UA_j as presented below. The expression also contains the two terms reflecting the heat transfer through the copper tube and the possible water-glycol ice, including the thermal conductivity k.

$$\mathrm{UA}_j = \frac{1}{\dfrac{1}{h_{i,\,j} A_{i,\,j}} + \dfrac{\ln\left(\dfrac{d_{tube,\,o}}{d_{tube,\,i}}\right)}{2\pi\ l_j\ k_{copper}} + \dfrac{\ln\left(\dfrac{d_{tube,\,o,\,eff}}{d_{tube,\,o}}\right)}{2\pi\ l_j\ k_{WG,\,ice}} + \dfrac{1}{h_{o,\,j} A_{o,\,j}}} \tag{4.4}$$

where the inner and outer areas are equated as

$$A_{i,\,j} = \pi\ d_{tube,\,i}\ l_j \tag{4.5}$$

$$A_{o,\,j} = \pi\ d_{\mathrm{tube,\,o,\,eff}}\ l_j \tag{4.6}$$

The effective outer tube diameter is found by including ice formations, if any, on the tubes.

$$d_{tube,\,o,\,eff} = d_{tube,\,i} + 2\,(t_{tube} + t_{ice}) \tag{4.7}$$

The equations and correlations used when calculating the inner and outer heat transfer coefficients and the pressure development through the entire PBU, are presented in the following sub-chapters.

4.2 Vaporizer design

The general principles for design and functionality of the Vaporizer, referring both to the PBU and the PVU, are described in Chapter 2.3. Below, more detailed parameters are discussed in order to build a functional Vaporizer unit. From Figure 4, it is evident that the product evaporator, the PVU, is just an enlarged version of the PBU. Thus, the model is built according to the PBU dimensions, and can easily be modified when applied on the PVU. The main simulations are performed with respect to the PBU capability and not that for the PVU. All PBU design parameters are extracted from available ship drawings from (Cryo AB - KV Bergen 2009) and presented in Table 11. The parameter values given in Table 11 are called the "reference design" of the PBU. The document provided values for some parameters, but the majority of the values had to be found by measuring the different lengths. Unfortunately, this leaves room for errors and misjudgments. The largest uncertainties concern the diameter of the tube, the diameter of the coil and the number of coils. Regarding the last, it is difficult to see whether there are 10 stand-alone coils with each nine turns or if there are 20 coils, where two and two are twinned together, each with 4.5 turns. The vertical height of the coils is equal for both designs. The last design will result in a lower pressure drop through the coils, but increase the total pipe surface inside the PBU and thus result in higher total heat transfer for a larger mass flow rate $\dot{m}_{PBU}$. For the simulations conducted for this master thesis, the stand-alone design has been used for the coil arrangement, while the twinned coils design is discussed in a separate chapter.

Parameter	Value	Unit	Description
N	9	[-]	Number of turns per coil (stand-alone design)
n	10	[-]	Number of coils in PBU
$d_{PBU,\,o}$	1.22	[m]	Outer diameter of PBU shell
$d_{PBU,\,i}$	0.76	[m]	Inner diameter of PBU shell
$d_{tube,\,i}$	0.03	[m]	Inner diameter of tubes in PBU
t_{tube}	0.001	[m]	Wall thickness of PBU tubes
spacing	0.01	[m]	Clearance between coil and the PBU shell, both to inner wall and outer wall
z_{BE}	0.90	[m]	Vertical height of entire PBU
z_{Bb}	0.20	[m]	Vertical height of lower straight section
z_{coil}	0.45	[m]	Vertical height of coils
z_{eE}	0.25	[m]	Vertical height of upper straight section
$d_{ring,\,lower}$	0.96	[m]	Diameter of lower LNG distribution ring
$d_{ring,\,lower,\,tube,\,i}$	0.06	[m]	Inner tube diameter of lower NG distribution ring
$l_{ring,\,lower}$	0.75	[m]	Average tube length for LNG in lower ring
$z_{ring,\,lower}$	0	[m]	Vertical height of lower LNG distribution ring
$d_{ring,\,upper}$	0.96	[m]	Diameter of upper NG collection ring
$d_{ring,\,upper,\,tube,\,i}$	0.06	[m]	Inner tube diameter of upper NG collection ring
$l_{ring,\,upper}$	0.75	[m]	Average tube length for NG in upper ring
$z_{ring,\,upper}$	0	[m]	Vertical height of upper NG collection ring
$\dot{V}_{WG}$	72.44	m^3/h	Water-glycol mixture flow rate
$T_{WG,\,avg}$	306 K	K	Average temperature of the water-glycol mixture through the PBU
t_{ice}	0	m	Thickness of ice layer on tubes inside PBU

Table 11 - Parameter description of the PBU design on KV Bergen, named "reference design"

In the following sub-chapters, the principles of the simulation models for LNG evaporation, NG condensation and pressure development are presented.

4.3 Inner heat transfer coefficient

The first paragraph of the equation for possible heat transfer from the water-glycol mixture to the LNG (Equation 4.1), is the inner heat transfer coefficient h_i, combined with the inner surface of the tubes, A_i. The capability of the LNG to receive heat from the tube wall is the key. A number of different parameters are determining these values: the tank conditions with filling ratio, tank pressure for a predefined LNG bulk composition and temperature, along with the PBU geometries such as $d_{tube,i}$ and coil height.

The inner heat transfer coefficient is calculated for all tube geometries by the Nusselt number and the thermal conductivity of the fluid. This calculation is performed for each of the small iterative spatial steps through the pipes, denoted "j" as explained in Chapter 4.1.

$$h_{i,\,\mathrm{j}} = \frac{k_j}{d_{tube,\,\mathrm{i}}} Nu_j \tag{4.8}$$

The thermal conductivity coefficient k_j is found by REFPROP for a given composition, pressure and temperature of the fluid. The Nusselt number for the different LNG/NG flow conditions and tube geometry are found through different correlations which are derived for the large temperature difference and the corresponding periodic large heat load. The different correlations used for finding h_i are specified for either liquid, two-phase or pure vapor conditions, for coiled or straight tubes, for laminar, transitional or turbulent flows and for nucleate boiling. These correlations are presented in the subsequent sub-chapters for liquid, two-phase and vapor flows, respectively.

In all the following expressions the Prandtl number and density are calculated by REFPROP, while the Reynolds number is expressed as:

$$\mathrm{Re}_j = \frac{\rho_j \, V_j \, \mathrm{d}_{tube,\,\mathrm{i}}}{\mu_{\mathrm{j}}} = \frac{\left(\frac{\dot{m}_{PBU}}{n}\right)}{\frac{\pi}{4} \, d_{tube,\,\mathrm{i}} \, \mu_{\mathrm{j}}} \tag{4.9}$$

where n, indicating the number of tubes which $\dot{m}_{PBU}$ is divided on, is 1 for the lower distribution ring.

4.3.1 Liquid flow

For the lower distribution ring and the lower straight section of the tubes, the following Nusselt number correlations have been found in (Incropera, Dewitt et al. 2013) and confirmed by (Whalley 1976). If the radius of the distribution ring is large, the small spatial steps can be assumed straight when handling a liquid flow. For a fully developed laminar flow with constant heat load, the Nusselt number can be expressed as:

$$Nu_j = 3.66 \quad ; \quad \mathrm{Re}_j < 3000 \tag{4.10}$$

and the correlation for transient and turbulent flows in smooth tubes is:

$$Nu_j = \frac{\frac{f_j}{8}\,(\mathrm{Re}_j - 1000)\;\mathrm{Pr}_j}{1 + 12.7\sqrt{\frac{f_j}{8}}\,(\mathrm{Pr}_j^{2/3} - 1)} \qquad ;\quad \mathrm{Re}_j > 3000 \tag{4.11}$$

where the Nusselt number is given as a function of the turbulent friction factor. Haaland's equation was, between several other explicit expressions, chosen as the main equation for the friction factor used in this work.

$$f_j = \frac{1}{-1.8\log_{10}\left[\left(\frac{e_{tube}/d_{tube,\,i}}{3.7}\right)^{1.11} + \left(\frac{6.9}{\mathrm{Re}_j}\right)^2\right]} \tag{4.12}$$

If the flow reaches the coils as pure liquid, the Nusselt number for laminar, transient and turbulent flows are expressed by correlations from the work of (Fernández-Seara 2013) on submerged helically coil heat exchangers.

$$Nu_{\mathrm{laminar,\,j}} = 3.65 + 0.08\left[1 + 0.8\left(\frac{d_{tube,\,i}}{d_{coil}}\right)^{0.9}\right]\mathrm{Re}_j^m\;\mathrm{Pr}_j^{1/3} \qquad ;\; \mathrm{Re}_j \le \mathrm{Re}_{critical} \tag{4.13}$$

$$Nu_{turbulent,\,\mathrm{j}} = \frac{\frac{f_j}{8}\;\mathrm{Re}_j\,\mathrm{Pr}_j}{1 + 12.7\sqrt{\frac{f_j}{8}}\left(\mathrm{Pr}_j^{2/3} - 1\right)}\left(\frac{\mathrm{Pr}_j}{\mathrm{Pr}_{j,\,wall}}\right)^{0.14} \qquad ;\quad \mathrm{Re}_j \ge 22\;000 \tag{4.14}$$

For transient flows ($\mathrm{Re}_{critical} < \mathrm{Re}_j < 22\;000$), the Nusselt number is determined from both the linear and the turbulent equations.

$$Nu_{transient,\,\mathrm{j}} = C\;\;Nu\,\big|_{\mathrm{Re}_j\,=\,\mathrm{Re}_{critical}} + \left(1 - C\right)\;\;Nu\,\big|_{\mathrm{Re}_j\,=\,22\;000} \tag{4.15}$$

In the above presented correlations, the following sub-equations are used:
critical Reynolds number:

$$\mathrm{Re}_{crit} = 2300 \left[1 + 8.6 \left(\frac{d_{tube,\,i}}{d_{coil}} \right)^{0.45} \right] \tag{4.16}$$

factor for determining the degree of transient flow in coils:

$$C = \frac{22\,000 - \mathrm{Re}_j}{22\,000 - \mathrm{Re}_{critical}} \tag{4.17}$$

exponent for the Reynolds number in the laminar correlation:

$$m = 0.5 + 0.2903 \left(\frac{d_{tube,\,i}}{d_{coil}} \right)^{0.194} \tag{4.18}$$

the friction factor in the tubes is for turbulent flow condition:

$$f_j = \left[\frac{0.3164}{\mathrm{Re}_j^{0.25}} + 0.03 \left(\frac{d_{tube,\,i}}{d_{coil}} \right)^{0.5} \right] \tag{4.19}$$

while for both laminar and transient flows conditions, the friction factor is equated as below:

$$f_j = \frac{64}{\mathrm{Re}_j} \left[1 + 0.015\, \mathrm{Re}_j^{0.75} \left(\frac{d_{tube,\,\mathrm{i}}}{d_{coil}} \right)^{0.4} \right] \quad ; \quad De_j \geq 11.6 \tag{4.20}$$

All relevant flow conditions have a Dean number greater than 11.6. The Dean number connects the Reynolds number to the ratio between the tube diameter and the curvature of the coil, expressed as:

$$\mathrm{De}_j = \mathrm{Re}_j \left(\frac{d_{tube,\,\mathrm{i}}}{d_{coil}} \right)^{0.5} \tag{4.21}$$

4.3.2 Two phase flow

A liquid sub-cooled compared to the pressure, can start boiling along the walls, when exposed to the large heat loads at the walls. In this model the principle of nucleate boiling is introduced at the starting locations of bubble formations along the tube walls at sufficiently large heat loads. The equations for nucleate boiling presented in (Incropera, Dewitt et al. 2013), where the principles for the correlations are confirmed by the works of (Næss 1990) and (Whalley 1984), can in a modified version be expressed as the Nusselt number:

$$Nu_{nucleate\ boiling,\,j} = h_{tp,\,j}\ \frac{\frac{f_j}{8}\left(\mathrm{Re}_j - 1000\right)\ \mathrm{Pr}_j}{1 + 12.7\sqrt{\frac{f_j}{8}}\ \left(\mathrm{Pr}_j^{2/3} - 1\right)} \tag{4.22}$$

where $h_{tp,\,j}$ is an adjustment factor for the intensity of the heat load $q''_{s,j}$ and the local vapor quality x_j, equated as:

$$h_{tp,\,j} = 0.6683\left[\left(\frac{\rho_{liquid,\,j}}{\rho_{vapor,\,j}}\right)^{0.1} x_j^{0.16}\left(1 - x_j\right)^{0.64} + 1058\left(\frac{q''_{s,j}}{G_{PBU,\,j}\ h_{fg,\,j}}\right)^{0.7}\left(1 - x_j\right)^{0.8}\right] \tag{4.23}$$

If $h_{tp,\,j}$ is less than 1, $h_{tp,\,j}$ is set to be 1. The correct local heat load $q''_{s,j}$ is found in an iterative procedure, where the entire calculation of the heat transfer for each spatial step is pre-formed multiple times. Found for all relevant calculations, the heat load required three iterations in order to converge.

The latent heat of evaporation is denoted $h_{fg,\,j}$ and calculated along with the densities and vapor fraction by REFPROP. The mass flow flux $G_{PBU,\,j}$ is expressed as the $\dot{m}_{PBU}$ divided on the cross sectional tube area:

$$G_{PBU,\,j} = \frac{\left(\frac{\dot{m}_{PBU}}{n}\right)}{A_{\text{cross-sectional, j}}} = \frac{\left(\frac{\dot{m}_{PBU}}{n}\right)}{\frac{\pi}{4}\ d_{tube,\,i}^2} \tag{4.24}$$

4.3.3 Vapor flow

When the LNG is completely evaporated into NG, the Nusselt number can be expressed with one equation independent of whether the heat transfer is taking place in the coil, in the upper straight section or in the upper collection ring (Whalley 1976). The Nusselt correlation for a gas being heated, presented as expressed in (Incropera, Dewitt et al. 2013):

$$Nu_j = 0.0243\ \mathrm{Re}_j^{0.8}\ \mathrm{Pr}_j^{0.4} \tag{4.25}$$

This correlation is valid for flows with Reynolds number > 10 000 and Prandtl number > 0.6 (Incropera, Dewitt et al. 2013). Calculations show that a fully evaporated flow satisfies these two requirements for all relevant flow conditions as temperature, pressure and mass flow rate, independent of location in the PBU.

4.4 Outer heat transfer coefficient

The outer heat transfer coefficient (h_o) of the PBU depends greatly on the design of the tube and the arrangement of the coil inside the PBU shell, as well as the water-glycol mixture flow rate. Since the design of the PBU had to be extracted from the drawings from KV Bergen as discussed in Chapter 4.2, only the methodology and correlations applied to calculating the outer heat transfer coefficient are presented in this section. Due to the close connection between the h_o, and the outer tube surface (A_o) in the overall heat transfer coefficient UA, as presented in Chapter 4.1, A_o is included in this sub-chapter. The evaluation of the influence of different PBU designs on both h_o and A_o are discussed in Chapter 5. The main focus of this section is the coiled part of the PBU, since it constitutes the larger part of the total tube length inside the PBU.

Similar to the inner heat transfer coefficient, h_o is calculated with an equation including both the Nusselt number and the thermal conductivity of the fluid, here the water-glycol mixture. The difference reflects not only in the Nusselt correlations, but also the geometry. Instead of operating with a flow in a circular tube, a hydraulic diameter for the flow has to be calculated for the cross sectional area and the tube walls inside the PBU. In the equation below, the subscript “WG“ indicates the water-glycol mixture, and “j“ gives the specific tube section.

$$h_{o,\,\mathrm{j}} = \frac{k_{WG}}{d_{hydraulic,\,\mathrm{j}}}\ \mathrm{Nu}_{WG,\,j} \tag{4.26}$$

The correlations used for the Nusselt number on the warm side of the heat exchanger for the different sections and geometries are presented in the rest of this sub-chapter.

In the coiled section, the water-glycol flows cross-directionally of the orientation of the tubes. Since the tubes in the coils inclines vertically very little, they can be simplified to be horizontal, while the water-glycol flows in a vertical direction. With coils consisting of several turns, a Nusselt correlation designed for rows of tubes in cross flow can be utilized (Incropera, Dewitt et al. 2013). The correlation is valid for Reynolds numbers between 10^3 and $2 \cdot 10^6$ and for Prandtl numbers between 0.7 and 500, and equated as:

$$Nu_{WG} = C_2 \; \mathrm{C}_1 \; \mathrm{Re}_{WG}^{\mathrm{m}} \; \mathrm{Pr}_{WG}^{0.36} \tag{4.27}$$

where both C_1 and m are determined by if the tubes, or here the turns of the coil, are aligned or staggered and by the Reynolds number. For the relevant flow rate range, the parameters have the values $C_1 = 0.27$ and $m = 0.63$. C_2 is a correction factor for the number of tubes in a row applicable if the total number is less than 20. In a case with nine turns, $C_2 \approx 0.965$.

For the straight sections the flows are counter-current. Using a hydraulic diameter for cross-sectional flow area, the shell annulus and the straight pipes may be viewed upon as a double pipe heat exchanger (Kern 1950), with the two Nusselt number correlations below:

$$Nu_{WG} = 1.86 \left[\mathrm{Re}_{WG} \, \mathrm{Pr}_{WG} \frac{d_{hydraulic}}{z_{\mathrm{section}}} \right]^{1/3} \left(\frac{\mu_{WG}}{\mu_{WG,\,\mathrm{wall}}} \right)^{0.14} \quad ; \; \mathrm{Re}_{WG} \leq 2100 \tag{4.28}$$

$$Nu_{WG} = 0.027 \; \mathrm{Re}_{WG}^{0.8} \; \mathrm{Pr}_{WG}^{1/3} \left(\frac{\mu_{WG}}{\mu_{WG,\,\mathrm{wall}}} \right)^{0.14} \quad ; \; \mathrm{Re}_{WG} \geq 2100 \tag{4.29}$$

For low Reynolds numbers, the Nusselt number is correlated with the ratio between the hydraulic diameter and the vertical height of the section. z_{section} differs between 0.20 m for the lower straight section and 0.25 m for the upper straight section (Table 11).

The warm fluid is in cross-flow with the lower and upper rings. From (Kern 1950) two correlations for single tubes in cross-flow can be used depending on whether the flow is turbulent or not:

$$Nu_{WG} = 0.6 \; \mathrm{Re}_{WG}^{0.5} \; \mathrm{Pr}_{WG}^{1/3} \quad ; \; \mathrm{Re}_{WG} \leq 10\,000 \tag{4.30}$$

$$Nu_{WG} = 0.36 \; \mathrm{Re}_{WG}^{0.55} \; \mathrm{Pr}_{WG}^{1/3} \left(\frac{\mu_{WG}}{\mu_{WG,\,\mathrm{wall}}} \right)^{0.14} \quad ; \; \mathrm{Re}_{WG} > 10\,000 \tag{4.31}$$

For both the straight sections and the two rings, the tube wall temperature is simplified and assumed to be at the freezing point of the water-glycol mixture for all NG temperatures below $T_{WG,\,freezing}$. This is explained by the large temperature difference between the warm and cold sides. In Chapter 2.2.1 $T_{WG,\,freezing}$ was found to be -33.97 °C (239.18 K). For higher NG temperatures, the wall temperature is set equal the NG temperature.

The Reynolds number is calculated by the hydraulic diameter and the mass flow flux of the water-glycol mixture:

$$\mathrm{Re}_{WG} = \frac{G_{WG}\ \mathrm{d}_{hydraulic}}{\mu_{WG}} \tag{4.32}$$

$$G_{WG} = \frac{\dot{Q}_{WG}\ \rho_{WG}}{A_{\text{cross-sectional}}} \tag{4.33}$$

$$d_{hydraulic} = \frac{4\,A_{WG,\,flow}}{\text{wetted perimeter of tubes}} \tag{4.34}$$

where A_{flow} is the available cross-sectional area for the water-glycol flow. For the straight section $A_{flow} = A_{cross\text{-}sectional}$. As the PBU may be assumed completely floated with the water-glycol, the whole surface of the tubes has to be included in the calculations of $d_{hydraulic}$ for the coils and the rings. Thus, in order to include the entire surface around the coiled tubes and the rings, a volumetric approach has been used to calculate $d_{hydraulic}$ for these sections.

The density, viscosity and Prandtl number for the water-glycol mixture are all calculated by the procedure presented in (M. Conde Engineering 2011) and (Code Consultants Inc 2010), with a 50 – 50 % concentration of water and ethylene glycol at $T_{WG,\,avg}$.

4.5 Pressure balance through the PBU circuit

The amount of LNG evaporated in the PBU is determined by the balance between the heat added in the heat exchanger and the drop in pressure throughout the entire PBU cycle, as discussed in Chapter 2. This sub-chapter is presenting the principles behind the different contributions to the pressure change throughout the entire thermosyphon cycle. The equations in the following two sub-sections are mainly taken from the text book ”Fluid Mechanics: Fundamentals and Applications” by (Cengel and Cimbala 2006). For the pressure losses in the two-phase flow, the textbook “Process Heat Transfer: Principles and Applications” by (Serth 2007) was primarily used.

The pressure calculations consists of the same three sections as presented in Figure 5 in Chapter 2.2.1. From the liquid surface inside the fuel tank to the inlet of the PBU is called

section AB, through the PBU is called section PBU, and the section from the PBU exit and back into the fuel tank is named section EA. Sections AB and EA are deemed to be one section for the evaluations: all the different contributions for the pressure development are added together. The reason is all the uncertainties regarding the pipe geometry. The PBU section is evaluated in more detail, as described in the introduction of Chapter 4, applying small spatial steps of 2 cm. For simplicity, the term 'section' is also used for the spatial steps in the PBU for the equations and their comments in the following two sub-chapter.

The values for the condition of the LNG or NG used in the calculations are taken from the inlet of a section. This simplification primarily affects the calculations of section AB and EA, and does not significantly reduce the accuracy of the pressure development for all the small sections in the PBU, where the values of the parameters do not materially change through each section.

4.5.1 General equations for single phase flow

The change in pressure, either for one small spatial step of the PBU or the entire pipe between the tank and the PBU, originates in three parts in this model. They are the change in static pressure ΔP_{static}, the friction induced pressure loss in the tubes $\Delta P_{friction}$, and the pressure losses due to valves, bends, tees and entry sections, ΔP_{minor}. The parameters for a single section and the corresponding pressure change are de-noted with "j", similar to the heat transfer procedure. The pressure change through a section is for single phase flow equated as:

$$\Delta P_j = \Delta P_{\text{static},j} + \Delta P_{\text{friction},j} + \Delta P_{\text{minor},\ j} \qquad (4.35)$$

Table 12 gives the geometry of the pipes connecting the PBU to the fuel tank. All the parameters required for the calculations inside the PBU are listed in Table 11.

Parameter	Value [m]	Description
e_{tube}	0.000004	Pipe roughness
$d_{tube,\ AB}$	0.028	Inner pipe diameter for AB
l_{AB}	3.00	Pipe length for AB
$\Delta z_{tank\text{-}to\text{-}B}$	1.55	Vertical height difference between the inner tank bottom and PBU inlet (B)
$d_{tube,\ EA}$	0.0603	Inner pipe diameter for EA
l_{EA}	5.00	Pipe length for EA
$\Delta z_{E\text{-}to\text{-}tank}$	5.33	Vertical height difference between PBU exit (E) and the inner tank top

Table 12 - Geometry of the pipes connecting the PBU to the fuel tank

The pressure loss in each section is determined by the geometric values and the friction factor, f_j. The mass flow rate is in the straight and coiled parts of the PBU divided equally between all "n" tubes, whereas it is set equal to 1 in the rest of the system.

$$\Delta P_{\text{friction, j}} = f_j \frac{8\, l_j \left(\frac{\dot{m}_{PBU}}{n}\right)^2}{\pi^2\, \rho_j\, d_{tube,\,j}^5} \tag{4.36}$$

The formula for deriving the friction factor f_j is governed by the Reynolds number. If the flow is fully developed and laminar, the Reynolds number is below the critical value:

$$f_j = \frac{64}{\mathrm{Re}_j} \quad ; \quad \mathrm{Re}_j \leq \mathrm{Re}_{critical} \tag{4.37}$$

If the flow is transient or turbulent, Haaland's equation was chosen as described in Chapter 4.3:

$$f_j = \frac{1}{-1.8\log_{10}\left[\left(\frac{e_{tube}/d_{tube,\,j}}{3.7}\right)^{1.11} + \left(\frac{6.9}{\mathrm{Re}_j}\right)^2\right]} \quad ; \quad \mathrm{Re}_j \geq \mathrm{Re}_{critical} \tag{4.38}$$

The Reynolds number is expressed as:

$$\mathrm{Re}_j = \frac{4\left(\frac{\dot{m}_{PBU}}{n}\right)}{\pi\, \mu_j\, d_{tube,\,j}} \tag{4.39}$$

For the coiled section of the PBU, the critical Reynolds number is equated as:

$$\mathrm{Re}_{critical} = 2300\left[1 + 8.6\left(\frac{d_{tube,\,j}}{d_{coil}}\right)^{0.45}\right] \tag{4.40}$$

In the rest of the system, the tubes are assumed to be straight, even if they should have small curvatures. The critical Reynolds number for straight tubes is 2300.

The static pressure change is the “driving force” of the thermosyphon. For the section between the tank and the PBU it contributes positively with increased pressure. Both through the PBU and in the return pipe, it contributes to a pressure reduction. The term can be expressed as:

$$\Delta P_{\text{static, j}} = \rho_j \; g \; \Delta z_j \tag{4.41}$$

where g is the gravitational constant. The vertical height for a spatial step Δz_j in the coiled section is calculated with the help of the ratio between the coil length and vertical height.

$$\Delta z_j = \frac{z_{coil}}{l_{coil}} \; l_j \tag{4.42}$$

For the vertical height of section AB and EA, the values listed in Table 12 needs to be adjusted for the liquid and vapor levels with varying filling ratios.

The term ‘minor losses’ is a collective term for all abnormalities in the pipes, covering bends, valves and the LNG leaving the tank and entering the pipe and the NG entering the tank. In addition, both the forking and the joining tees where the straight tubes are connected to the lower and upper rings in the PBU are included. The pressure drop is equated as:

$$\Delta P_{\text{minor}, j} = \left(\sum_k K_j \right) \frac{8 \left(\frac{\dot{m}_{PBU}}{n_j} \right)^2}{\pi \; \rho_j \; d^4_{tube, \text{j}}} \tag{4.43}$$

where the pressure loss coefficient K, representing the severity of the different minor losses, is summed up for each section. Table 13 gives the K-values used in this thesis, all found in (Cengel and Cimbala 2006).

Parameter	Comment	K-value	Location	Number in section
Pipe inlet	Sharp edged	0.5	AB - between tank and pipe	1
90 ° - bend	Smooth, threaded	0.9	AB - pipe EA – pipe PBU - transition between straight and coiled sections	AB : 3 EA : 4 PBU : 2
45 ° - bend	Threaded elbow	0.4	AB - pipe EA - pipe	AB : 1 EA : 1
Globe valve		10	AB - pipe EA - pipe	AB : 1 EA : 1
Pipe outlet	Fully turbu-lent flow	1.05	EA - between pipe and tank	1
Tee	Branch flow, threaded	2	PBU – connection between rings and tubes/coils	2 for each of the n tubes

Table 13 - Pressure loss coefficient for minor losses - (Cengel and Cimbala 2006)

4.5.2 Two-phase pressure drop

This section reviews the pressure change during the evaporation phase. The change in pressure encompasses the static pressure, the two-phase pressure gradient and the acceleration of the fluid caused by the change in density from liquid to vapor. The equations used in this section are, as already referred to, based on (Serth 2007). Instead of Equation 4.35, the summation of the pressure change contributions is given by:

$$\Delta P_j = \Delta P_{\text{static},\,j} + \Delta P_{\text{friction},\,j} + \Delta P_{\text{acceleration},\,j} \tag{4.44}$$

The static pressure change is derived with an averaged two-phase density of the fluid in the section $\rho_{avg,j}$, calculated with the help of the void fraction, ε_{void} and the liquid and vapor densities:

$$\Delta P_{\text{static},\,j} = \rho_{avg,\,j}\ \mathrm{g}\ \Delta z_j \tag{4.45}$$

$$\rho_{avg,\,j} = \varepsilon_{void}\ \rho_{vap,\,j}\ +\ (1-\varepsilon_{void})\ \rho_{liq,\,j} \tag{4.46}$$

The void fraction describes the ratio between the parts of the cross sectional flow area that is used for the vapor compared to that for the the liquid. x_j is the vapor mass fraction.

$$\varepsilon_{void} = \frac{x_j}{x_j + SR\ \left(1-x_j\right)\ \left(\dfrac{\rho_{vap,\,j}}{\rho_{liq,\,j}}\right)} \tag{4.47}$$

The void fraction is found through the slip ratio (SR) for which the correct equation is determined by the Lockhart-Martinelli parameter (X_{tt}). For X_{tt} larger than 1:

$$SR = \left(\frac{\rho_{liq,\,j}}{\rho_{\mathrm{hom}ogenous,\,j}} \right)^{0.5} \tag{4.48}$$

and for X_{tt} lower than 1:

$$SR = \left(\frac{\rho_{liq,\,j}}{\rho_{vap,\,j}} \right)^{0.25} \tag{4.49}$$

The Lockhart-Martinelli parameter is equated as:

$$X_{tt} = \left[\frac{1-x_j}{x_j} \right]^{0.9} \left(\frac{\rho_{vap,\,j}}{\rho_{liq,\,j}} \right)^{0.5} \left(\frac{\mu_{vap,\,j}}{\mu_{liq,\,j}} \right)^{0.1} \tag{4.50}$$

Finally, the homogenous two-phase density is calculated for the use in one of the slip ratio equations:

$$\rho_{\mathrm{homogenous},\,j} = \frac{1}{\dfrac{x_j}{\rho_{vap,\,j}} + \dfrac{1-x_j}{\rho_{liq,\,j}}} \tag{4.51}$$

After calculating the average two-phase density in order to find ΔP_{static}, the two-phase pressure gradient $\overline{\varphi}^2_{\mathrm{LO}}$, needs to be calculated in order to account for the two-phase turbulence in the friction induced pressure loss. Modified from (Serth 2007), the following equation for the friction related losses can be present:

$$\Delta P_{friction} = \bar{\varphi}^2_{LO,\,j} \; f_j \; \frac{8\, l_j \left(\dfrac{\dot{\mathrm{m}}_{PBU}}{n} \right)^2}{\pi^2 \; \rho_{liq,\,j} \; \mathrm{d}^5_{tube,\,\mathrm{j}}} \tag{4.52}$$

where the friction factor is calculated in the same way as for the single phase. The two-phase pressure gradient can be expressed as:

$$\bar{\varphi}_{LO,j}^2 = \frac{Y_j^2}{9} + \left[1 + \frac{2}{3}(Y_j^2 - 1)\right]\left(\frac{2}{3}\right)^{1/3} \tag{4.53}$$

where Y is a coefficient relating the density and viscosity of the two phases.

$$Y_j = \left(\frac{\rho_{liq,j}}{\rho_{vap,j}}\right)^{0.5} \left(\frac{\mu_{vap,j}}{\mu_{liq,j}}\right)^{0.2585/2} \tag{4.54}$$

The evaporation accelerates the fluid. This is due to the immense reduction in density between the LNG and the NG, resulting in the pressure loss expressed below:

$$\Delta P_{\text{acceleration},j} = \Delta\gamma_j \frac{16\left(\frac{\dot{m}_{PBU}}{n}\right)^2}{\pi^2 \rho_{liq,j} d_{tube,j}^4} \tag{4.55}$$

$\Delta\gamma_j$ describes the amount of evaporation in each section, including both the change in the void fraction and in the densities. The values for the end of a step ("j+1") are assessed through an iterative procedure, similar to that for the heat load $q''_{s,j}$ in Chapter 4.3.2.

$$\Delta\gamma_j = \gamma_{j+1} - \gamma_j = \left(\frac{(1-\chi_{j+1})^2}{1-\varepsilon_{void,j+1}} + \frac{\rho_{liq,j+1}\chi_{j+1}^2}{\rho_{vap,j+1}\varepsilon_{void,j+1}}\right) - \left(\frac{(1-\chi_j)^2}{1-\varepsilon_{void,j}} + \frac{\rho_{liq,j}\chi_j^2}{\rho_{vap,j}\varepsilon_{void,j}}\right) \tag{4.56}$$

For the simulations where the PBU does not completely evaporate the LNG, the above presented equations for two-phase flow are used when calculating the pressure change through the return pipe from the PBU outlet to the fuel tank.

4.6 Evaporation capacity in PBU

From the correlations and equations presented in the previous sub-chapters, it is evident that the evaporation capacity of the PBU will vary significantly with both the filling ratio of the fuel tank and with P_{tank}. These variations will be found in mass evaporation capacity, in return vapor quality and in return temperature. The design of the PBU and other system configurations will also directly determine the PBU capacity. In this sub-chapter the reference design of the PBU, as presented in Chapter 4.2 is used to assess the evaporation capacity. In later chapters, the capacity for other designs and system configurations will be outlined.

On MF Korsfjord DiRenzo measured an average NG return temperature from the PBU (T_{return}) of 227 K (DiRenzo 2014a), and thus this is used as target temperature (T_{target}) in the models developed for this thesis. The target temperature for the NG return flow is 18 - 24 K above the vapor saturation temperature, which is assumed to be a sufficient superheating of the vapor. It must be underlined that T_{target} is the targeted minimum NG return temperature, and not the desired temperature. Higher T_{return} will increase the tank pressure faster, as described in detail in Chapter 4.7.

The focus for finding the evaporation capacity is determined by the most relevant range of tank conditions according to the de-loading events, presented in Chapter 1.3, and for normal operation ranges for KV Bergen. On KV Bergen, the PBU is activated when the tank pressure falls below 4.5 bar and de-activated when 4.95 bar is reached (DiRenzo 2014a). Thus, the most relevant tank pressure range is between the de-loading pressure of 3.6 bar and the de-activation pressure for the PBU of 4.95 bar. Of interest is also what happens below 3.6 bar, when the NG Engines are shut off and the pressure builds up again. For simplicity, the pressure range used in the simulations is from 3.0 bar to 5.0 bar. Pressure levels above 5.0 bar are not relevant since the PBU then will be de-activated, and pressures down to 2.99 bar is relevant due to data used from (DiRenzo 2014a).

In the de-loading reports, the fuel tank was reported to be newly bunkered. This indicates that the filling ratio was high, in the area of 0.8 -0.9 (Cryomar 2015) indicated that typically a fuel tank is bunkered to a filling ratio of 0.9. For further simulations, a filling ratio of 0.9 is the focal point, but lower filling ratios are used for the purpose of evaluating the pressurization capacity. High filling ratios secures a large “driving force” for the thermosyphon effect, but correspondingly demands a larger heat transfer capacity in the PBU in order to evaporate all of the circulated LNG.

The reference PBU design (Table 11) is used when depicting the effects on $\dot{m}_{PBU}$ and T_{return} with varying P_{tank} and the filling ratio. The simulation results indicate a clear trend in increasing mass flow rate through the PBU, $\dot{m}_{PBU}$, for increasing P_{tank} and filling ratios, as shown in Figure 13.

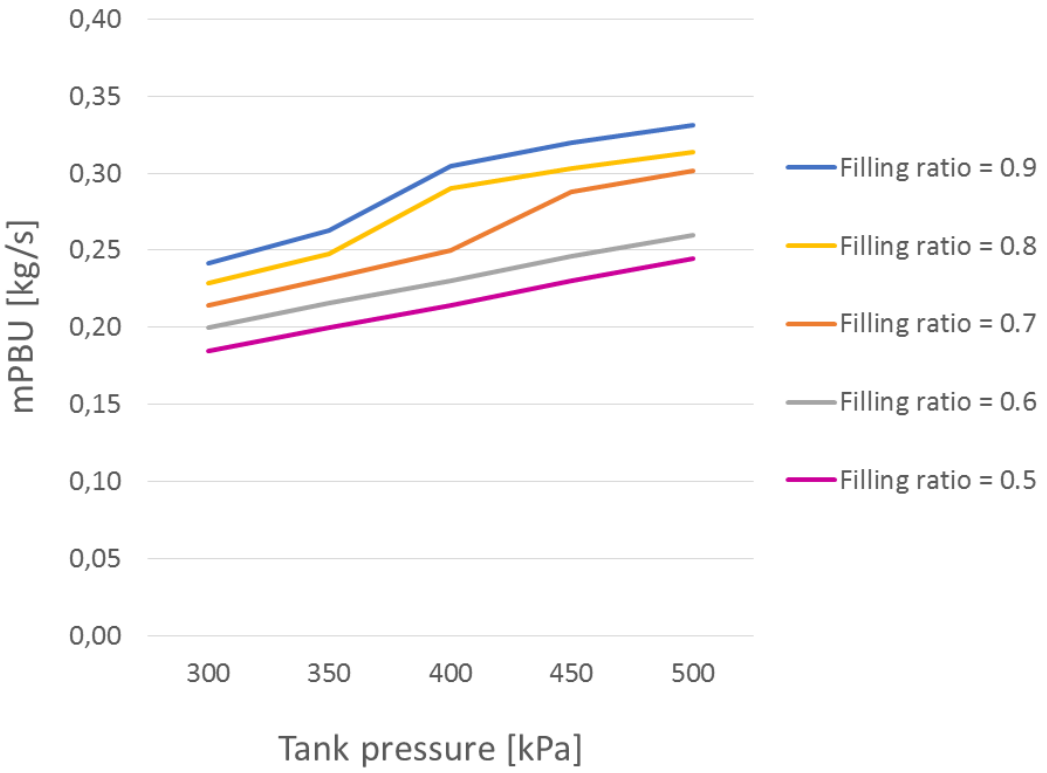

Figure 13 - $\dot{m}_{PBU}$ for the reference design with different filling ratios and varying P_{tank}

The kinks in Figure 13 indicate pressure regions with faster increase in flow rate for a given filling ratio. To understand these, one must observe the conditions at the tank inlet for the returning NG. Studying the return temperatures, they are falling with increasing $\dot{m}_{PBU}$. This is logical since a higher flow rate necessitates more heat to reach the same T_{return}, but the enhanced flow rate only partly manages to increase the heat transfer rate. For the highest filling ratios, T_{return} is for all relevant pressure levels below T_{target} = 227 K, and if returning dry vapor, it only takes place at low tank pressures, as presented in Figure 14.

The kinks are in both figures only present for filling ratios where the return flow experience a phase transition for increasing P_{tank}. The explanation is that the pressure losses through the return pipe is reduced. Lower vapor temperature results in a higher density and correspondingly lower velocity, results in lower friction related pressure losses. The equations handling the pressure drops in the model, gives a lower pressure loss for a colder two-phase flow than for a warm vapor flow. This is not intuitive and may be wrong, but whereas the warm vapor is turbulent, the two-phase flow may for long sections consist of separated phases, with vapor streaming above the liquid, both being cold and laminar. These two factors results in an increased $\dot{m}_{PBU}$, despite that the "driving force" for the thermosyphon is reduced with lower density differences in the system.

The entire area below the red dashed line and above the red dot-dashed line indicates the two-phase region. The band between the green dashed line for T_{target} and the red dashed line for the vapor saturation temperature ($T_{sat,\ vap}$) is assumed to be the necessary security margin for avoiding partly re-condensation of the NG returning back to the fuel tank.

Above T_{target}, the NG is assumed to be sufficiently superheated to avoid any droplets forming and causing enhanced condensation in the tank. As Figure 14 clearly reveals, high filling ratios result in T_{return} far from the targeted temperature. In fact, the filling ratio must be as low as 0.6 in order to achieve $T_{return} \geq T_{target}$ for P_{tank} = 350 kPa.

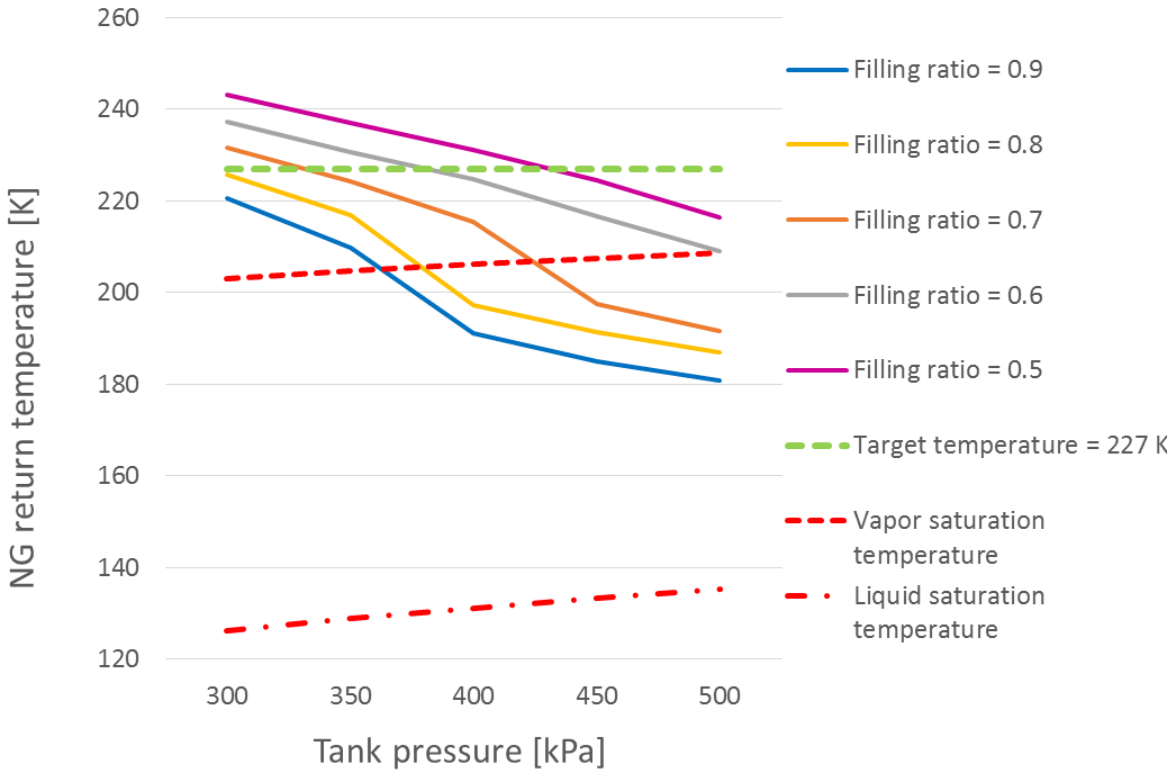

Figure 14 – NG return temperature for reference design with different filling ratios and varying P_{tank}

The lack of heat transfer capability of the PBU compared to the mass flow rate through the system observed in Figure 14, indicates three issues. First, the balancing mass flow rate is too high due to too low pressure drops throughout in the system. The reason can either be that not all 'minor losses' are included or that the equations used are not the optimal choice for this PBU design. Second, the correlations used to calculate the inner and/or outer heat transfer coefficients are underestimating the heat transfer at such large temperature differences. And finally, the design is not correct and optimal for maximizing the heat transfer.

In Chapter 5 the reference design used for the simulations above is modified to achieve $T_{return} > T_{target}$ for filling ratios up to 0.9 and P_{tank} up to 5.0 bar. The modifications are performed for a series of different parameters in order to indicate their effect on the NG return flow.

4.7 Fuel tank pressurization

The pressurization model of the fuel tank is developed with a mass and an internal energy balance for each time step of the pressure development. As discussed in (Hernes 2014), the volumetric change of vapor and liquid sections in the fuel tank is negligible for the time frames of interest. Neither fuel consumption, in-tank condensation nor evaporation through the PBU has a significant impact on the vapor volume during the relative short periods used in this thesis. The vapor volume, and correspondingly the filling ratio, are therefore assumed to be constant for a simulation. Both the increasing density of the vapor due to added mass from the PBU and the fact that the evaporated mass keeps a higher temperature than the vapor in the tank, contributes to increasing the tank pressure. Equally, the condensation reduces the NG density and thus P_{tank}. The above mentioned balance for volume, mass and internal energy for the vapor region can be equated as:

$$V_{vapor}(t+dt) = V_{vapor}(t) \tag{4.57}$$

$$m_{NG,\,\text{tank}}(t+dt) = m_{NG,\text{tank}}(t) + \left[\dot{m}_{PBU}(t) - \dot{m}_{con}(t)\right]dt \tag{4.58}$$

$$U_{NG,\,\text{tank}}(t+dt) = U_{NG,\,\text{tank}}(t) + \left[u_{PBU}(t)\cdot\dot{m}_{PBU}(t) - u_{con}(t)\cdot\dot{m}_{con}(t)\right]\text{dt} \tag{4.59}$$

where “t” indicates a specific time during the pressurization and “dt” is the time step. The left side of the equations noted with “t+dt” represent the situation at the end of a time step, equal to the starting values for the next time step. The time step used in this model is one second.

4.7.1 Idealized pressurization

For ideal pressurization, with $\dot{m}_{con}$ = 0 kg/s, the most rapid pressurization possible is obtained. This pressure development simulation indicates the minimum time and evaporated mass of LNG for a certain rise in pressure. No fuel consumption is accounted for and the vapor volume is assumed constant, as explained above.

Combining this model with the pressurization on MF Korsfjord in the measurement campaign of (DiRenzo 2014a), with details of the fuel tank and LNG system presented in Table 14, the necessary mass of the LNG evaporated for the ideal pressurization of 43.27 m^3 from 299 kPa to 495 kPa, is 71.37 kg. This is achieved in 496 seconds, when the simulated return temperature from the PBU is used for the internal energy calculations. These two numbers are utilized when calculating the condensation rate and thermal conductivity layer thickness between the liquid and the vapor sections, described later in Chapter 4.8.

Parameters	Value
$P_{tank,\ initial}$	299 kPa
$T_{vapor,\ initial}$	202.97 K
$T_{LNG,\ bulk}$	121 K
V_{vapor}	43.27 m^3
filling ratio	0.622
$\dot{m}_{cond}$	vary
$\dot{m}_{PBU}$	varying with P_{tank}
$\dot{V}_{WG}$	72.44 m^3/h

Table 14 - Parameters of LNG tank and the PBU on MF Korsfjord before pressurization from 299 kPa to 495 kPa (DiRenzo 2014a)

The increasing evaporation capacity of the PBU as the P_{tank} increases, are presented in Table 15 together with the NG return temperatures from the PBU. In Table 17 located in the next sub-chapter, details around the ideal pressurization are compared to those of the pressurization including condensation. The mass flow rate through the PBU is significantly lower on MF Korsfjord than those on KV Bergen presented in Figure 13. The reason is that the fuel tank on MF Korsfjord is almost half the size of that on KV Bergen (Table 4, Table 6), resulting in less required evaporation for a given pressure lift.

P_{tank}	$\dot{m}_{PBU}$	T_{return}
kPa	*kg/s*	*K*
300	0.132	266.52
350	0.140	263.47
400	0.149	260.08
450	0.156	257.37
500	0.165	253.94

Table 15 - PBU capacity on MF Korsfjord at a filling ratio of 0.622 and $\dot{V}_{WG}$ = 72.44 m^3/h

4.7.2 Influence of the filling ratio

One must keep in mind that for low filling ratios, the vapor volume is larger than for high filling ratios. A half-full tank needs more evaporated mass per unit pressure increase than an almost full tank. Thus, for a system struggling to keep the pressure above 3.6 bar and avoid de-loading, the pressurization takes much longer time at low filling ratios than for higher filling ratios. Figure 15 gives the amount of time required for an ideal pressurization of MF Korsfjord from 299 kPa to 495 kPa at different filling ratios. It shows that the idealized pressurization time depends strongly on the filling ratio.

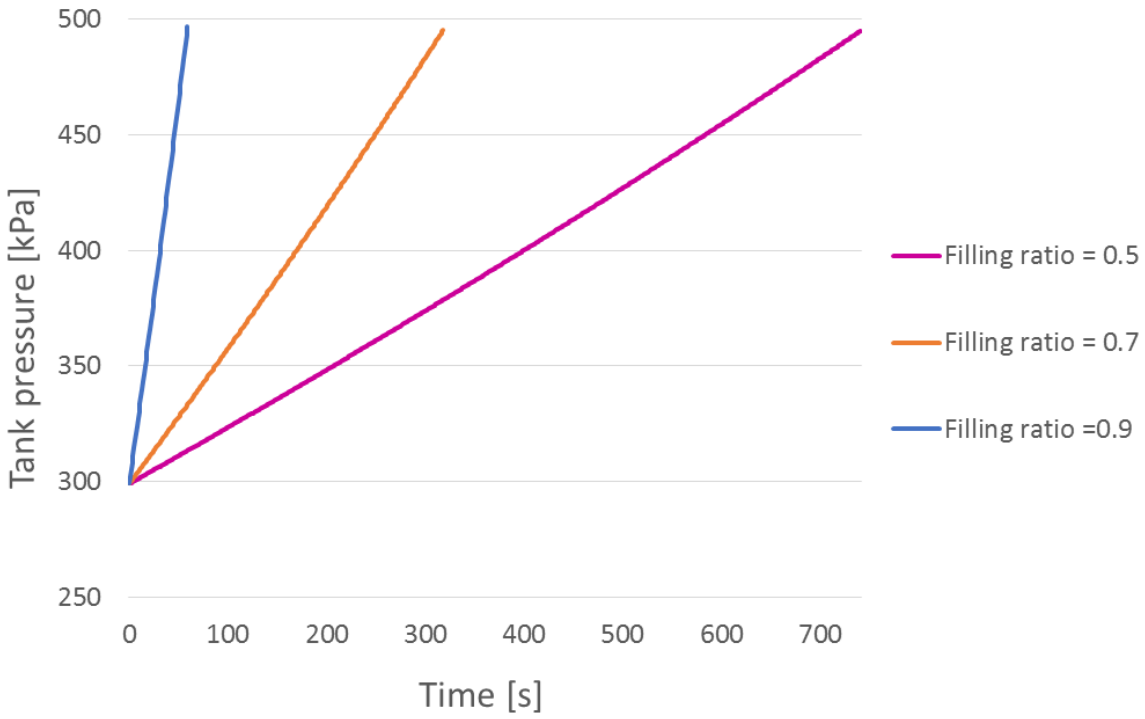

Figure 15 - Ideal pressurization time on MF Korsfjord from 299 to 495 kPa for different filling ratios

In Figure 15, 495kPa is used as target pressure. This is the tank pressure when the flow through the PBU was shut off on both MF Korsfjord and on KV Bergen (DiRenzo 2014a). The pressurization time is more than five-doubled from 59 s to 318 s, for a filling ratio of 0.7 compared to a higher filling ratio of 0.9. This is mainly due to two reasons. First, the vapor volume is much larger for a lower filling ratio, thus more LNG needs to be evaporated to increase the density sufficiently. Secondly, the mass flow through the PBU is smaller for lower filling ratios, due to the lowered driving force of the thermosyphon with smaller difference between the hydrostatic forces through the system. Table 16 gives in addition to the pressurization time, the mass flow rate for the P_{tank} = 500 kPa.

Filling ratio	**Pressurization time**	**$\dot{m}_{PBU}$ (P_{tank} = 500 kPa)**
-	*s*	*kg/s*
0.5	741	0.145
0.7	318	0.175
0.9	59	0.205

Table 16 - Results for ideal pressurization from 299 to 495 kPa, including $\dot{m}_{PBU}$(P_{tank} = 500 kPa) for different filling ratios on MF Korsfjord

4.8 Condensation rate in the fuel tank

The essential factor for keeping P_{tank} above the de-loading pressure is that the PBU can evaporate more mass than what condenses inside the tank. It is therefore crucial to understand the condensation rate for different tank conditions. The only useful measurements available for this purpose are those performed on MF Korsfjord by (DiRenzo 2014a). Other reports with pressurization time have been gathered, but they lack sufficient information about the fuel tank and evaporation system to allow designing the models. The necessary pressurization time when MF Korsfjord was in calm sea, was 18 minutes in order to raise the pressure from 299 kPa to 495 kPa for a vapor volume of 43.27 m^3 (DiRenzo 2014a). Before pressurization on MF Korsfjord, the tank and system conditions were as presented in Table 14.

By coupling the pressurization time needed in an idealized model designed for this thesis and the 18 minutes measured on MF Korsfjord, the re-condensation rate of the evaporated LNG can be found. The re-condensation rate is a simplification connecting the vapor that condenses during the pressurization to the calculated $\dot{m}_{PBU}$, equated as:

$$\text{re-condensation rate} = \frac{\dot{m}_{\text{con, required}}}{\dot{m}_{PBU}} \tag{4.60}$$

The $\dot{m}_{con,required}$ is the condensed mass flow rate required in order for the pressurization to take 18 minutes - as in the measurement conducted on MF Korsfjord. The re-condensation rate states how much NG condenses in a specific situation, and is used to calculate the liquid boundary layer thickness with the help of a modified version of Fourier's law, as described by (Scurlock 2006) and presented below in Equation 4.61.

The evaporation model was modified to MF Korsfjord by primarily reducing the tank diameter to 3.6 m and the height difference between the tank bottom and the inlet at the bottom of the PBU to zero, both according to the ship drawings (Linde Cryo AB 2008). Available information on MF Korsfjord was far from sufficient to establish a precise and independent model of the evaporation capacity. Therefore, the design of the PBU was kept as for KV Bergen, even though the design differs somewhat. The vertical height of the PBU unit was scaled down to 0.74 m to match the size of the PBU on MF Korsfjord (Linde Cryo AB 2008), with a correspondingly down-scaling of the internal vertical sections.

Applying the model with the measured time of 18 minutes, or 1080 seconds, the re-condensation rate is found to be 60.5 %. By keeping this rate constant, the actual $\dot{m}_{con}$ will vary with the $\dot{m}_{PBU}$. Since the pressurization takes approximately twice the time found for the ideal pressurization in Chapter 4.7.1, more warm NG is added to the tank, in total 157.12 kg. Consequently, the higher specific internal energy in the vapor phase results in a higher final temperature. The final vapor temperature increases from 219.9 K to 229.9 K. Thus, the necessary net added mass in vapor phase declines from 71.37 kg for the ideal pressurization to 62.09 kg when including condensation.

Parameter	Idealized pressurization		Real pressurization
Time	496 s		1080 s
$T_{vapor,\ final}$	219.9 K		229.9 K
$m_{PBU,\ tot}$	71.37 kg		157.12 kg
$m_{con,\ tot}$	0 kg		95.04 kg
Re-condensation rate	0 %		60.5 %

Table 17 - Ideal vs real pressurization on MF Korsfjord from 299 kPa to 495 kPa with filling ratio of 0.622 and $\dot{V}_{WG}$ = 72.44 m³/h

The re-condensation rate of 60.5 % is directly linked to the tank conditions under the measurements performed on MF Korsfjord. In order to implement the condensation in the simulations for other tank conditions (varying filling ratios and P_{tank}) as well as for other PBU designs resulting in different $\dot{m}_{PBU}$, the thickness of the thermal conductivity layer must be calculated. As mentioned above, this can be done with a modified version of the Fourier's law (Incropera, Dewitt et al. 2013) inspired by (Scurlock 2006). The result is an expression for the effective thickness of the thermal conductivity layer, where the heat, or energy leaving the vapor section accompanying the condensing mass, is represented by $\dot{Q}_{con}$. The condensation rate is proportional with the area of the liquid-vapor interface, A_{ht}.

$$\chi_{conduction,\ eff} = \frac{k_{conduction}\ A_{ht}\ \left[T_{sat,\ liq}(P_{\text{tank}}) - T_{bulk}\right]}{\dot{Q}_{con}} \tag{4.61}$$

Furthermore, the heat transfer is expressed as the enthalpy change from vapor to saturated liquid for the given mass flow rate.

$$\dot{Q}_{con} = \dot{m}_{con}\ \left(h_{vapor} - h_{sat,\ liq}\right) \tag{4.62}$$

Using these equations, it is possible to determine the thickness of the thermal conductivity layer ($\chi_{conduction}$) for calm conditions ($A_{ht} = A_{calm}$), to be 1.23 mm for the pressurization on MF Korsfjord. Implementing this thickness in the pressurization simulation for calculating $\dot{m}_{con}$, the same results were achieved as when using $\dot{m}_{con} = 0.605\ \dot{m}_{PBU}$.

In order to transfer this knowledge to the system on KV Bergen, some assumptions must be made:

- The LNG bunkered on both ships are similar, both in composition and in T_{bulk}
- The pressure operation range is similar
- The temperature of the vapor phase is similar
- The pressurization is performed in calm sea

With these assumptions, the thickness of the thermal conductivity layer for the fuel tank on KV Bergen in calm sea can be assumed equal to that calculated for MF Korsfjord. Thus, for all further simulations $\chi_{conduction}$ is set to be 1.23 mm.

Since the sea is hardly at such calm conditions as during the described pressurization on MF Korsfjord, an effective thickness of the thermal conductivity layer, $\chi_{conduction,\ eff}$ needs to be used in the simulations. This is to handle both the destruction of the thermal boundary layer and the assumption that the layer gets thinner with the wave-induced increase of the liquid-vapor interface area. These elements are further discussed in the next sub-chapter.

On KV Bergen, where the fuel tank is larger than on MF Korsfjord, higher $\dot{m}_{con}$ is found due to the larger liquid-vapor interface. When the PBU is not operating, the condensation will gradually reduce P_{tank}. The required time for a drop in pressure from 5.0 bar to below the de-loading pressure of 3.6 bar, varies with the filling ratio of the tank. The condensation mass flow rate is determined by the tank pressure and the liquid-vapor interface area, as described by Equation 4.61. For a specific drop in pressure, the amount of vapor required to condense, is coupled to the volume of the vapor section. In Figure 16 the pressure development is illustrated for the fuel tank on KV Bergen in calm sea when the PBU is de-activated.

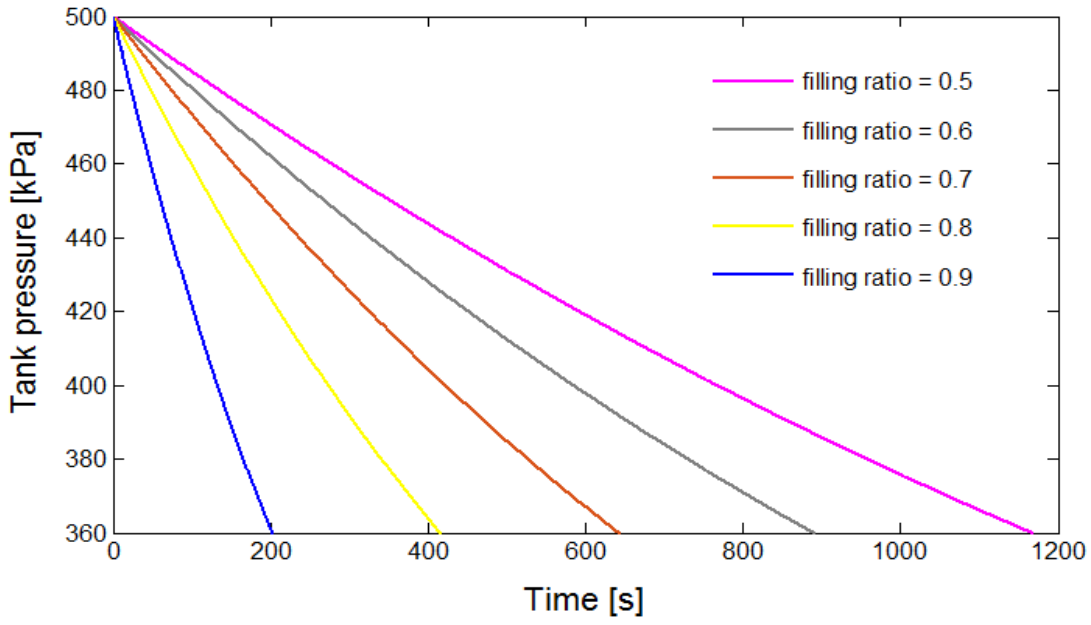

Figure 16 - Time for a drop in pressure from 5.0 bar to 3.6 bar when the PBU is de-activated

As observed, the pressure reduction occurs faster for a small vapor cushion than for a large cushion. At high filling ratios, the required time is more than tripled from 203 seconds to 640 seconds when the filling ratio is reduced from 0.9 to 0.7. The important aspect is the pressure development of for the fuel tank, including both the condensation and the evaporation. The pressure development is in Chapter 7 presented for various tank conditions and system configurations.

4.9 Sloshing and destruction of thermal boundary layer

One of the main objectives of the project work (Hernes 2014) was to address what effects sea-waves are causing on in-tank fluid movements and correspondingly enhanced $\dot{m}_{con}$. Essential for the analysis was the two terms Sloshing factor and Destruction ratio, both describing the conditions of the liquid- vapor interface.

The Sloshing factor (SF) is given as the factor the area of the liquid-vapor interface increases with compared to the calm sea area, due to in-tank motions of the fluid. The heat transferring area A_{ht}, introduced in the previous sub-chapter is thus related to the liquid-vapor interface area for calm sea A_{calm}, with the given expression:

$$A_{ht} = SF\ A_{calm} \tag{4.63}$$

The value of the SF increases from 1, when there is no motion in the fluid, to "infinity" for a complete mixing of vapor and liquid.

$$Sloshing\ factor = SF \quad ; \quad 1 < SF < \infty \tag{4.64}$$

It is analogous to a sinus-curve, where the length of the line increases with a ratio of $\pi/2 \approx 1.57$ compared with the straight line, but the averaged location of the line does not change.

Even though the sloshing factor will differ over time, a simplification assuming constant SF for pressurization is both necessary and acceptable when designing the model. This is explained by the large uncertainties in the re-condensation ratio and the thermal conductivity layer thickness. In practice, the re-condensation ratio will vary with the conditions of the tank: pressure, temperatures, liquid surface, the heat transfer coefficient, the boundary layer thickness and motions of the fluid. These factors are only partly included and compensated for in the pressure development models in this thesis.

When the sloshing results in liquids, either as bulk or droplets, falling over the vapor-liquid interface, parts of this layer are destroyed. The destruction will mainly occur locally and create areas with enhanced heat transfer and thus condensation (Zhang 2005). These spots have been described as "cold spots". Although the conduction layer is destroyed locally, the destruction can on average be described as a reduction in conduction layer thickness, referred to as the destruction ratio. A destruction ratio of 0 implies that the conduction

layer is intact, whereas a destruction ratio of 1 implies a complete elimination of the thermal conduction layer.

$$Destruction\ ratio\ =\ DR\ =\ 1\ -\ \frac{V_{BL,\ remaining}}{V_{\mathrm{BL},\ initial}}\qquad ;\quad 0 < \mathrm{DR} < 1 \tag{4.65}$$

As the heat transferred with condensation rapidly escalates with an introduction of in-tank waves, the model has to be adjusted for the effective thermal layer thickness. For calculation purposes, the initial $\chi_{conduction}$ is adjusted according to the amount of sloshing and presence of the cold spots. Based on four equations connecting the volume and surface of the boundary layer with the sloshing factor and the destruction ratio, the effective thermal conduction thickness can be expressed by the $\chi_{conduction}$, the SF and the DR:

$$V_{BL,\ \mathrm{initial}} = A_{calm}\ \chi_{conduction} \tag{4.66}$$

$$V_{BL,\ \mathrm{remaining}} = A_{ht}\ \chi_{conduction,\ \mathrm{eff}} \tag{4.67}$$

$$V_{BL,\ \mathrm{remaining}} = \left(1-DR\right)\ V_{BL,\ \mathrm{initial}} \tag{4.68}$$

$$A_{ht} = A_{calm}\ SF \tag{4.69}$$

Combined, they can be equated as:

$$\chi_{conduction,\ \mathrm{eff}} = \frac{V_{BL,\ \mathrm{remaining}}}{A_{ht}} = \frac{\left(1-DR\right)\ A_{calm}\ \chi_{conduction}}{A_{calm}\ SF} = \frac{\left(1-DR\right)}{SF}\chi_{conduction} \tag{4.70}$$

The challenge is thus to make adequate assumptions for the amount of sloshing and for the degree of destruction of the thermal layer. It is evident that the DR must be positively correlated with the sloshing factor; the DR increases with more extensive sloshing. The strength of this correlation is likely to depend on the sloshing regime, the vapor and bulk temperatures and the LNG composition. More than an educated guess requires laboratory experiments with LNG under real conditions, and the possibility to enforce different sloshing regimes onto the LNG, similar to the Nitrogen experiment described in the Literature Study conducted by (Ludwig, Dreyer et al. 2013).

The educated guess used for coupling the destruction ratio to the sloshing factor in this master thesis, is:

$$DR = 1 - \frac{1}{SF} \tag{4.71}$$

The destruction ratio is 0.5 for a sloshing factor of 2, and increasing towards 1 for higher SF. For SF = 2, the effective thickness of the thermal boundary layer would thus only be 25 % of the initial $\chi_{conduction}$. In addition would the liquid-vapor interface be twice as large as A_{calm}, multiplying $\dot{m}_{con}$ with a total factor of 8 compared to calm sea conditions, without any increase in evaporation capacity. The condensation rate is thereby related to the sloshing factor to the third power, and can by modification of the equations presented in Chapter 4.8 and in this chapter, be expressed as:

$$\dot{m}_{con} = \frac{k_{conduction} \left[T_{sat,\,liq}(P_{\text{tank}}) - T_{bulk} \right]}{\left(h_{vapor} - h_{sat,\,liq} \right)} \frac{A_{calm}}{\chi_{conduction}} SF^3 \tag{4.72}$$

5 Sensitivity analysis of the PBU design and system configurations

As described in Chapter 4, the heat transfer capability does not only depend on the tank conditions in terms of filling ratio and pressure level, but also on the design of the PBU itself. As described in Chapter 4.6, the PBU geometry and system configuration labeled the 'reference design' (Table 11) is not capable of delivering sufficient heat for securing a complete evaporation and the required superheating for high filling ratios at relevant tank pressure levels for the system on KV Bergen.

The objective of this chapter is to evaluate different geometries of the PBU and system configurations in order to establish a Vaporizer system design that is capable of delivering dry vapor above a desired T_{target}, returning to the tank. In this thesis, a measured return temperature in (DiRenzo 2014a) is used as the desired return temperature, fixing T_{target} = -46.15 °C (227 K).

The analysis of the parameters listed in Table 18 reveal the sensitivity regarding the effects the parameters have on the pressure development and the heat transfer rates, and thus the necessary changes in order to obtain $T_{return} > T_{target}$.

Parameter	Unit	Description
$d_{tube,\ i}$	m	Inner tube diameter
spacing	m	Space between coil and PBU shell
z_{coil}	m	Vertical height of coiled section
n & N	-	Coil arrangement, number of coils and turns in each coil
$\dot{V}_{WG}$	m^3/h	Water-glycol mixture flow rate
$T_{WG,\ avg}$	K	Average temperature of the water-glycol mixture through the PBU
T_{return}	K	Implementing a thermal PID-controller, ensuring $T_{return} > T_{target}$
t_{ice}	m	Ice thickness

Table 18 – List of parameter: variations of the design and operational conditions of the PBU

The criteria for choosing these parameters are both the difficulties to extract their values from the drawings of KV Bergen (Cryo AB 2010), and the possibility for some adjustments of the system without undertaking extensive retrofitting of the LNG fuel system.

In the discussions on heat transfer capacity and pressure drop, in short the thermosyphon balance, all parameters that are not explicitly stated to differ from the reference system design, are equal to the values given in Table 11. In Chapter 5.1, the geometry of the PBU is evaluated, while the system configurations are discussed in Chapter 5.2.

5.1 PBU design variations

The objective of this sub-chapter is to explain how parameters for the PBU geometry influence both the heat transfer capability of the PBU and the pressure drop through the entire circuit: both affecting the $\dot{m}_{PBU}$, the return temperature and vapor quality.

5.1.1 Inner tube diameter

The impact of changing the inner tube diameter is discussed in this sub-chapter, whereas the quantification of the effects on $\dot{m}_{PBU}$ and T_{return}, when varying $d_{tube,\,i,}$ are given in the tables in Chapter 5.1.2, together with the spacing between the coil and the PBU shell walls.

The inner tube diameter is of large importance for balancing the thermosyphon effect. In short, for a fixed mass flow rate, a larger tube diameter will increase h_o and the heat transferring tube surfaces A_i and A_o, but also decrease h_i and the friction induced pressure drop due to reduced fluid velocities. In practice, a reduced pressure drop will be compensated with an enhanced mass flow rate through the PBU in order to maintain the pressure balance. The increase in $\dot{m}_{PBU}$ will partly compensate for the reduction in h_i caused by the increased inner tube diameter.

The equation below gives the friction induced pressure loss for a single-phase flow in a given tube section, was first expressed in Chapter 4.5. The friction factor calculated by Haaland's equation increases slightly for larger $d_{tube,\,i}$ and tube circumference, but it is by far not sufficient to compensate for the fact that the pressure drop is correlated to the tube diameter in the minus 5th power.

$$\Delta P_{friction,\,j} = f_j \frac{8\, l_j \left(\frac{\dot{m}_{PBU}}{n}\right)^2}{\pi^2\, \rho_j\, d_{tube,\,i}^5} \tag{5.1}$$

This equation gets a bit more complicated for a two-phase flow, but the principle of a lower pressure drop for increasing $d_{tube,\,i}$ is the same. This is explained in more detail in Chapter 4.5, where the pressure development through the entire PBU is examined.

The effect of the tube diameter on the outer heat transfer coefficient h_o is caused by the reduced flow area for the water-glycol mixture when the total tube volume inside the PBU increases. For both h_o and the outer heat transfer capability $h_o A_o$ (as presented in Chapter 4.4), the results of the tube diameter are presented in Table 22 and Table 23 in Chapter 5.1.2.

The inner heat transfer coefficient, as presented in Chapter 4.3, depends in most cases to some degree on the Reynolds number, the friction factor and directly with the $d_{tube,\,i}$. Since the Reynolds number decreases proportionally with increasing $d_{tube,\,i}$, h_i decreases for larger tube diameters.

If the inner tube diameter is the only parameter for the PBU that differ compared to the reference design, the effect is illustrated in Figure 17 and Figure 18. Both figures are based on a filling ratio of 0.9 and $\dot{V}_{WG}$ = 72.44 m^3/h. In Figure 17 the effect on the $\dot{m}_{PBU}$ may not look too dramatic as the $\dot{m}_{PBU}$ depends more on tank pressure than on the $d_{tube,\,i}$. On the other hand, in Figure 18 the huge difference in return temperature is revealed. The explanation why the amount of $\dot{m}_{PBU}$ necessary to balance the pressure of the thermosyphon differs so little between the three designs, is that the parameters gas velocity and length of the two-phase region are contributing in opposite directions of each other with respect to the pressure balance. A smaller $d_{tube,\,i}$ results in lower return temperature of the NG, which lowers the pressure drop through the return pipe between the PBU and the fuel tank. This is caused by an increased density in the vapor phase. On the other hand, a larger diameter results in a lower pressure drop through the PBU for equal $\dot{m}_{PBU}$. This duplex effect for different tube diameters results in relatively small variations in $\dot{m}_{PBU}$ at a given P_{tank}, as shown in Figure 17. The difference is mainly connected to whether dry vapor or a two-phase flow is returned to the tank.

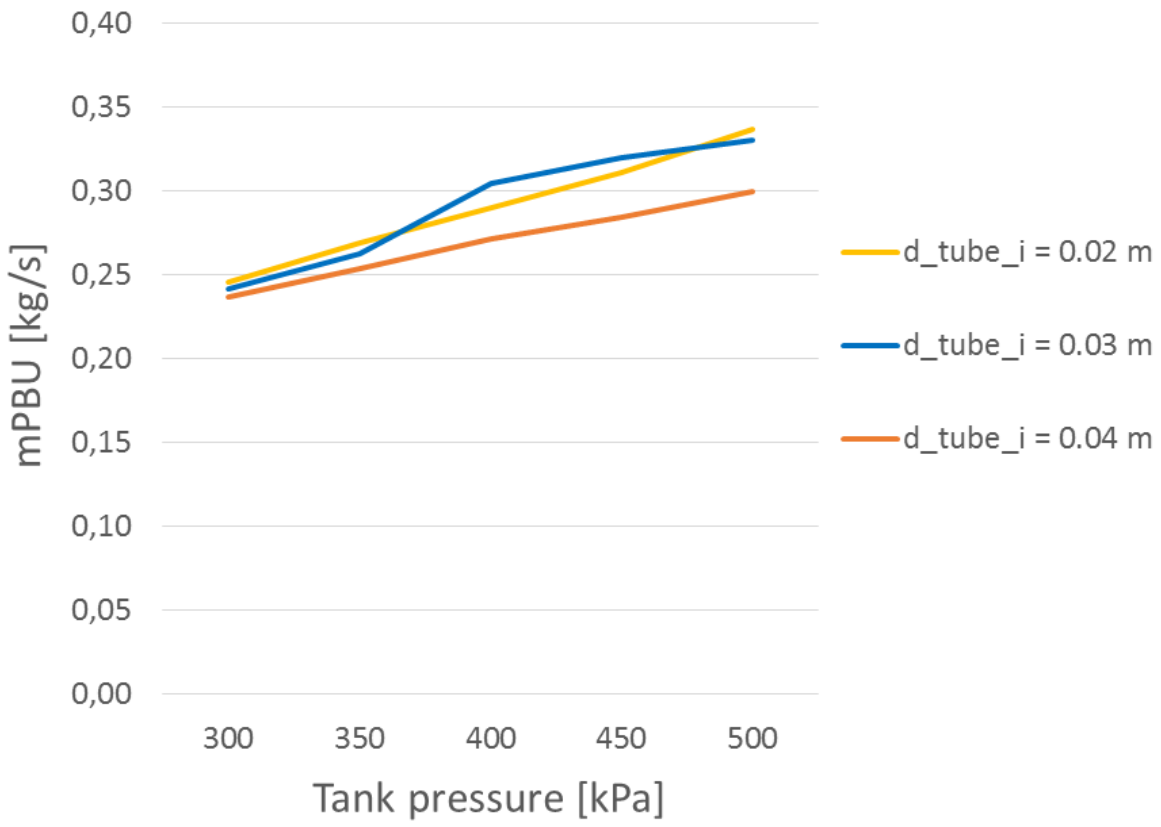

Figure 17 - $\dot{m}_{PBU}$ for different $d_{tube,\,I}$ with varying P_{tank} (filling ratio = 0.9 and reference design)

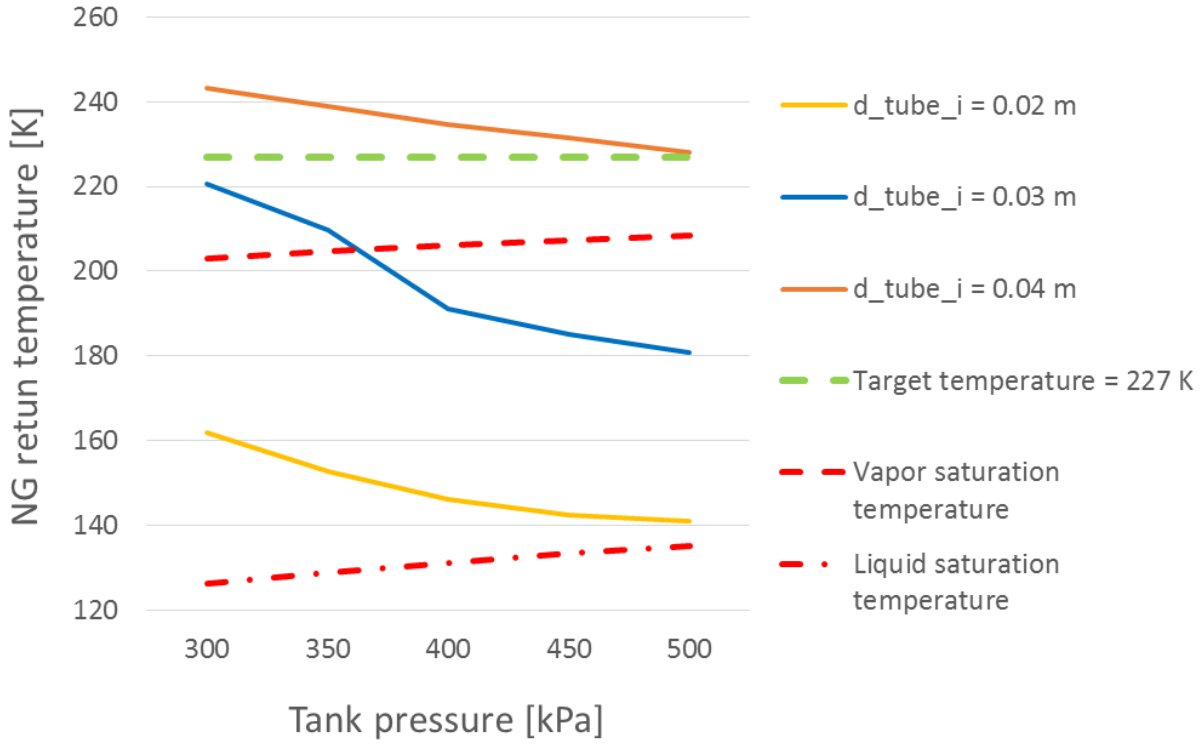

Figure 18 - NG return temperature for different $d_{tube,\,i}$ with varying P_{tank} (filling ratio = 0.9 and reference design)

From the figure above, it is evident that $d_{tube,\,i}$ must be increased to 0.04 m in order to configure the PBU design after the measured T_{target} = 227 K (DiRenzo 2014a). The T_{return} for P_{tank} = 500 kPa at a filling ratio of 0.9 will then be 227 K.

Given the existing PBU design on KV Bergen, there are some restrictions on how large the tube diameter can be. For a coil consisting of nine turns and having a height of 0.45 m, the distance between the centers of two turns, the pitch, is z_{pitch} = 0.05 m. The pitch is illustrated in Figure 19, where tubes in two consecutive turns of a coil are showed from the side.

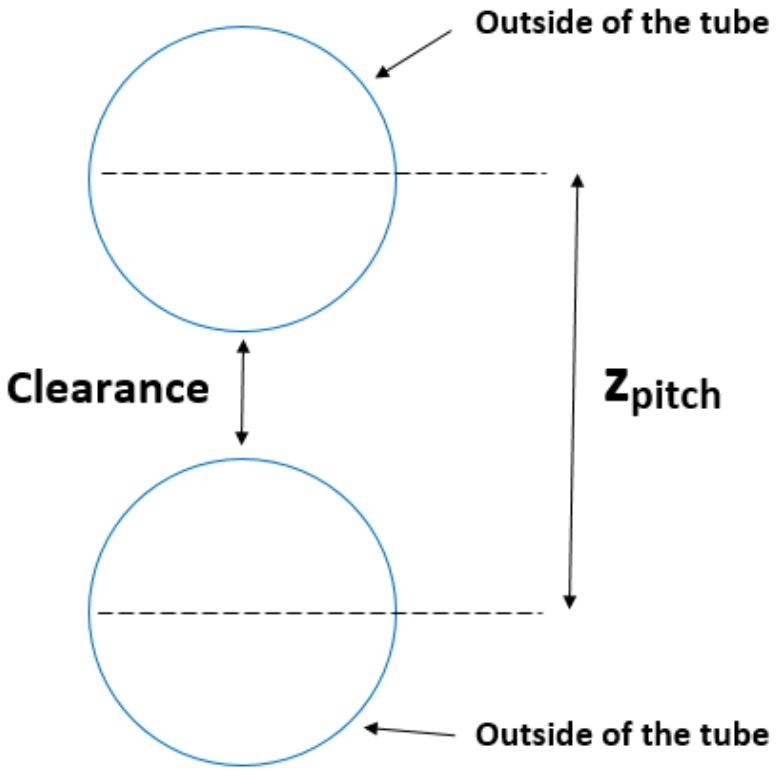

Figure 19 – Clearance and z_{pitch} illustrated with a side view of a coil in the PBU

It is important to secure that a reasonable amount of the water-glycol mixture is able to pass around the top and the bottom of the coiled tube in all the turns, implying that the tubes cannot have a dimension that hinders these flow patterns. This can be described with two equations, where the term clearance is the distance between the outside of two consecutive tubes:

$$z_{pitch} = 2\left(\frac{d_{tube,\,o}}{2}\right) + clearence = 2\left(\frac{d_{tube,\,i}}{2} + t_{tube}\right) + clearence \tag{5.2}$$

$$d_{tube,\,i} \leq z_{pitch} - 2\,t_{tube} - clearence \tag{5.3}$$

The clearance is pictured in Figure 19. An inner tube diameter of 0.03 m, as in the reference design in Table 11, with z_{pitch} = 0.05 m and t_{tube} = 0.001 m, gives a clearance of 0.018 m. The clearance for different $d_{tube,\,i}$ is given in Table 19. For an inner tube diameter of 0.04 m, the clearance is only 8 mm, and it is from a flow-perspective probably close to the minimum acceptable clearance and thus the maximum $d_{tube,\,i}$.

$d_{tube,\,i}$ *[m]*	**clearance** *[m]*
0.01	0.038
0.02	0.028
0.03	0.018
0.04	0.008

Table 19 - Clearance between the tubes in a coil (z_{pitch} = 0.05 m, t_{tube} = 0.001 m, z_{coil} = 0.45 m, N = 9)

For a design with several coils inside the PBU shell, tubes with a larger diameter are only possible if the z_{pitch} is increased in order to preserve a minimum acceptable clearance. This can only be achieved by either increasing the coil height for the same number of turns, or reducing the number of turns for the existing coil height. A combination of these two is also a solution. The latter will reduce the overall coil length. A different design principle for the Vaporizer is to let the coils turn around the whole PBU annulus. For such a design, an frequently used approach is to let several tubes be twinned into each other. Two or three parallel rings with tubes are used. This or other possible PBU designs are not further discussed in this thesis.

5.1.2 Wall spacing

The diameter of the coils has a significant impact on the total possible heat transfer, both through the outer heat transfer coefficient and through the total tube length. The method used for this work to determine the coil diameter is to apply a fixed space between the outer PBU shell and the coil, and similarly between the inner PBU shell and the coil, without considering any ice formations. Thereby, for a given spacing, the outer diameter of the coil is fixed, independent of the inner tube diameter. To clarify the terms used, Figure 20 shows the schematics of the coiled sections from a top view.

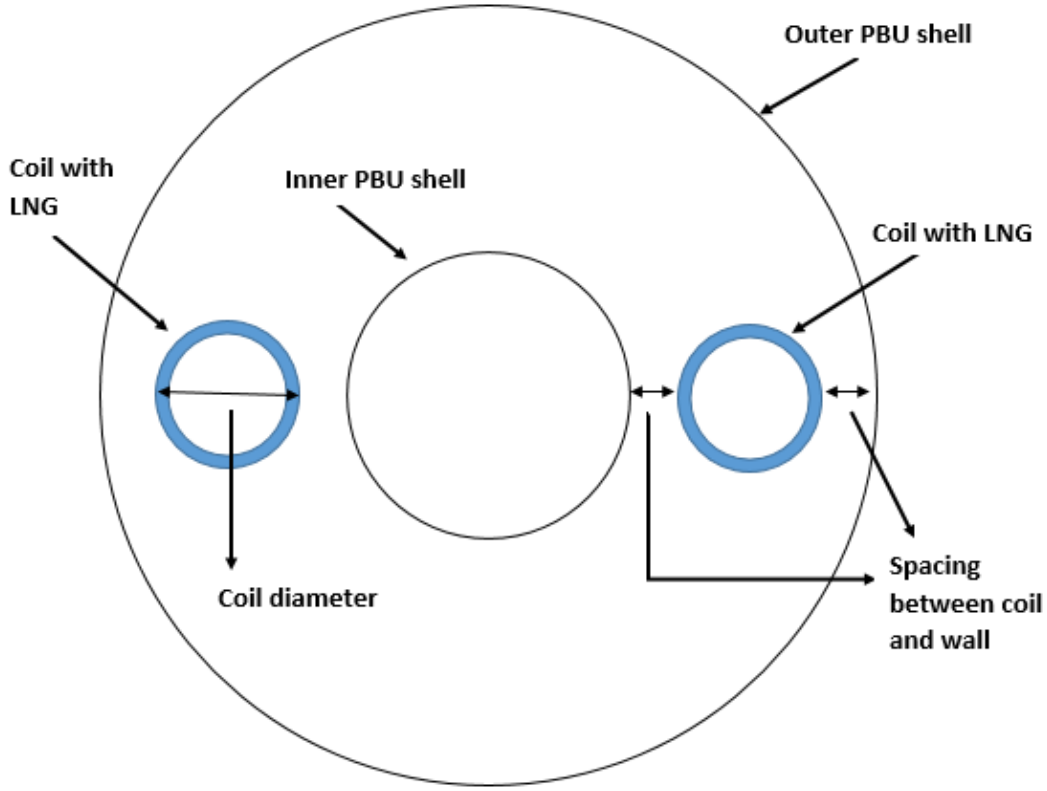

Figure 20 - Top view of the PBU showing the wall-coil spacing. Not correctly scaled, only for illustration purpose.

The length of the coil is important for two reasons: friction related pressure drop through the pipes and the total heat transferring area. Since the length of the coiled section is a function of $d_{tube,\,i}$ and the spacing in terms of the coil diameter, the equations below reveal that a coil's length decreases with increasing spacing and increasing $d_{tube,\,i}$.

$$d_{coil} = \frac{d_{coil,\,o} + d_{coil,\,i}}{2} = \frac{d_{PBU,\,o} - d_{PBU,\,i}}{2} - 2\ spacing - \left(d_{tube,\,i} + 2\ t_{tube}\right) \tag{5.4}$$

$$l_{coil} = N\ \sqrt{(\pi\ d_{coil})^2 + z_{pitch}{}^2} \tag{5.5}$$

For some combinations of the spacing and the $d_{tube,\,i}$, the length of the coil is presented in Table 20.

Spacing *[m]*	l_{coil} *[m]*			
	$d_{tube,\ i}$ = 0.01 m	$d_{tube,\ i}$ = 0.02 m	$d_{tube,\ i}$ = 0.03 m	$d_{tube,\ i}$ = 0.04 m
0.005	5.90	5.62	5.33	5.05
0.01	5.62	5.33	5.05	4.77
0.02	5.05	4.77	4.49	4.21
0.03	4.49	4.21	3.93	3.65

Table 20 - Length of one coil, varying wall spacing and inner tube diameter (reference design)

As in contrast to the lengths given in the table above, the total average length of the rest of the tubes inside the PBU sums up to 1.95 m (reference design in Table 11). Only the variation in the coil lengths in Table 20 is larger than the length of the rest of the tube inside the PBU, confirming the dominant position of the coil for the thermosyphon effect. Another factor underpinning the relative importance of the coils is the fact that the LNG flow is divided into several tubes in the coiled section (and for the straight sections) contrary to the single distribution ring at the bottom and the collection ring at the top of the PBU.

The tube surface is of interest for the heat transfer. For the outer surface of one coil, the area ($A_{coil,\ o}$) is shown in Table 21, using the same $d_{tube,\ i}$ and spacing as in Table 20. In the PBU there are 10 coils, so the total outer tube area of the coiled section is ten times higher. The same trend will be present for the inner surface area of a coil ($A_{coil,\ i}$).

Spacing *[m]*	$A_{coil,\ o}$ *[m^2]*			
	$d_{tube,\ i}$ = 0.01 m	$d_{tube,\ i}$ = 0.02 m	$d_{tube,\ i}$ = 0.03 m	$d_{tube,\ i}$ = 0.04 m
0.005	0.222	0.388	0.536	0.667
0.01	0.212	0.369	0.508	0.630
0.02	0.191	0.330	0.451	0.555
0.03	0.169	0.291	0.395	0.481

Table 21 - Outer area of one coil, varying wall spacing and inner tube diameter (reference design)

In terms of surface area, the increase in $d_{tube,\ i}$ more than compensates for the reduced coil length caused by the larger tube diameter (Table 20). For a spacing of 0.01 m, tripling the $d_{tube,\ i}$ from 0.01 m to 0.03 m increases the outer surface of one coil with 140 %, even though the coil length decreases with 10 %.

For a given tube diameter, a larger coil diameter will reduce the flow area for the water-glycol mixture and thereby increase the velocity for a fixed water-glycol flow rate. Reverting to the equations for the outer heat transfer coefficient in Chapter 4.4, larger Reynolds numbers result in larger h_o. Summing up, h_o increases with reduced spacing and increasing $d_{tube,\ i}$, as presented in Figure 21 and in Table 22.

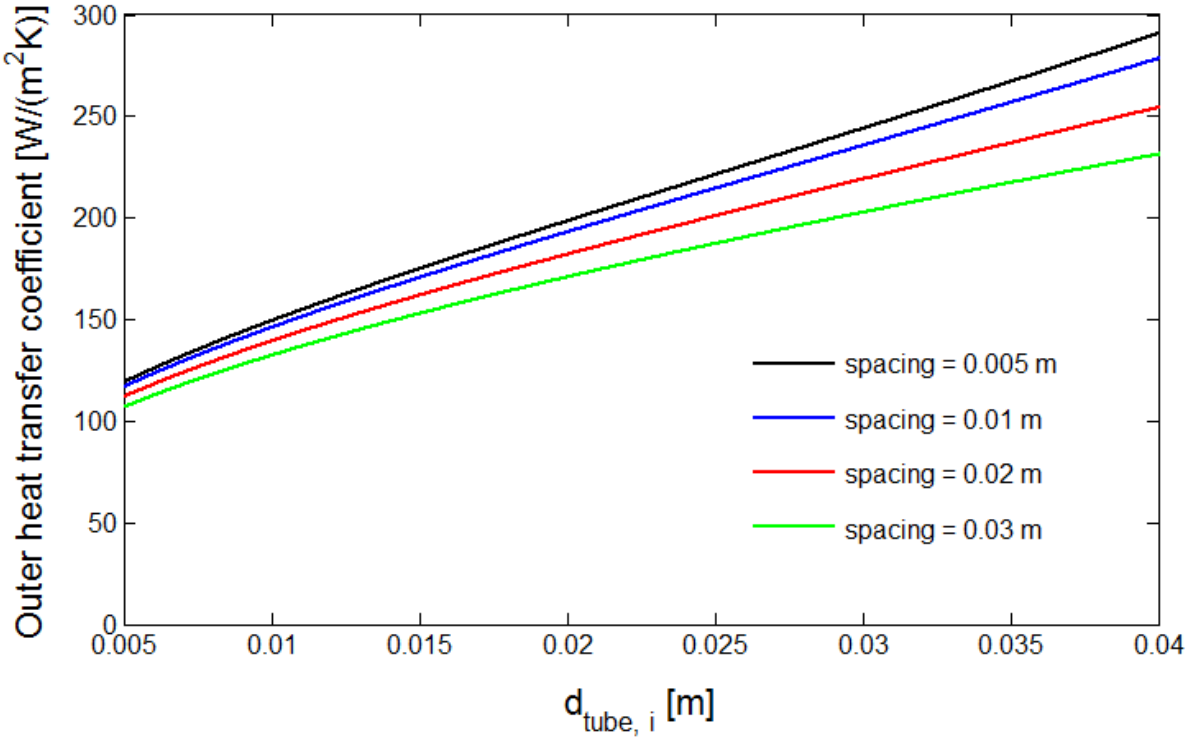

Figure 21 - h_o for the coiled section of the PBU with different spacing for varying $d_{tube,\,i}$ (reference design)

Spacing *[m]*	$\mathbf{h_{o,\,coil}}$ *[W / m²K]*			
	$d_{tube,\,i}$ = 0.01 m	$d_{tube,\,i}$ = 0.02 m	$d_{tube,\,i}$ = 0.03 m	$d_{tube,\,i}$ = 0.04 m
0.005	149.25	198.35	243.88	290.76
0.01	145.97	192.91	235.50	278.25
0.02	139.24	181.93	218.96	254.22
0.03	131.22	170.75	202.60	231.19

Table 22 - h_o for the coiled section of the PBU with different spacing and $d_{tube,\,i}$ (reference design)

The heat transferred through a tube is given by the overall heat transfer coefficient UA, which includes the difference between the inner and outer surfaces of the tube, as presented in Equation 4.1 in Chapter 4.1. Thus, it makes sense to discuss the amount of heat that possibly can be transferred from the warm water-glycol to the tube. It does not matter whether the heat transfer capability of the inside of the tube is infinite or not as long as the outer heat transfer capability (h_o A_o) is much smaller. For simplicity, and described above, the temperature of the water-glycol mixture is assumed to be constant through the PBU and thus h_o will be constant for a given geometry. For each coil, the outer heat transfer capability will be:

$$\left(A_o\ h_o\right)_{coil} = \pi\ d_{tube,\,o,\,eff}\ \ l_{coil}\ h_{o,\,\mathrm{coil}} \tag{5.6}$$

Assuming no ice formation, the trends for h_o in Table 22 are strengthened relative to those for the heat transfer capability per degree of temperature difference, presented in Table 23. The significance of the different parameters are striking: the $d_{tube,i}$ is much more important than the spacing. For an increase in $d_{tube,i}$ from 0.01 m to 0.03 m, $(h_o A_o)_{coil}$ rises with 260 - 295 % dependent on spacing, whereas $(h_o A_o)_{coil}$ increases with only 39 - 58 % for a reduction of the spacing from 0.03m to 0.01m for the different inner tube diameters. Larger tube diameters are more sensitive to reduced spacing, while smaller spacing is the same for increasing tube diameter.

Spacing *[m]*	**$(h_o A_o)_{coil}$** *[W / K]*			
	$d_{tube,\,i}$ = 0.01 m	$d_{tube,\,i}$ = 0.02 m	$d_{tube,\,i}$ = 0.03 m	$d_{tube,\,i}$ = 0.04 m
0.005	33.13	76.96	130.72	193.94
0.01	30.90	71.13	119.63	175.30
0.02	26.53	60.00	98.84	141.09
0.03	22.22	49.67	80.01	111.20

Table 23 - Heat transfer capability of the outside of one tube for the coiled section (reference design)

This suggests that larger tubes will contribute to a higher evaporation capacity in the PBU. For $d_{tube,i}$ = 0.03 m, the effect on $(h_o A_o)_{coil}$ of cutting the spacing in half from 0.01 m to 0.005 m, is 9.3 %. The risk of icing, and a subsequent ice blocking of the water-glycol flowing path between the coil and the shell walls, is dramatically increased when the spacing is reduced down to 0.005 m. Later in this sub-chapter the effects of the increase in $(h_o A_o)_{coil}$ are studied in the terms of $\dot{m}_{PBU}$.

The coil length is also important for the pressure drop caused by friction inside the tubes. For a tube of otherwise identical geometry, any extra length would proportionally increase the pressure drop, as can be derived from Equation 5.1 in the sub-chapter 5.1.1. Since the ratio $d_{tube,\,i}$ over d_{coil} decreases with decreasing wall spacing, the critical Reynolds number used for determining the friction factor correlation for the coil (presented in Chapter 4.5), will decrease. The consequence is that the friction factor on average will increase and thus the pressure drop through the coils will be larger.

With a larger pressure drop through the coils and the PBU, a smaller mass flow rate will balance the thermosyphon effect. Less heat must be transferred in order to achieve complete evaporation and the desired superheating. For a system with too low average heat transfer capacity, an increase in the pressure drop can be a good design choice. The additional pressure drop implies that a lower mass flow rate is required for the pressure balance, and thereby to enable a fully evaporated and sufficient superheated return flow.

Adding both the differences for the pressure development and for the heat transfer, Figure 22**Error! Reference source not found.** and Figure 23 show the consequences of different spacing for the $\dot{m}_{PBU}$ and the NG return temperature respectively. For a 0.02 and 0.03 m spacing, Figure 23 shows that Table 24the return flow is in two-phase for all the relevant

P_{tank} at a high filling ratio. Not even a reduction of the spacing to 0.005 m, secures a complete evaporation for the highest P_{tank} at a filling ratio of 0.9.

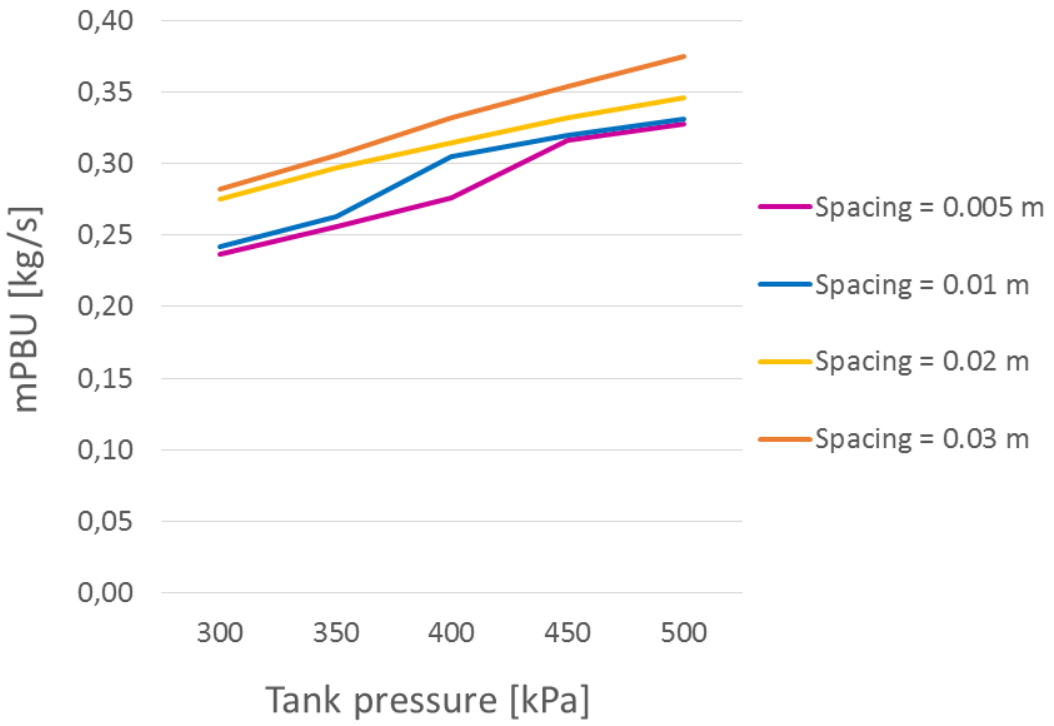

Figure 22 - $\dot{m}_{PBU}$ for different spacing with varying P_{tank} (filling ratio = 0.9 and reference design)

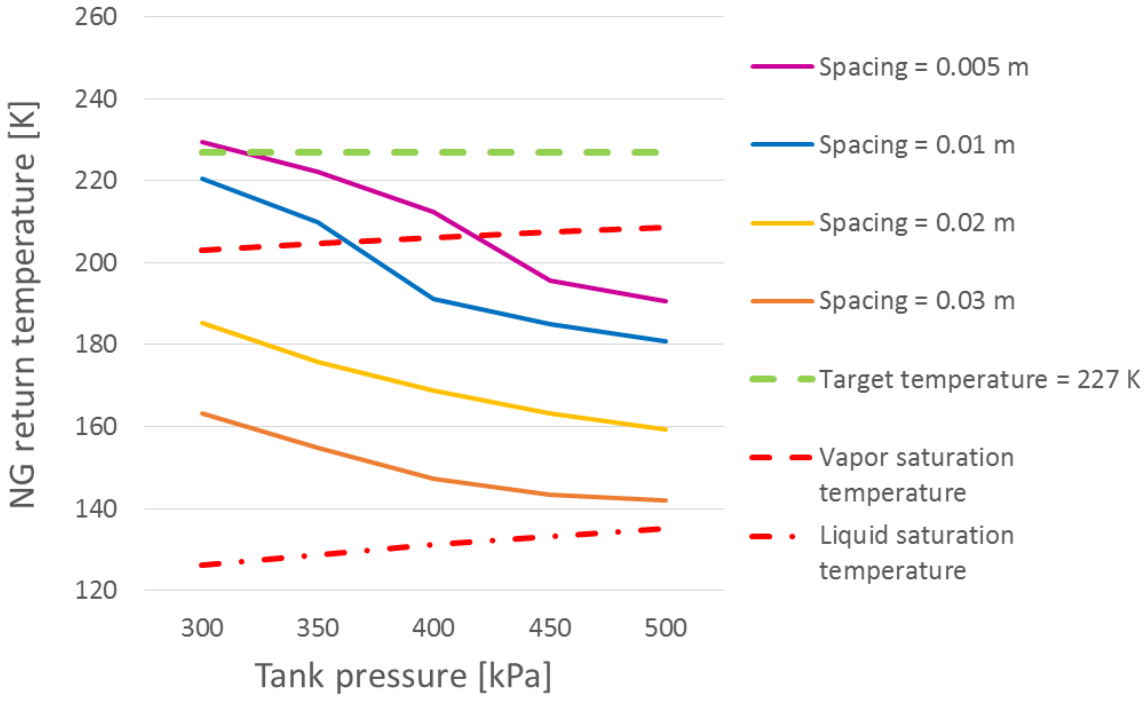

Figure 23 –NG return temperature for different spacing with varying P_{tank} (filling ratio = 0.9 and reference design)

Importantly, for very small wall spacing, the risk for ice formations blocking the entire area between the coil and the PBU shell wall will increase. The exact minimum spacing that can be justified is difficult to determine, since it is closely linked to the ice formation risk, $\dot{V}_{WG}$ and $\dot{m}_{PBU}$. Reducing the spacing down to 0.005 m is probably too risky considering the possibility for ice formation. Thus, ice formation of the water-glycol mixture inside the PBU should be further investigated.

5.1.3 Coil height

As earlier described, the coil length is important for both the total heat transfer capability of the PBU and the pressure drop through the PBU. An alternative to reducing the wall spacing in order to obtain a larger coil length, is simply to increase the vertical height of the coil. This results in a larger total height of the Vaporizer unit, unless other parts are correspondingly shortened. Since the Vaporizer, along with the rest of the LNG fuel management equipment, is located inside the cold box, connected to the fuel tank, the available space must be considered when enlarging the Vaporizer. According to the ship drawing of KV Bergen in Figure 4, the total Vaporizer height is 3.32 m, of which the PBU section contributes with 0.90 m. In Figure 24 the location of the Vaporizer is indicated with the number 4 inside the Cold Box (number 5) and connected to the fuel tank (number 2). The drawing indicates that there could be space for a moderate increase of the coiled section in the PBU and the Vaporizer. However, the area above the Vaporizer is likely to be used for other purposes, but this does not rule out changes to the design allowing a slightly higher Vaporizer. Otherwise, the total height of the cold box could be increased to enable larger coils in the PBU. A retrofitting of the cold box on KV Bergen would be expensive, but should be done rather easily when designing the system for a new LNG fueled vessel.

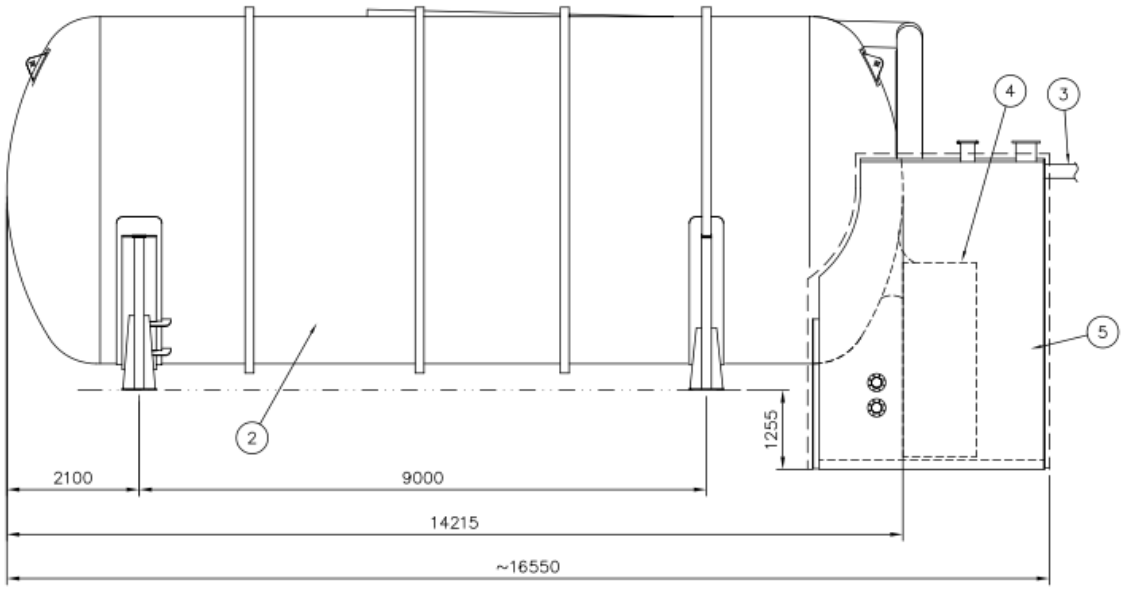

Figure 24 - Fuel tank and Cold Box on KV Bergen, vaporizer indicated with nr 4 - (Cryo AB 2012)

Several designs are possible for increasing the length of the coils, but this thesis only addresses an extension of the coils in the reference design (Table 11) with additional turns. Thus, the coil height is increased until the return temperature of the NG is above T_{target} = 227 K for a filling ratio of 0.9 and P_{tank} = 500 kPa, and keeping the z_{pitch} = 0.05 m. The development of T_{return} for increasing coil height is presented in Figure 25.

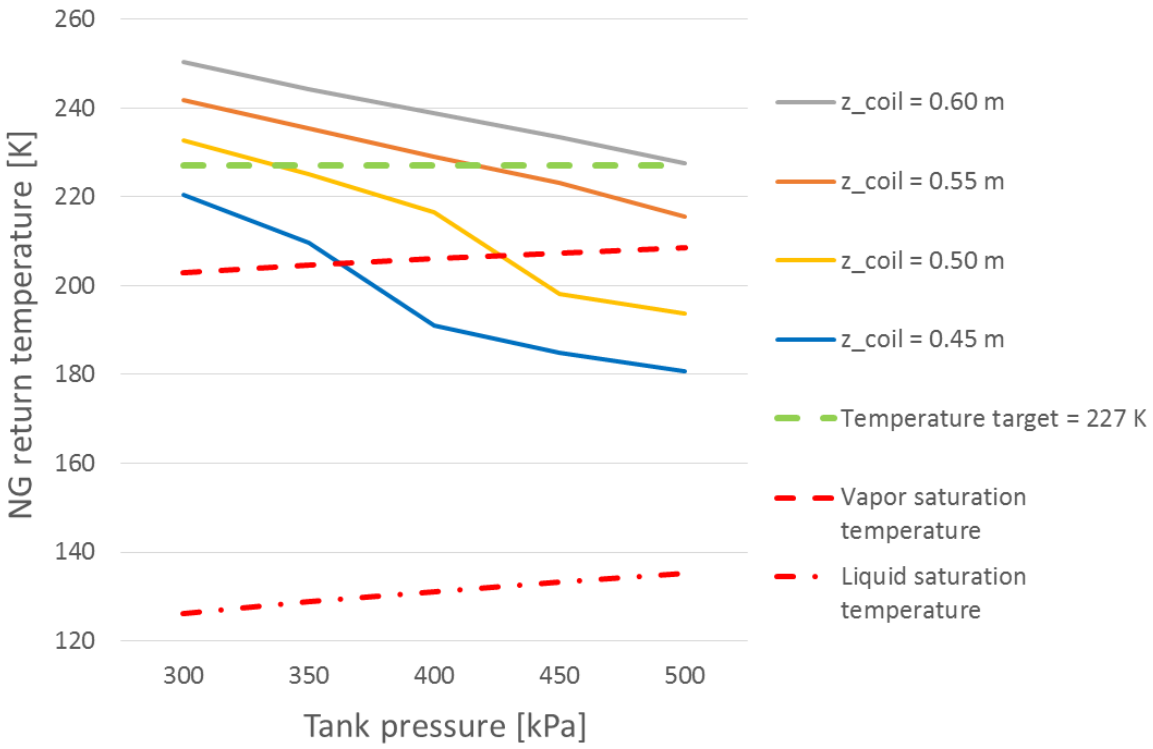

Figure 25 – NG return temperature for different vertical coil heights with varying P_{tank} (filling ratio = 0.9 and reference design)

The coil height must be increased by one third, from 0.45 m to 0.60 m, to obtain T_{return} larger than T_{target}. The NG return temperature is 227.68 K for filling ratio of 0.9 at P_{tank} = 500 kPa.

As can be seen from Figure 26, the $\dot{m}_{PBU}$ decreases for longer coils due to the enhanced NG return temperature. As previously discussed the density decreases with higher temperatures, causing higher velocities and correspondingly larger pressure drop in the return tube, which result in lower $\dot{m}_{PBU}$. In Figure 26 the $\dot{m}_{PBU}$ is a significant lower when consisting of dry vapor compared to a two-phase flow. As shown, the designs with z_{coil} = 0.45 m and z_{coil} = 0.50 m returns dry vapor even for high P_{tank}, whereas z_{coil} = 0.55 m and z_{coil} = 0.60 m is only able to deliver dry vapor at low P_{tank}.

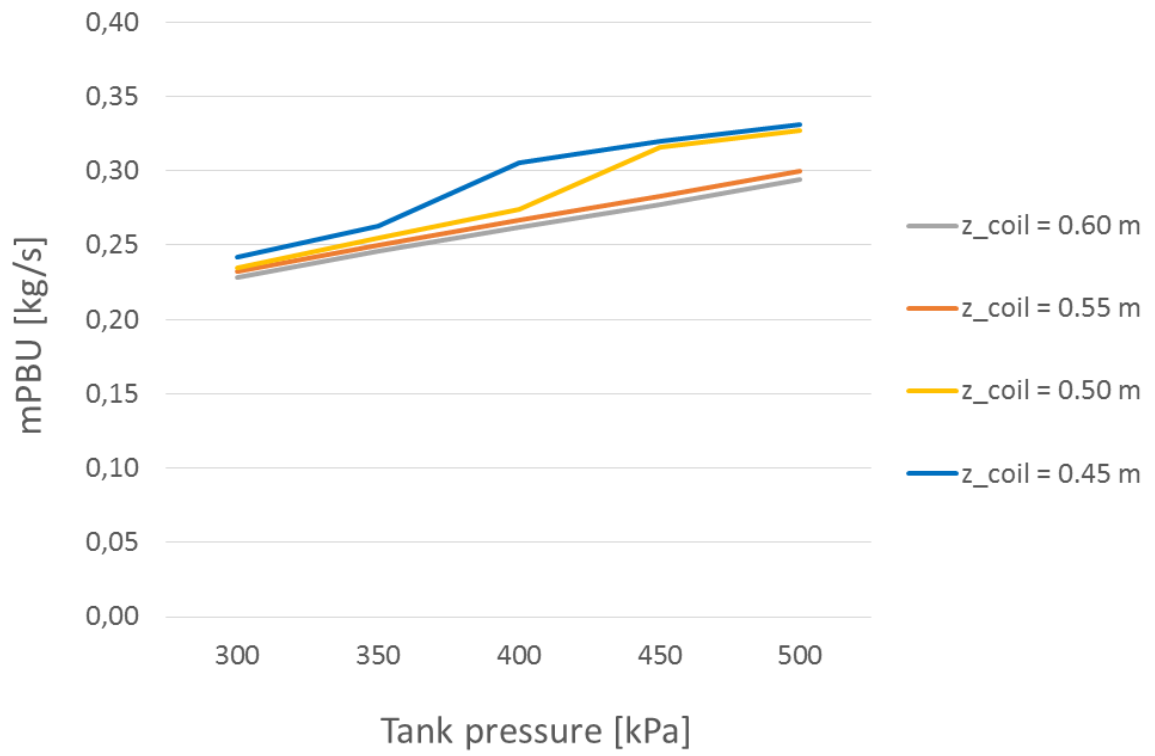

Figure 26 - $\dot{m}_{PBU}$ for different vertical coil heights with varying P_{tank} (filling ratio = 0.9 and reference design)

5.1.4 Stand-alone coils or dual-twinned coils

In the drawing of PBU design for KV Bergen (Cryo AB - KV Bergen 2009) in Figure 4, it is not obvious if there are ten pairs of two coils twinned together (dual-twinned) or ten single coils (stand-alone and reference design, Table 11) with each twice as many turns. As briefly discussed in Chapter 4.1, the two designs result in different pressure drops and heat transfer rates through the PBU for the same mass flow rate. The consequences of these design differences are assessed in more detail in this sub-chapter.

In Table 24, the differences between the return conditions for the same mass flow rate with the two designs are presented. The balancing $\dot{m}_{PBU}$ for the reference design at a filling ratio of 0.9 and P_{tank} = 500 kPa, 0.331 kg/s is used. When balancing the pressure in the thermosyphon, a tolerance level of 1.0 kPa is used between the tank pressure and the pressure of the NG returning from the PBU to the tank. For the dual-twinned design simulation, the returning pressure is a slightly higher, thus the thermosyphon is not balanced and the corresponding $\dot{m}_{PBU}$ would be higher, reducing T_{return}, $P_{PBU,\ exit}$ and the returning vapor quality x_{return} somewhat compared to that the values presented in the table. Figure 27 and Figure 28 below provide further insight into the effect of the coil design.

Parameter	Stand-alone coils	Dual-twinned coils
n	10	20
N	9	4.5
$P_{PBU,\ exit}$	517.14 kPa	518.75 kPa
P_{return}	500.82 kPa	501.86 kPa
T_{return}	180.80 K	199.68 K
x_{return}	0.979	0.996

Table 24 - Comparison of return conditions for Stand-alone and Dual-twinned coil design for $\dot{m}_{PBU}$ = 0.331 kg/s (filling ratio = 0.9, P_{tank} = 500 kPa and reference design)

Due to both shorter coiled sections and lower fluid velocities since the LNG/NG is divided between twice as many tubes, the pressure drop is reduced for dual-twinned coils compared to stand-alone coils. The result is a larger $\dot{m}_{PBU}$ for the dual-twinned design.

For a given $\dot{m}_{PBU}$, the inner heat transfer coefficient is reduced for the dual-twinned coils, due to the lower flow rates through each tube. On the other hand, the required heat transfer to heat the fluid inside one tube is cut in half when the mass flow rate in each tube is halved. Together with the additional overall tube length, the overall heat transfer is in fact larger for the dual-twinned design than for the stand-alone design. The inner heat transfer coefficient is also reduced with the lower flow velocities, but this reduction is less than the gain achieved by the additional piping surface. The stand-alone coil arrangement has in total 10 pipes á 5.50 m, and the dual-twinned design results in 20 pipes á 3.01 m. Both straight sections of the tubes are included in these numbers. In total, the dual-twinned coil arrangement consists of 5.20 m more piping than the stand-alone or reference design.

As Figure 27 illustrates with dotted lines for the dual-twinned design, the return temperature from the PBU is larger than for the stand-alone design, indicated by the solid lines. It is evident that by only changing the coil arrangement, a complete evaporation and $T_{return} > T_{target}$ cannot be secured for a combination of both high filling ratios and tank pressures.

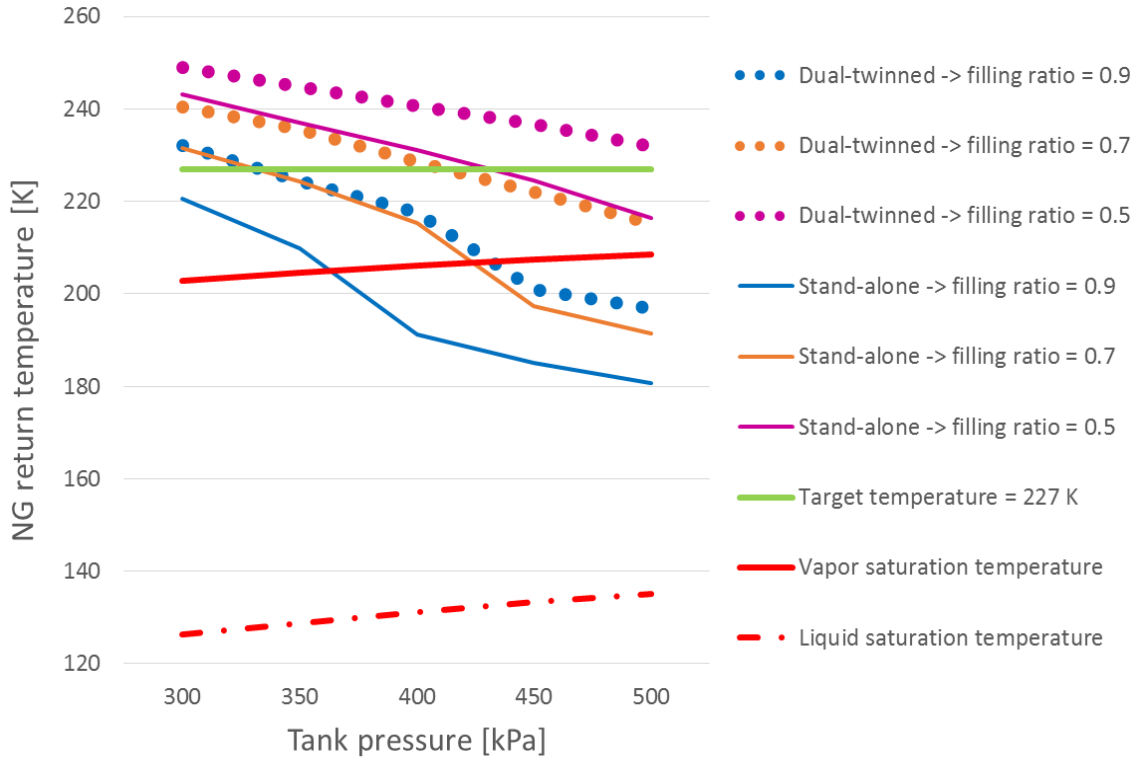

Figure 27 - NG return temperatures for Dual-twinned versus Stand-alone coil arrangement (filling ratio = 0.9 and reference design)

Due to the higher NG return temperatures and the corresponding pressure losses, the resulting $\dot{m}_{PBU}$ for the dual-twinned design is not that different from that for the stand-alone design (reference design). Depending on P_{tank}, and thus if the return flow consists of vapor or two-phase flow, the mass flow rate can also be lower for the dual-twinned design as shown in Figure 28. The explanation for this is similar to that used in Chapter 5.1.1.

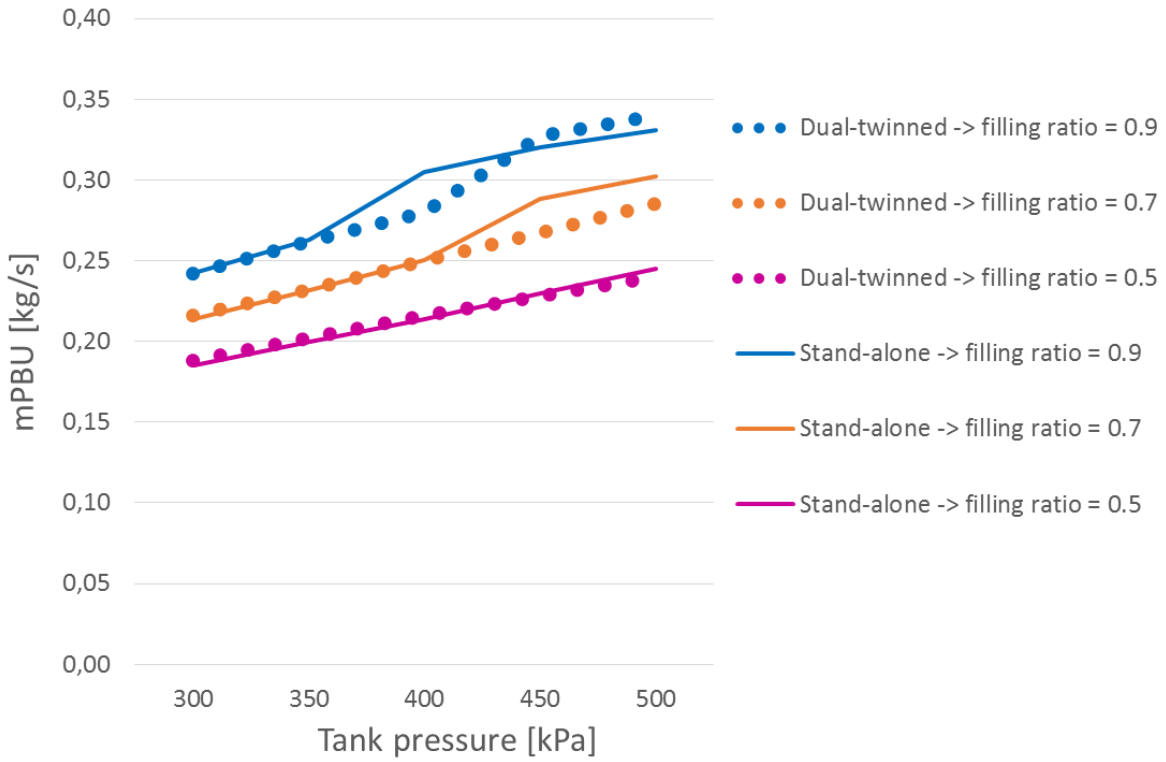

Figure 28 - $\dot{m}_{PBU}$ for Dual-twinned versus Stand-alone coil arrangement (filling ratio = 0.9 and reference design)

5.2 System configurations

Improving the geometry of the PBU is one method to secure sufficient heat transfer to the LNG. The other major option is to adjust the warm side flow in the heat exchanger, either through increasing the flow rate of the water-glycol mixture or by lifting the temperature. A third option is to modify the control system of the PBU. Introducing a thermal governed PID-controller for the NG stream after the PBU, the mass flow rate can be controlled to be as low as necessary in order to secure the desired NG return temperature, independent of differing tank and system conditions. These three options are discussed in this section together with the consequences of ice formations on the tubes.

5.2.1 Water-glycol mixture flow rate

For a given PBU design, the outer heat transfer coefficient is fixed when assuming non-varying temperatures and non-varying ice formations on the hot side. By increasing the water-glycol flow rate, the velocity on the hot side increases and thus the Reynolds number, which directly influences the h_o through the Nusselt number correlations. In the above-mentioned measurement campaign on KV Bergen, the flow rate of the water-glycol mixture was on average found to be 72.44 m^3/h (DiRenzo 2014a), 12.44 m^3/h above the value from the ship manual (Cryo AB - KV Bergen 2009).

Ignoring any capacity constraints in the water-glycol system, the improvement in h_o for increasing $\dot{V}_{WG}$ is illustrated in Figure 29 for 72.44, 100 and 120 m^3/h. In Figure 29, h_o is given for the different sections of the piping through the PBU. From left to right: lower distribution ring, lower straight section, coil, upper straight section and the upper collection ring.

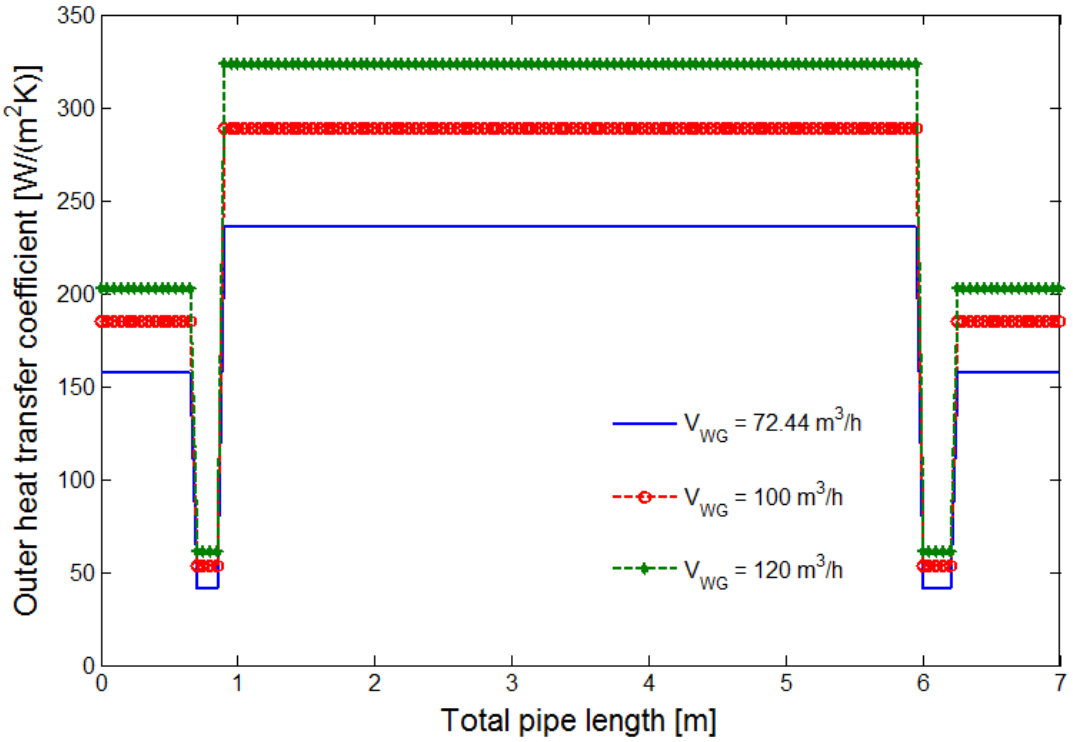

Figure 29 - Outer heat transfer coefficient for the entire PBU tube length with different $\dot{V}_{WG}$ (reference design)

Given the assumption used in this work, the outer heat transfer coefficient is constant for each section with a given geometry. If the temperature of the water-glycol mixture had been significantly reduced due to the heat transfer to the LNG/NG through the PBU, h_o would have declined with the decreasing temperature. Compared to the averaged T_{WG} used in this work, h_o would have been slightly higher than indicated in Figure 29 at the top of a PBU section, and slightly lower at the bottom of that section.

As discussed in Chapter 5.1, the heat transfer capability for the warm side of the tubes (h_o A_o) is probably the most important coefficient when investigating the impact of enhanced water-glycol flow rates, since it is lower than the inner heat transfer capability (h_i A_i). In Figure 30, the h_o A_o for an entire coil is drawn for the three water-glycol flow rates introduced above.

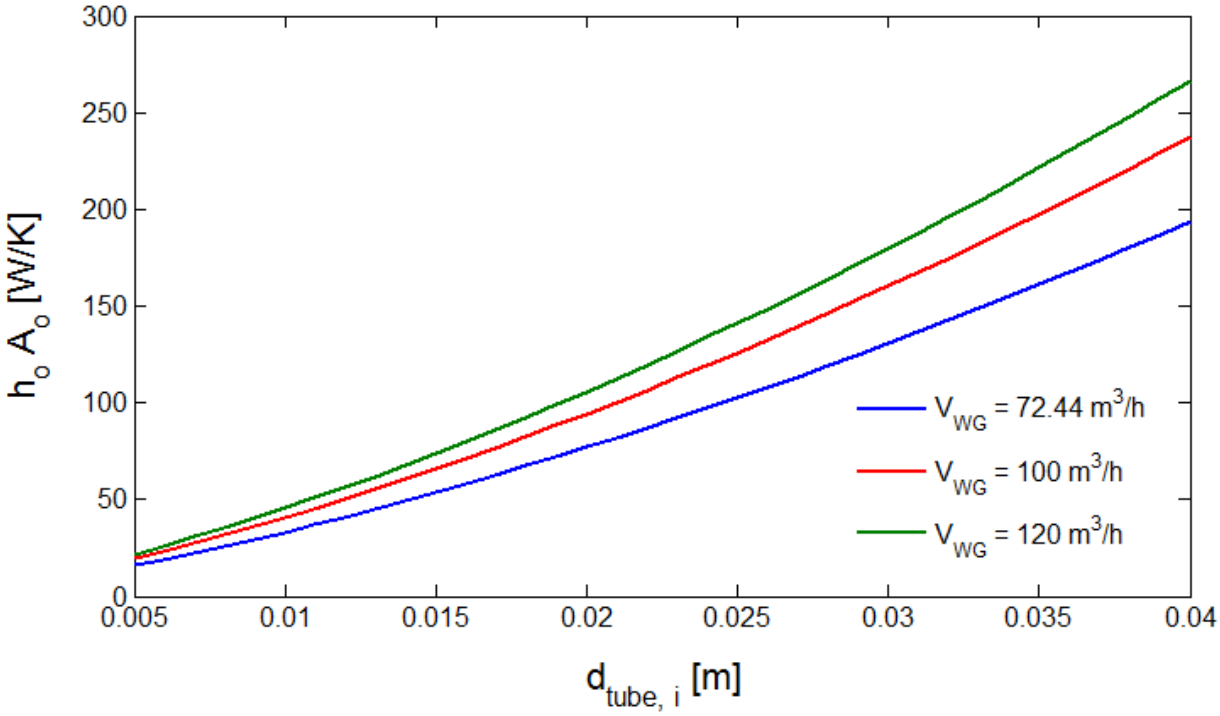

Figure 30 - Heat transfer capability for the outside for the coiled section of one tube with different $\dot{V}_{WG}$ for varying $d_{tube,\,i}$ (reference design)

With the knowledge from Chapter 5.1.2 regarding the nature of $h_o A_o$, the shape of the lines in Figure 30, is as expected. The heat transfer capability increases significantly when the $\dot{V}_{WG}$ goes from the reference design to 100 and 120 m^3/h.

As Figure 31 shows, $\dot{V}_{WG}$ needs to be 120 m^3/h to secure $T_{return} \geq 227$ K for a filling ratio of 0.9 and P_{tank} = 5.0 bar. Even if the filling ratio should be a few percentage points higher, the NG returning will still be dry. Playing Russian roulette, and allowing the NG return temperature to decrease below 227 K and towards $T_{sat,\,vapor}$ (P_{tank} = 5.0 bar) = 208.6 K, the water-glycol flow rate can be reduced to 100 m^3/h and still returning dry vapor, as also indicated in Figure 31.

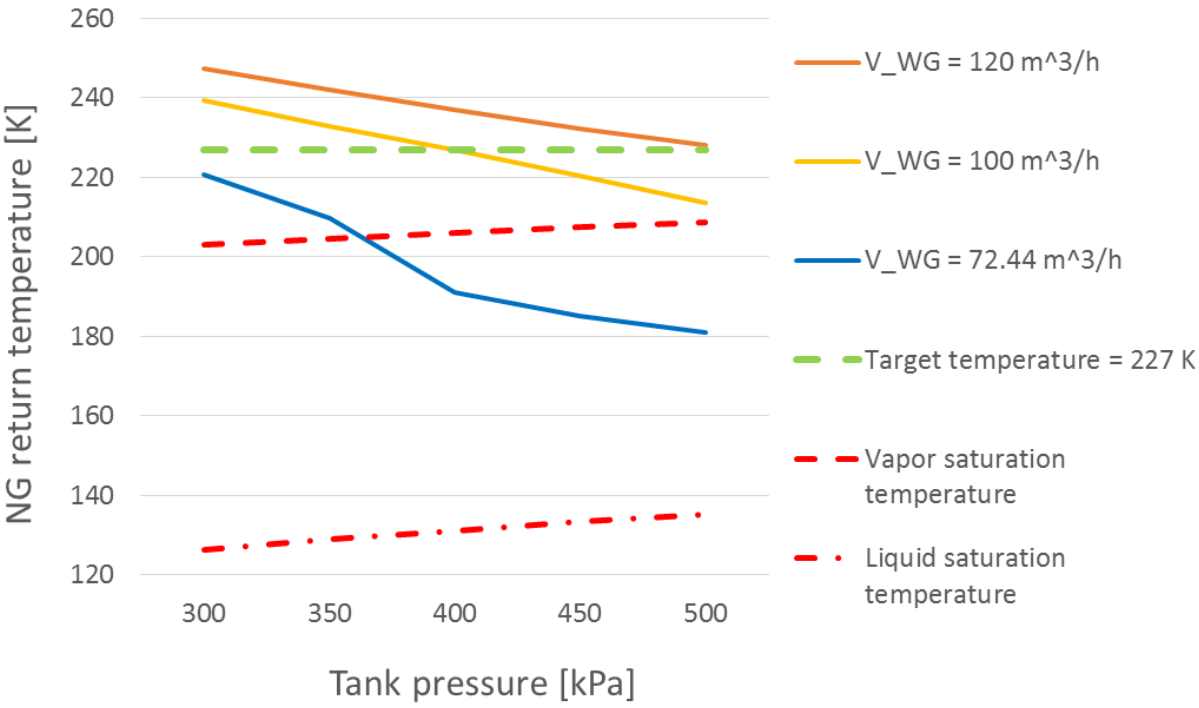

Figure 31 – NG return temperature for different $\dot{V}_{WG}$ with varying P_{tank} (filling ratio = 0.9 and reference design)

In addition to securing the desired superheating, the increase in $\dot{V}_{WG}$ impacts the $\dot{m}_{PBU}$. For flow rates of 100 m^3/h and 120 m^3/h, the $\dot{m}_{PBU}$ is reduced compared to a flow rate of 72.44 m^3/h. Figure 32 shows this development:

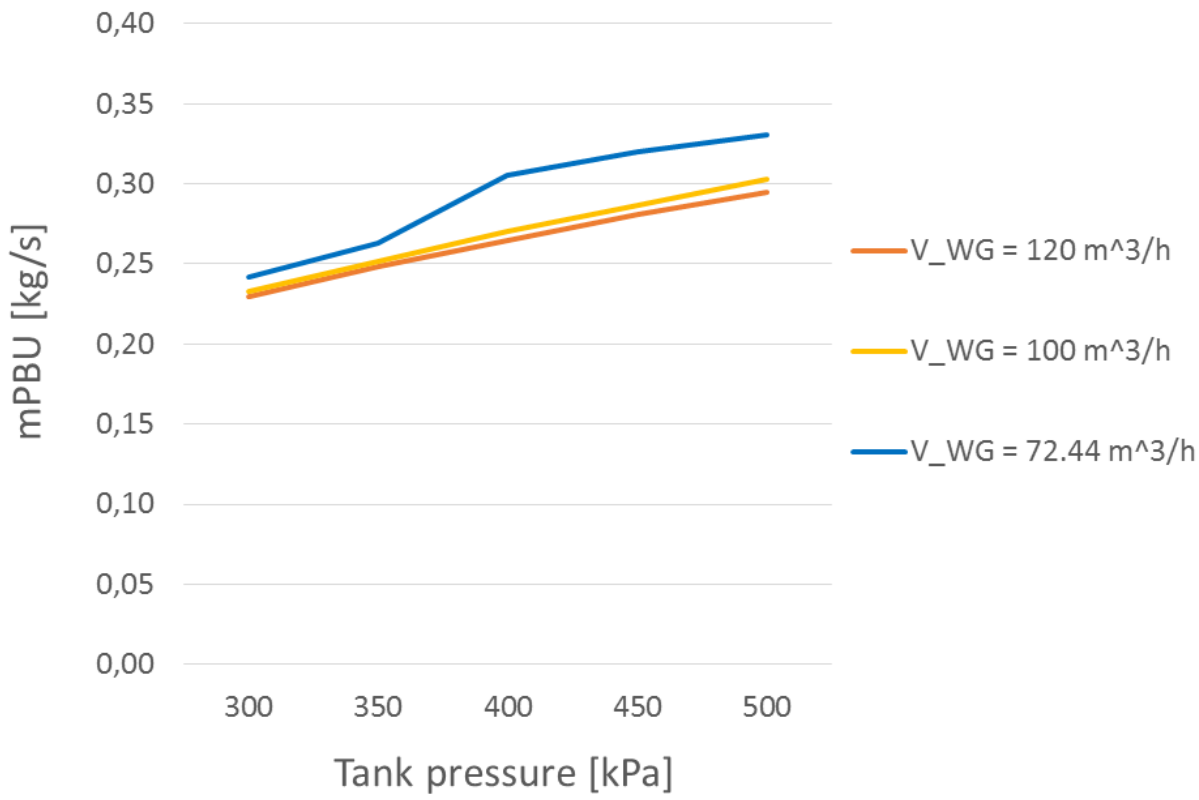

Figure 32 - $\dot{m}_{PBU}$ for different $\dot{V}_{WG}$ with varying P_{tank} (filling ratio = 0.9 and reference design)

Part of the reason why the mass flow rate declines with increasing $\dot{V}_{WG}$, is that the pressure drop through the return pipe to the fuel tank increases rapidly when the flow is fully evaporated and further superheated. The corresponding higher temperature, lower density and higher velocity in the return pipe enhance the friction-induced pressure drop. The different drops in pressure through the return pipe are illustrated in Figure 33. This indicates that in order to achieve the pressure balance of the thermosyphon, the pressure losses in the rest of the system must be higher when returning a two-phase flow, explaining the necessity of a higher LNG/NG mass flow rate.

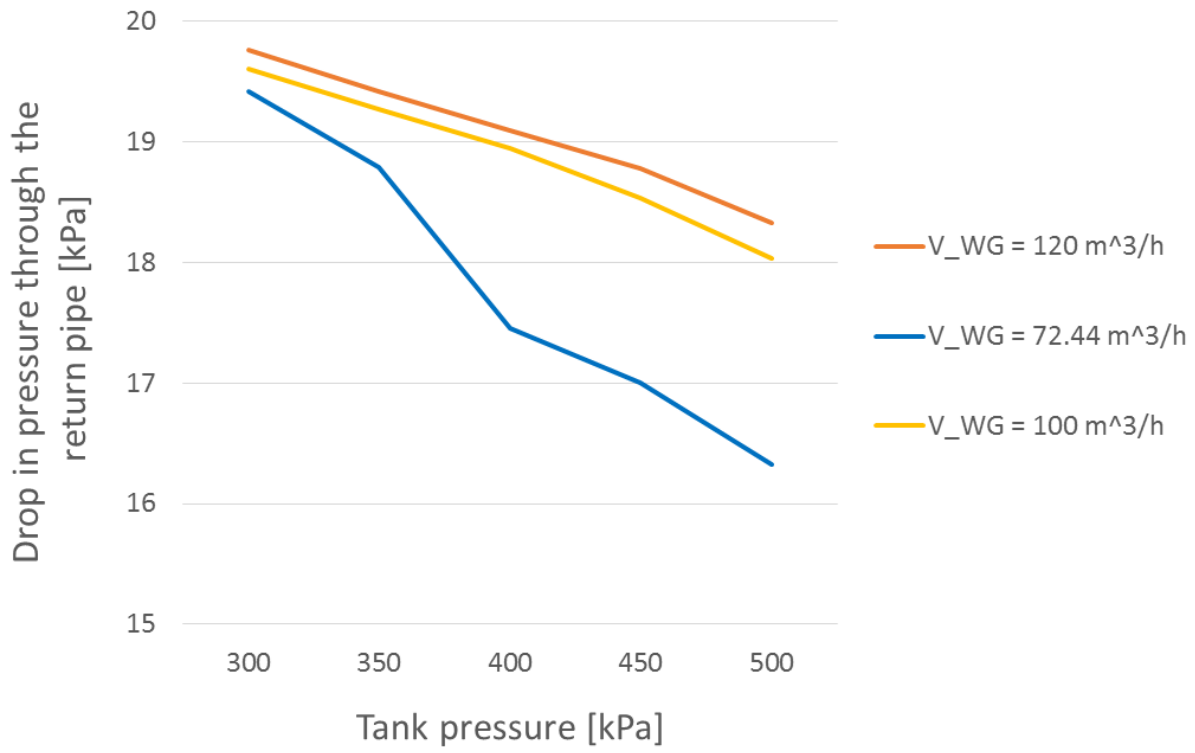

Figure 33 - Drop in pressure through the return pipe from the PBU for different $\dot{V}_{WG}$ with varying P_{tank} (filling ratio = 0.9 and reference design)

The restrictions regarding the water-glycol flow rate in the PBU are primarily based on the capacity of the circulation pumps and the allowed flow velocities through both heat exchangers. The heat exchangers being the PBU and the heat exchanger on the engine side, the circuits heat source. The last two are difficult to determine without detailed descriptions of the heat exchangers and their inner flow pattern, but the circulation pump capacity is described in the operation manual. On KV Bergen there are two circulation pumps installed in parallel, each with a capacity of 60 m^3/h with water-glycol mixture (Cryo AB - KV Bergen 2009). Assuming that the pumps are the active constraint, the maximum water-glycol flow rate is 120 m^3/h. By chance this is also the required $\dot{V}_{WG}$ to operate the PBU with $T_{return} \geq T_{target}$ for the relevant filling ratios and pressure levels. If it is possible to operate the system with a flow rate of 120 m^3/h or not, is not further investigated. In case it is not be possible to increase the flow rate up to 120 m^3/h, the flow rate most likely be increased somewhat.

5.2.2 Water-glycol mixture temperature

Using an arithmetic approach, the heat transferred from the water-glycol mixture to the LNG is proportional with the temperature difference between the warm and the cold fluid, as shown in Equation 4.1 in Chapter 4.1. Thus, by increasing the water-glycol mixture temperature $T_{WG, avg}$, the heat transfer in the PBU can be raised.

As described in Chapter 4.1, average temperatures are used on both tube sides when calculating the heat transferred in one spatial step of the tube. On the warm side, an average for the entire PBU is used, $T_{WG, avg}$. For the LNG/NG, the temperature at the start of a section is set as the temperature for that small tube section. The actual temperature of the LNG/NG is increasing through a small spatial step, but not materially for the heat transfer, and is thus neglected when calculating the heat transfer coefficients for each iterative spatial step. In this sub-chapter, the effect of the $T_{WG, avg}$ on the overall results for the PBU is evaluated.

The operational manual for KV Bergen suggests an inlet temperature of 30 °C for the water-glycol mixture into the Vaporizer. According to the manual, the temperature will sink to 26 °C at the top of the PBU and to 22 °C at the outlet of the PBU and the Vaporizer. In the measurement campaigns conducted by (DiRenzo 2014a), both the inlet and outlet temperatures of the Vaporizer were measured. The average results are given in Table 25, where an average for the entire Vaporizer is given at the bottom.

Parameter	Measurement 1	Measurement 2
$T_{WG, in, avg}$	33.09 °C	41.56 °C
$T_{WG, out, avg}$	32.60 °C	41.41 °C
$T_{WG, avg}$	32.85 °C	41.49 °C

Table 25 - Water-glycol mixture temperatures, data from (DiRenzo 2014a)

In the reference design (Table 11), the temperature from the first measurement is used, $T_{WG, avg}$ = 32.85 °C (306 K). The relative temperature increase between the two measurements must be viewed in the light of the PBU LNG inlet temperature, T_{bulk} = -152.15 °C (121 K). The temperature difference ($\Delta T = T_{WG, avg} - T_{LNG, in}$) increases with 4.67 % from 185.00 °C to 193.64 °C. As the LNG/NG temperature increases towards the top of the PBU, the difference to the water-glycol-mixture decreases. Thus, the relative increase in $T_{WG, avg}$ from 32.85 °C to 41.49 °C becomes larger. When the NG passes T_{target} = 227 K, the temperature difference across the tube is increased from 79.00 °C to 87.64 °C, or with 10.94 % for the same rise in $T_{WG, avg}$. For a PBU design equal to that of the reference design, the effect of the warm side temperature on both the NG return temperature and the $\dot{m}_{PBU}$ are found in Figure 34 and Figure 35, respectively.

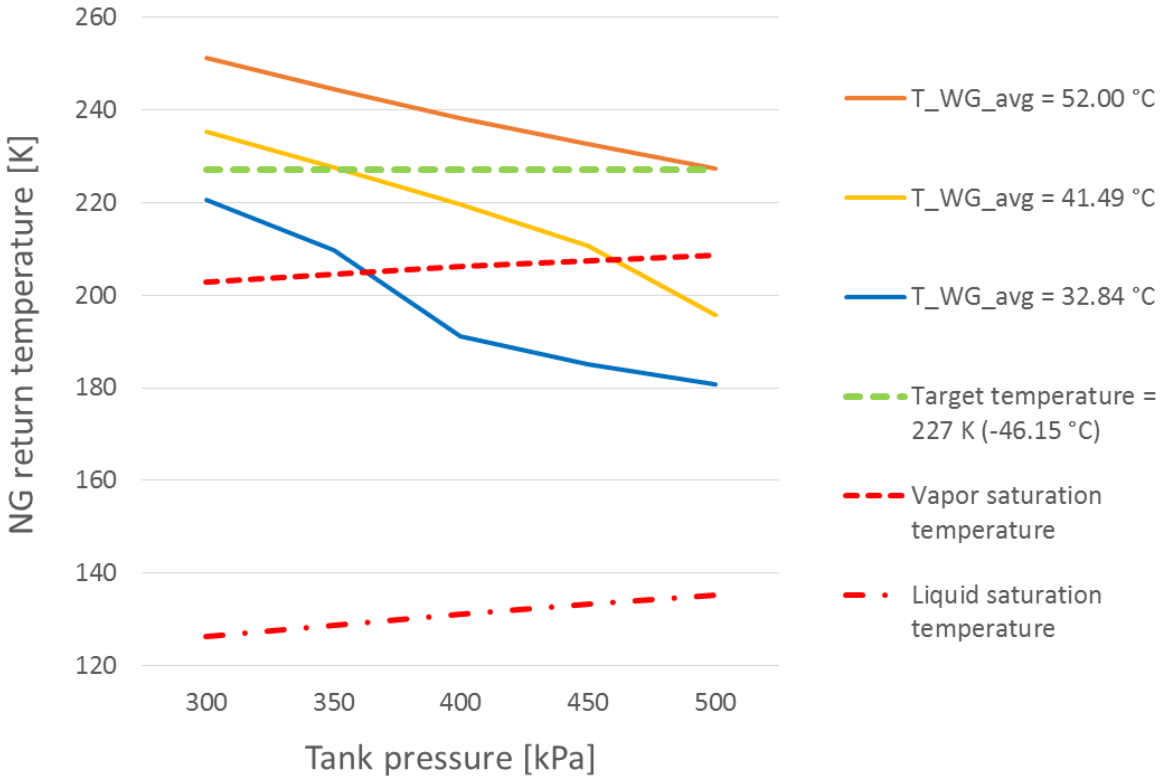

Figure 34 - NG return temperature for different $T_{WG,\,avg}$ with varying P_{tank} (filling ratio = 0.9 and reference design)

As shown in Figure 34, the increase of $T_{WG,\,avg}$ to 41.49 °C is neither sufficient to secure that $T_{return} > T_{target}$ nor sufficient to ensure complete evaporation at the highest filling ratio and P_{tank}. The water-glycol mixture temperature must be raised to 52 °C in order to secure T_{return} to exceed 227 K for all relevant tank conditions, as indicated in the graph above.

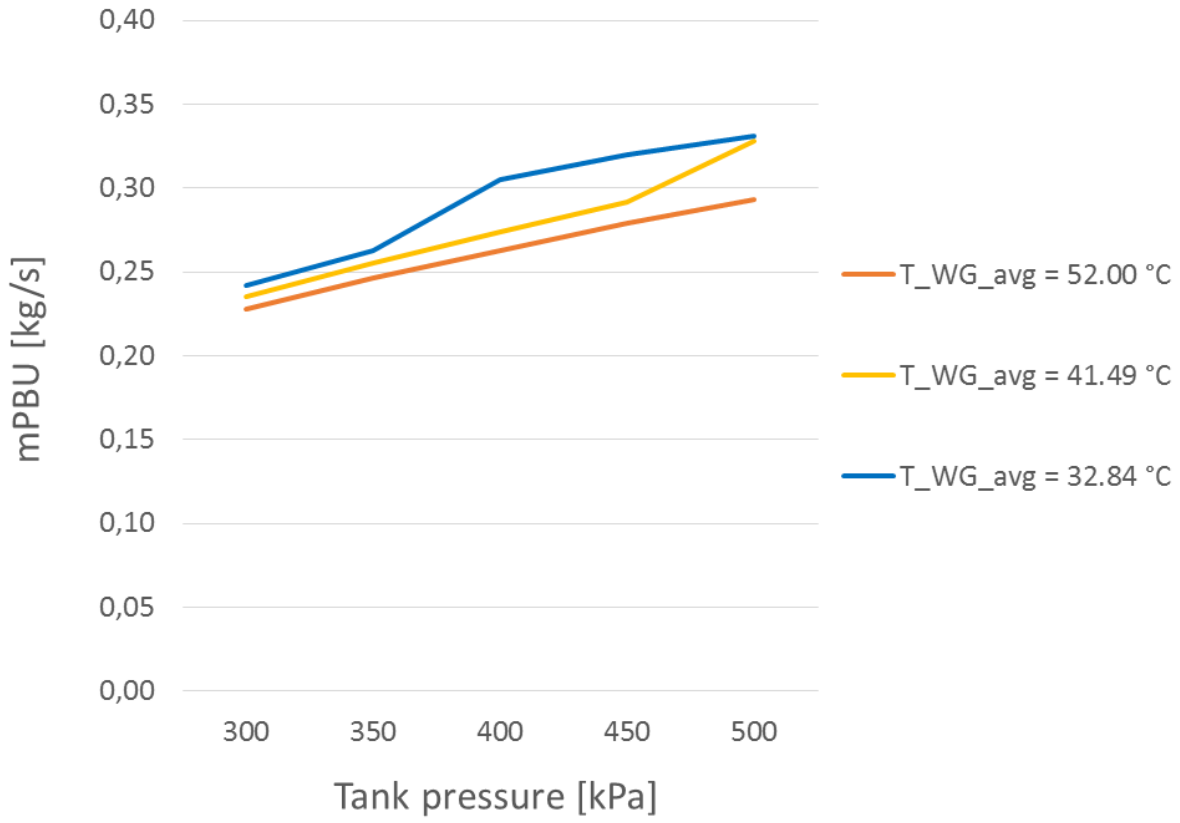

Figure 35 - $\dot{m}_{PBU}$ for different $T_{WG,\,avg}$ with varying P_{tank} (filling ratio = 0.9 and reference design)

When comparing the $\dot{m}_{PBU}$ for the higher $T_{WG,\,avg}$ found above, with that for the reference design temperature 32.85 °C, the mass flow rates are slightly lower. Only for tank pressures where the return stream is fully evaporated instead of returning as a two-phase flow, the $\dot{m}_{PBU}$ is significantly lower with the enhanced $T_{WG,\,avg}$. The reason is the same as for similar result for the previous parameter modifications.

Operating the water-glycol flow at a temperature above 52 °C will demand large energy input in order to increase the temperature after a longer standstill of the system. An electric warmer may be required. When the operational temperature is reached, the extra heat needed from the NG Engines compared to lower $T_{WG,\,avg}$, is not that large. At higher temperatures there will be larger heat leakages to the surroundings, but the heat transferred to the LNG does not vary that much for a given tank condition (filling ratio and P_{tank}). As shown in Figure 35, the mass flow rate is reduced when the flow is fully evaporated. Thus, the total heat rate transferred from the water-glycol does not increase as much as the higher NG return temperature indicates. An overview of the heat required for heat transfer to the LNG for the different water-glycol temperatures at a filling rate of 0.9 and P_{tank} = 5.0 bar, is given in Table 26.

$T_{WG, avg}$		$\dot{m}_{PBU}$	T_{return}	h_{bulk}	h_{return}	Δh_{PBU}	$H_{tot} = \dot{Q}_{needed}$
°C	*K*	*kg/s*	*K*	*kJ/kg*	*kJ/kg*	*kJ/kg*	*kW*
32.85	306.00	0.331	180.80	16.79	616.63	599.84	198.55
41.49	314.64	0.328	195.79	16.79	654.89	638.10	209.30
52.00	325.15	0.293	227.39	16.79	724.13	707.34	207.25

Table 26 - Total required heat transfer for different $T_{WG, avg}$ (filling ratio = 0.9, Ptank = 5.0 bar and reference design)

As can be seen in the table, the heat transfer differ by only 5.4 % for the three cases;, it is evident that the total heat rate transferred in the PBU $\dot{Q}_{needed}$ is not a limiting factor. The NG Engines should, depending on the heat transfer design before the water-glycol loop, be capable of delivering the temperatures needed for $T_{wg, avg}$ = 52 °C.

5.2.3 Ice formation on the tubes

The temperature difference between the warm and cold sides of the PBU at the LNG inlet is enormous. With the temperatures used in this work, the difference is 185 K - from $T_{WG, avg}$ = 32.85 °C (306 K) to $T_{LNG, in}$ = 121 K. At the PBU top, the difference is lowered to 79 K, if $T_{NG, out} = T_{return}$ is 227 K. The minimum NG return temperature set to be -46.15 °C (227 K), found from measured data in (DiRenzo 2014a), is below the freezing point of the 50 - 50 % water-glycol mixture, $T_{WG, freeze}$ = -33.97 °C (239.18 K) (see Chapter 2.3). Thus, there is a potential risk for ice formation on the tubes for the entire PBU. The filling ratio and tank pressure are therefore determining the ice formation risk through the $\dot{m}_{PBU}$, together with the system parameters $\dot{V}_{WG}$ and $T_{WG, avg}$.

The real amount of ice forming and the nature of the ice forming and melting outside the tubes are unknown due to the difficulties in conducting measurements as well as observing the inside of the PBU under normal operations. It is not even sure if the water-glycol mixture is forming ice on the coils or just turns into an ice-slurry flowing past the coils and melting again after leaving the PBU. (Cryomar 2015) stated that they had not experienced any problems caused by ice formation in the systems they had provided. This does not imply that there has not been any ice forming in the PBUs, only that the amount of ice have not impacted the operation of the systems noticeably. Ice formation is thus still a relevant topic, and a potential threat, especially if the heat rejected from the engines to the water-glycol loop is for any reason significantly reduced.

Measuring the water-glycol temperature in and out of the PBU gives an indication of the amount of heat transferred to the LNG, but not the complete picture. Since the temperature of the water-glycol mixture in the tube leaving the PBU may vary circumferentially, containing ice chunks or ice slurry, the real amount of heat rejected can vary significantly compared to that calculated from the averaged inlet and outlet temperature difference. Similarly, ice will melt inside the PBU and contribute to reducing the average water-glycol temperature, without increase in the LNG temperature. Due to the difficulties to predict the nature of ice and slurry formation and melting, these are not included in the further research in

this thesis. Nevertheless, both factors are of importance and should be investigated in a later project. What's remaining is the solid formation of ice on the tubes inside the PBU, for which some of the possible consequences are evaluated in this sub-chapter.

The first assumption made is that the solid ice is forming a homogenous layer around all the tubes inside the PBU. This would not be the case in practice, due to the above-mentioned temperature development of the LNG/NG through the PBU, but is a necessary simplification for simulation purposes. Further, no slush, melting or freezing are considered. The enthalpy released when the water-glycol freezes could either be transferred to the LNG or internally in the warm fluid. The ratio of the released heat by the formation of ice, which actually ends up transferred to the LNG, is rather difficult to predict. The same considerations applies for the melting and of the slush formation, for which the heat transfer contributions are not included in further work of this thesis.

A control system to avoid complete freeze-out of the PBU is installed on KV Bergen and is acting on the water-glycol outlet temperature. The ice is affecting the system in four ways: increasing h_o due to smaller cross sectional flow area for the water-glycol mixture and increasing A_o due to larger effective outer tube diameter $d_{tube,\,o,\,eff}$. On the other hand, the thermal conductivity of the additional layer is almost nothing compared with that for copper, $k_{WG,\,ice}$ = 0.415 W/mK compared to k_{copper} = 420 W/mK. The additional thermal resistance due to the ice forming is thus severe, irrespective of the ice thickness, reducing the overall heat transfer coefficient according to the equation for UA in Chapter 4.1. In Table 27 the consequences for an ice layer are represented by some important parameters for determining the heat transfer for the coiled section, along with the corresponding mass flow rate and the NG return temperature for a filling ratio of 0.9 and P_{tank} = 300 kPa. The conduction resistance per length unit for both the tube wall and the ice can be expressed as:

$$\text{Conduction resistance per length unit} = \frac{\ln\left(\frac{d_{tube,\,o}}{d_{tube,\,i}}\right)}{2\,\pi\,k_{copper}} + \frac{\ln\left(\frac{d_{tube,\,o,\,eff}}{d_{tube,\,o}}\right)}{2\,\pi\,k_{WG,\,ice}} \qquad (5.7)$$

t_{ice}	$(h_o A_o)$ per tube length	Conduction resistance for tube wall and ice per tube length	$\dot{m}_{PBU}$	T_{return}
			filling ratio = 0.9 P_{tank} = 300 kPa	filling ratio = 0.9 P_{tank} = 300 kPa
m	*W/mK*	*mK/W*	*kg/s*	*K*
0	23.68	$2.446 \cdot 10^{-5}$	0.242	220.58
0.0005	24.94	0.0118	0.277	179.37
0.001	26.25	0.0233	0.288	157.25
0.002	28.99	0.0452	0.342	131.21

Table 27 - Consequences of ice formation for the coiled section of the PBU (filling ratio = 0.9 and reference design)

From the table above, it is evident that no matter how much the $(h_o A_o)_{coil}$ increases due to ice formation, the conduction resistance dominates the heat transfer capability, when ice is forming on the tube walls. The NG return temperature is significant reduced for even the thinnest ice layer.

It must be stated, that the approach with non-varying homogenous ice formation on the tubes throughout the entire PBU, seems to be overestimating the consequences of ice formation. The ice would probably be formed locally and in the lower part of the coiled section of the PBU.

5.2.4 Thermal-control of the $\dot{m}_{PBU}$

On KV Bergen, the valve controlling the mass flow rate into the PBU is over-ruled by the water-glycol mixture outlet temperature of the PBU. A similar system can be installed for the NG outlet temperature from the PBU. By using a PID-valve, $\dot{m}_{PBU}$ can be controlled securing that T_{return} is larger than T_{target} = 227 K, or any other desired temperature, for any relevant tank and system condition. Thermal-governed PID-valves for securing the desired return temperature have recently been taken into use by the industry (Cryomar 2015). This is a comparatively small retrofitting, and it secures that no droplets enters the fuel tank. Thus, a potential source for enhanced condensation rates is avoided. Should the heat source become unstable, the mass flow rate is adjusted correspondingly. The same applies for the pressurization at high filling ratios and tank pressures, where the reference design (Table 11) used in this thesis for KV Bergen is not capable of delivering sufficiently high NG return temperatures.

Applying thermal control to the reference PBU design as described in Table 11, the effects are presented in Figure 36 and in Figure 37. In the first figure, the excess pressure for the flow returning into the tank is plotted. The red dashed tolerance level indicates the allowable deviation between the tank pressure and the pressure of the returning NG into the tank. For the pressure balance of the thermosyphon effect used in the simulation model when calculating $\dot{m}_{PBU}$, the tolerance level was fixed at 1.0 kPa.

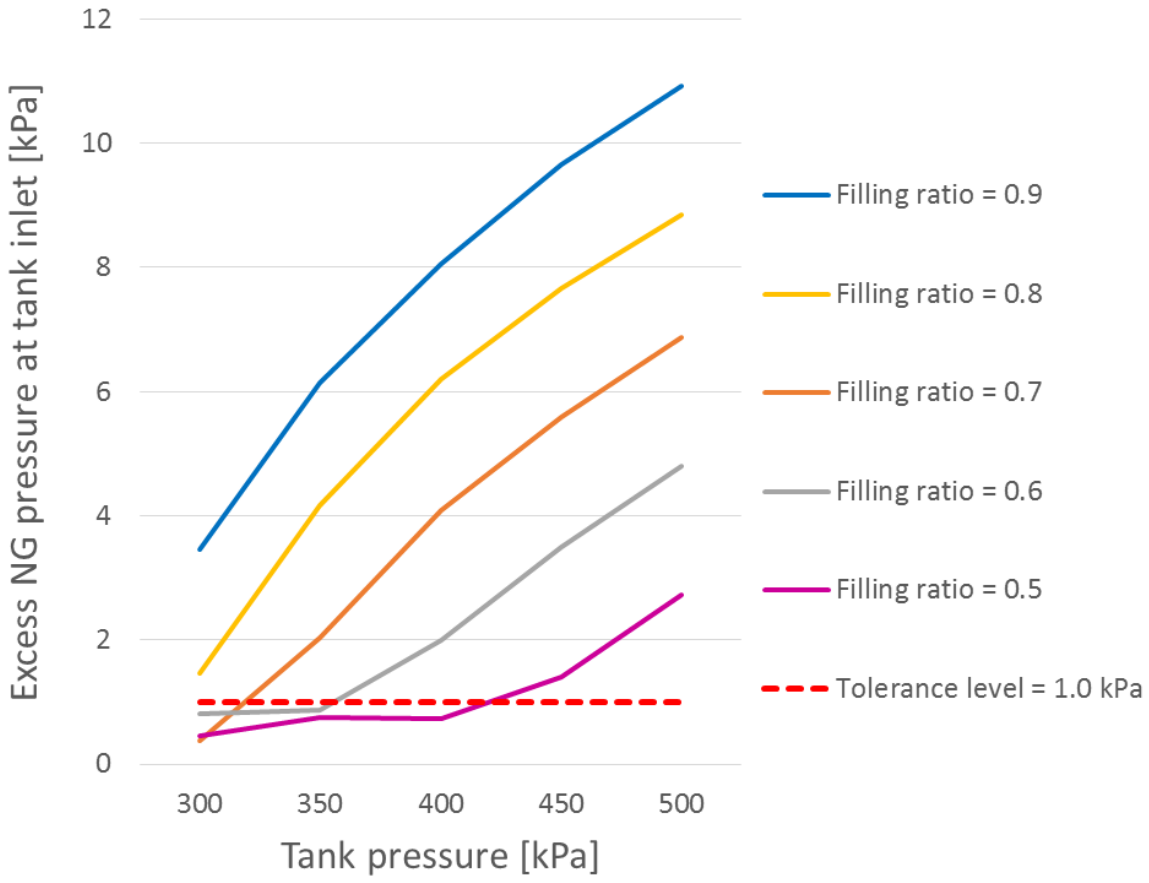

Figure 36 – Excess pressure for the flow at tank inlet when applying thermal PID-control $T_{return} \geq 227$ K (filling ratio = 0.9 and reference design)

The higher pressure of the returning flow is equalized when entering the fuel tank, which can induce mixing in the vapor section. The velocity of the returning NG into the tank contributes to determine the extent of mixing. For the highest filling ratio, the return velocity is lower for high P_{tank} than for lower P_{tank} and thus compensating for the larger pressure difference that must be equalized. The simulations give a return velocity of 16.19 m/s for P_{tank} = 500 kPa, which increases to 26.78 m/s for P_{tank} = 300 kPa. It is thus assumed that neither the pressure equalization for up to 11 kPa or 1-2 % of P_{tank} nor the entry velocity, contributes significantly to a mixing of the vapor, which can enhance the condensation rate.

Figure 36 of the excess pressure of the returning NG, indicates that the PID-controller does not affect the simulations with those tank conditions where the NG anyway is superheated to at least T_{target} = 227 K. This is indicated with the area below the dotted red line, where the returning NG flow is found for low filling ratios and P_{tank}. For all other simulations, the PID-controller must reduce the mass flow rate in order to keep the NG return temperature above T_{target}. The result is that the mass flow rate remains almost unchanged for filling ratio at high tank pressures P_{tank}, but vary significant with filling ratio at low P_{tank}, as shown in Figure 37.

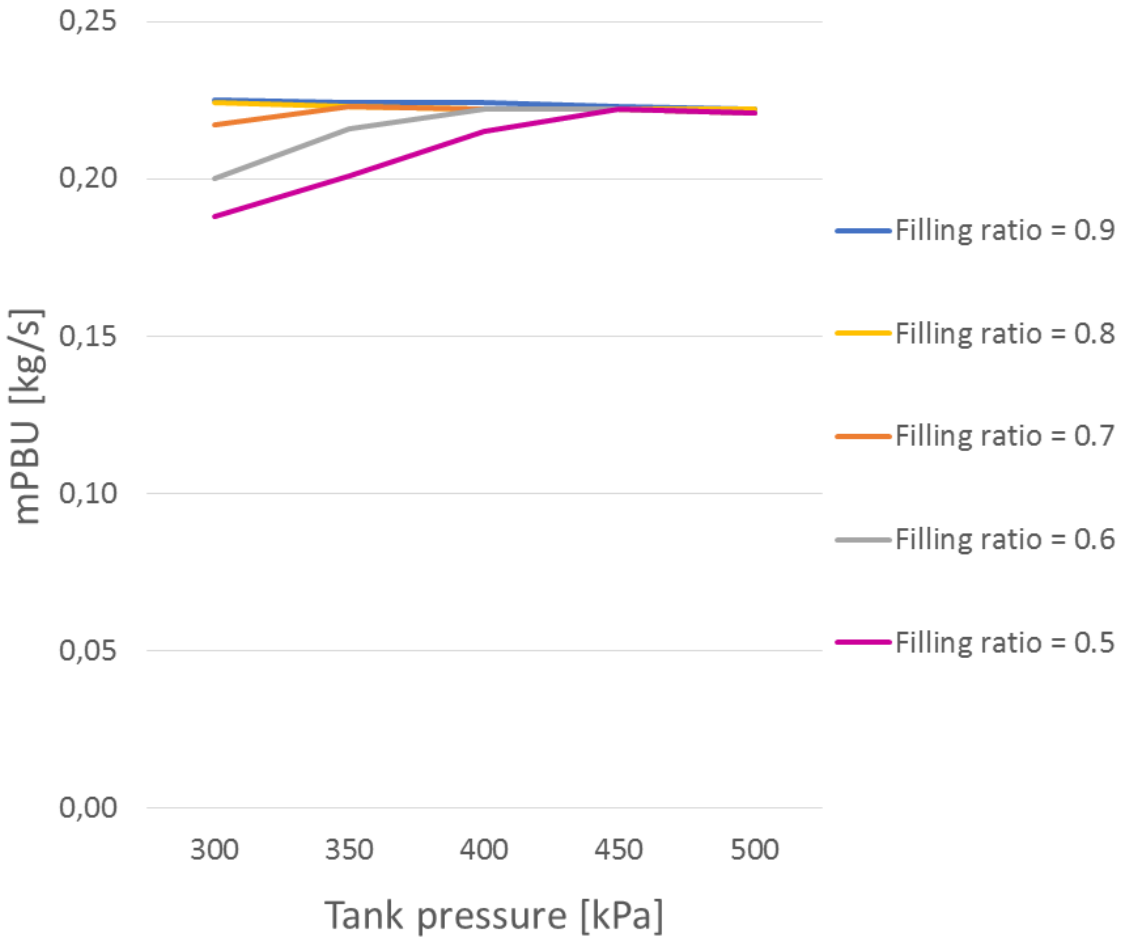

Figure 37 - $\dot{m}_{PBU}$ when applying thermal PID-control $T_{return} \geq 227$ K (filling ratio = 0.9 and reference design)

6 Passive and active measures to avoid engine de-loading

Further to modifying the PBU geometry and the system configurations as outlined in Chapter 5, actions can be taken in order to reduce the rapid drop in pressure inside the fuel tank. Some of these measures will be reducing the condensation rate, others will supplement the PBU and increase the pressure build-up capacity. Not all of them will in their own capacity be sufficient to fully eliminate the NG Engine de-loading risk, but they will all contribute to maintaining the pressure in the LNG fuel systems for ships exposed to rough sea.

Therefore, both active and passive measures need to be investigated for each vessel. Some measures imply significant investment costs and are thus primarily relevant for newbuilds. Others may involve smaller modifications, additions of equipment or changes in the set points of the control system. A combination of two or more of these measures will result in lower risk for de-loading; either by reversing the drop in pressure, slowing down the process until the vessel gets better coverage from the sea, or even removing the possibility for de-loading all together.

6.1 Nitrogen injection

If the drop in tank pressure is too large to be compensated by the conventional method using the PBU, or if the PBU for any reason is out of service, Nitrogen can be injected into the tank. This will trigger a rapid increase of the pressure caused by the increased density in the vapor region. The advantage of using Nitrogen as an inert gas is that vessels already possess a nitrogen infrastructure for purging of the LNG system. This will simplify a retrofitting of the LNG system. The Nitrogen capacity needed for KV Bergen and both the short and long term consequences of injecting larger amount of Nitrogen into the NG/LNG are reviewed below.

6.1.1 Required injection capacity

Most ships sailing using LNG as fuel, have a Nitrogen gas bottle battery onboard for purging purposes, as do both KV Bergen. From these bottles Nitrogen can be injected into the fuel tank if the tank pressure drops below a set value. Importantly, it operates fully independent of the PBU, which is important from an availability perspective. The amount of Nitrogen injected corresponds to what is needed in order to increase the tank pressure to an upper set point. In this thesis, these set points are chosen to be 3.8 bar and 5.5 bar, respectively. The lower set point must be somewhat above $P_{de\text{-}loading}$ = 3.6 bar, required to increase the pressure before the de-loading occurs. For the upper limit, the pressure is chosen more freely to be above the pressure for which the PBU on KV Bergen is de-activated, 4.95 bar (DiRenzo 2014a). If the PBU is not operational, it is recommended to include an extra safety margin for the pressure. This explains why the upper target is set half a bar above the PBU de-activation pressure.

The mass of Nitrogen needed for the pressure rise is calculated by applying the ideal gas law, adjusted with the compressibility factor z_{N2}. The procedure is chosen because the N2-injection is assumed to be so rapid that the Nitrogen does not have time to interact with the liquid in the tank. In addition, the higher temperature of the Nitrogen than for the NG will establish a NG buffer layer between the colder LNG and the warmer Nitrogen, hindering enhanced mixing (Ludwig, Dreyer et al. 2013). Utilizing that the number of moles is corresponding to the partial pressure of the added Nitrogen, an equation for the required injected Nitrogen mass is given by:

$$m_{\mathrm{N2,\ inert}} = \frac{(p_{\mathrm{upper\ target}} - p_{\mathrm{lower\ limit}})\ V_{\mathrm{vapor}}}{Z_{\mathrm{N2}} \frac{\bar{R}}{M_{\mathrm{N2}}} T_{\mathrm{tank}}} = \frac{(550kPa - 380kPa)\ V_{\mathrm{vapor}}}{Z_{\mathrm{N2}} \frac{\bar{R}}{M_{\mathrm{N2}}} T_{\mathrm{tank}}} \quad (6.1)$$

Throughout the pressurization, the vapor temperature increases according to the increased vapor density and pressure. For each small incremental addition of Nitrogen, the new temperature was calculated by NIST REFPROP, along with the compressibility factor z_{N2}.

Table 28 gives the required Nitrogen for the pressurization from 3.8 bar to 5.5 bar, with different filling ratios. From the bunkered LNG composition given in Table 9, the molar fractions prior to the N2 injection was found from vapor-liquid equilibrium at 3.8 bar. The molar fraction of Nitrogen in the vapor-phase was 6.55 mole % before and 35.17 mole % after. These values are independent of filling ratio and injected mass, as the increase in pressure is the same. The initial vapor temperature used is the vapor saturation temperature at 3.8 bar.

Filling ratio	**m_{N2} injected**
-	*kg*
0.5	327.8
0.6	244.9
0.7	165.5
0.8	93.4
0.9	34.2

Table 28 - Required mass of Nitrogen for pressurizing the fuel tank on KV Bergen from 3.8 bar to 5.5 bar for varying filling ratio

A typical vessel using Nitrogen for purging purposes has 12 gas bottles put in a battery. A standard bottle contains 50 L Nitrogen at 200 bar. Due to pressure losses from the bottle to the tank, it is only possible to utilize the gas until a pressure level of approximately 10 bar is reached. Assuming an ambient temperature of 15 °C (288 K) and a 190 bar pressure reduction, each bottle can deliver 11.17 kg of Nitrogen according to Equation 6.2. Thus, in

order to increase the pressure from 3.8 bar to 5.5 bar with a filling ratio of 0.9, 3.1 bottles are required according to the results in Table 28.

$$m_{\mathrm{N2,bottle}} = \frac{(p_{full} - p_{\mathrm{exploited}})\, V_{\mathrm{vapor}}}{Z_{\mathrm{N2}} \frac{\bar{R}}{M_{\mathrm{N2}}} T_{\mathrm{ambient}}} = \frac{(20MPa - 1MPa)\ 0.05m^3}{Z_{\mathrm{N2}} \frac{\bar{R}}{M_{\mathrm{N2}}} 288K} \tag{6.2}$$

Already at a filling ratio of 0.8, 8.4 bottles must be used, which makes Nitrogen injection more of a once-per-voyage option using the existing onboard Nitrogen storage capacity. Reducing the target pressure down to 5.0 bar, 24.2 kg of Nitrogen or 2.2 bottles are needed at a filling ratio of 0.9 and 66.0 kg or 5.9 bottles at a filling ratio of 0.8. This reduction of the pressurization requirement does not solve the problem with too little Nitrogen in a "12 bottle battery". It is still insufficient to make Nitrogen injection a reliable means to prevent multiple critical drops in pressure. One bottle can increase the pressure with 38.37 kPa respectively 19.18 kPa for filling ratios of 0.9 and 0.8, given an initial vapor temperature equal the saturation temperature for 3.8 bar 205.5 K. If the filling ratio should be significantly lower, for example 0.5, one N2-bottle would only rise the pressure with 7.67 kPa. This implies that a total of 29.4 bottles are needed for the pressurization from 3.8 bar to 5.5 bar. For higher initial vapor temperatures, the pressurization effect of each bottle is slightly higher. If the vapor kept on average 227 K, the effect would be 38.46 kPa and 19.23 kPa (instead of 38.37 kPa and 19.18 kPa) for the same filling ratios. Thus, initial NG temperatures above the saturation point give only a negligible pressurization contribution and it is therefore not further investigated.

In order to make Nitrogen injection a useful means for preventing de-loading, the ship owner has the option to add more Nitrogen bottle batteries on the vessel, or install an air-separation unit to produce the Nitrogen onboard. The latter would cost somewhere in the range of 1.2 -1.5 mill NOK and would be accompanied with a N2-storage tank (Cryomar 2015). According to the same company, over time this will be a cheaper solution than the use of Nitrogen bottle batteries. Thanks to less hassle when replacing empty N2-bottles, a well-functioning air-separator unit can save some time for the crew when using the Nitrogen system.

A Nitrogen tank should be large enough to contain enough gas to handle a series of pressurizations at low filling ratios. Three pressurizations at a filling ratio of 0.5 should contribute to a significant reduction in the de-loading risk. A total of 983.4 kg Nitrogen would than be needed. The corresponding Nitrogen tank must have an inner tank volume of 4.41 m^3 when applying the same constraints on the tank as for the bottles: the tank only can be depleted to 10 bar, a final pressure of 200 bar and an ambient temperature of 15 °C. Both the deck area and volume needed are small compared to that for the LNG fuel tank and accompanying systems, but nevertheless significant.

Since the de-loading risk is most threatening at high filling ratios, a Nitrogen tank capacity designed to handle a sequence of three pressurizations at a filling ratio of 0.7 should be sufficient. This would require 496.5 kg Nitrogen and an inner tank volume of 2.23 m^3, with same conditions as above. Most of the times when Nitrogen is expected to be used for pressurization, the filling ratio should be higher than 0.7, thus increasing the number of consecutive pressurizations possible for the above mentioned inner tank volume.

6.1.2 Consequences of injecting Nitrogen

For increasing concentrations of the Nitrogen, the heating value of the fuel is reduced as Nitrogen has a heating value of zero. Furthermore, for the changing compositions, the liquid saturation temperature determining the boundary layer conditions at the liquid-vapor interface, will change. Adding Nitrogen will decrease $T_{sat,\ liq}$, which again will influence the condensation rate, as described in the equation 4.72 in Chapter 4.9.

Compared to the large mass of the LNG, the injected Nitrogen from a single pressurization does not constitute a challenge. Variations in the Nitrogen content of the LNG are larger; suppliers can add Nitrogen in order to adjust the heating value of the LNG according to the different countries requirements, resulting in a Nitrogen concentration of up to 3 mole % (Coyle 2007). The LNG used in this paper contains only 0.5 mole % Nitrogen. The Nitrogen vapor will start to mitigate into the LNG in order to establish equilibrium for the Nitrogen between the two phases. Therefore, if this back-up system for pressurization is used frequently, an accumulation of Nitrogen in the fuel tank may occur, causing some of the challenges described above.

As described in the previous sub-chapter, the molar fraction of Nitrogen in the vapor is 35.17 % immediately after the described pressurization, irrespective of filling ratio. This is valid for the initial LNG composition given in Table 10. As time passes, and the Nitrogen in the vapor section starts to mitigate into the liquid LNG in order to establish equilibrium between the two phases for the Nitrogen. After a series of Nitrogen pressurizations, the system will gradually be affected. Table 29 gives the development of the molar concentration for Nitrogen in the bulk LNG when a tank with filling ratio = 0.9 is pressurized from 3.8 bar to 5.5 bar multiple times. Between each pressurization, the Nitrogen is allowed to mitigate into the LNG and establish equilibrium.

Injection number	Molar concentration of N2 in the bulk LNG
0	0.50 %
1	0.52 %
2	0.55 %
5	0.62 %
10	0.75 %
20	1.02 %
30	1.31 %
50	1.92 %
82	3.03 %
100	3.72 %

Table 29 - Development of Nitrogen in the bulk LNG for multiple N2-pressurizations from 3.8 bar to 5.5 bar with filling ratio = 0.9

As the table shows, the Nitrogen concentration in the bulk LNG increases very slowly. First after 20 pressurization cycles has the molar concentration doubled from 0.50 % to 1.02 %. In order to reach the 3.0 % - limit recommended in (Coyle 2007), 82 pressurizations are necessary. Thus, it should be safe to conclude with that injecting Nitrogen does not affect the fuel noticeable and is thus a safe method for rapidly increasing the tank pressure.

A consequence of higher Nitrogen concentrations in the fuel is larger Nitrogen emissions, NO_x from the NG Engines. Since the engines are operating with air containing about 79 mole % Nitrogen, the extra emissions of NO_x due to Nitrogen pressurization is negligible, also in an ECA (Emission Control Area) context as described in Chapter 1. This should thus not prevent the use of Nitrogen as a NG Engine de-loading preventer.

6.2 Increased LNG temperature at bunkering / Bunkering warm LNG

From the equation determining the condensation rate presented in Chapter 4.9, the condensation rate is proportional to the temperature difference between the bulk LNG and the liquid saturation temperature at the tank pressure. Thus, $\dot{m}_{con}$ should decrease with warmer LNG bulk, as the temperature difference is reduced. Confirming this theory, (Cryomar 2015) states that when bunkering warm LNG on ships using their design, the condensation rate decreases compared to cold bulk LNG.

The de-loading events on KV Bergen occurred shortly after bunkering (DiRenzo 2014a), thus little heat is added to the LNG/NG through the PBU. When operating the PBU, heat is added to the system and contributing to heat the bulk LNG. Thus, if the PBU is allowed to operate for an extended period of time, significant heat can be added and thus reducing the condensation rate, as described above. (Cryomar 2015) presented test results for an LNG-fueled vessel operating on the Norwegian coast. When the vessel shortly after bun-

kering was exposed to rough sea and heavy rolling, a rapid drop in P_{tank} was experienced despite an active PBU. For a tank of 398 m^3 with a filling ratio of 0.857, P_{tank} dropped by 2.1 bar, from 6.2 bar to 4.1 bar, in 14 minutes. At this filling ratio, the PBU, which was active, is able to increase the pressure with 1 bar per 10 minute at calm sea. After allowing the PBU to operate for 12-15 hours, there was no signs of a notable drop in pressure when rolling in rough sea, even though the PBU was de-activated. During the test in rough sea, both with and without the PBU operative, exact temperatures for neither the LNG nor the NG could be presented. The important aspect to investigate is the effect on the drop in pressure and the pressurization when applying warmer bulk LNG, irrespective of the LNG has been heated before bunkering or heated by operating the PBU.

The LNG used as reference in this thesis, kept -152.15 °C (121 K) when bunkered. In a measurement documented by DiRenzo, the LNG bulk temperature was 147.95 °C (124.2 K). (Cryomar 2015) reported that upfront a bunkering of a ship, the LNG temperature in the fuel tank was approximately -135 °C (138.15 K). Keeping these temperatures in mind, the effect of T_{bulk} on the pressure development is assessed for relevant temperatures and the corresponding liquid saturation pressures given in Table 30.

T_{bulk} *[K]*	$P_{sat,\ liq}(T_{bulk})$ *[kPa]*
118	175.52
121	215.04
124	261.00
127	314.00
130	374.68
133	443.68
136	521.62

Table 30 - LNG bulk temperatures with corresponding liquid saturation pressures (LNG composition given in Table 9)

The absolute minimum pressure in the tank is the liquid saturation pressure of the fluid. At tank pressures lower that $P_{sat,\ liq}$, the liquid would start to evaporate in order to establish equilibrium. A complete mixing of vapor and liquid in a fuel tank will result in the minimum possible tank pressure, as modeled in the project work (Hernes 2014). After complete mixing, the final P_{tank}, was slightly larger, a few kPa, than the $P_{sat,\ liq}$ for the bulk LNG temperature. Thus, for the scope of this thesis, to present different solutions to avoid de-loading of the NG Engines, one possibility is to keep the LNG temperature sufficiently high. For the LNG composition used, T_{bulk} = -143.15 °C (130 K) secures a minimum pressure of 374.67 kPa, which is above $P_{de\text{-}loading}$ = 360 kPa. Actually, securing an LNG bulk temperature high enough that $P_{sat,\ liq}$ is higher than the required pressure at the GRU inlet on the vessel, would solve the entire de-loading challenge.

Since the condensation rate is equated being proportional to the difference between $T_{sat,\,liq}$ and T_{bulk} in Equation 4.72 in Chapter 4.9, any rise in temperature for T_{bulk} will reduce the condensation rate if P_{tank} is fixed. Thus, in addition to increase the minimum possible pressure, an increase in T_{bulk} would also reduce the condensation mass flow rate. As shown in Table 30, a small increase in T_{bulk} results in a sharp increase in $P_{sat,\,liq}$ and correspondingly lower $\dot{m}_{con}$.

Keeping the pressure range used on KV Bergen for the LNG fuel system, the LNG bulk temperature can be increased up to 133 K. At higher temperatures, the saturation pressure exceeds the existing operation pressure on the vessel. For the relevant T_{bulk}, the NG return temperature for tank pressures of 400 kPa to 500 kPa are presented in Figure 38. Otherwise, the reference design (Table 11) is applied for all other parameters. As shown, the NG temperature increases rapidly, almost with one degree Kelvin per degree Kelvin increase for the T_{bulk}. When the NG return flow is fully evaporated (as for T_{bulk} = 130 K and P_{tank} = 400 kPa), it is evident that the T_{return} increases significantly. For T_{bulk} = 133 K, the saturation pressure is 444 kPa, therefore is not the NG return temperature at 400 kPa plotted.

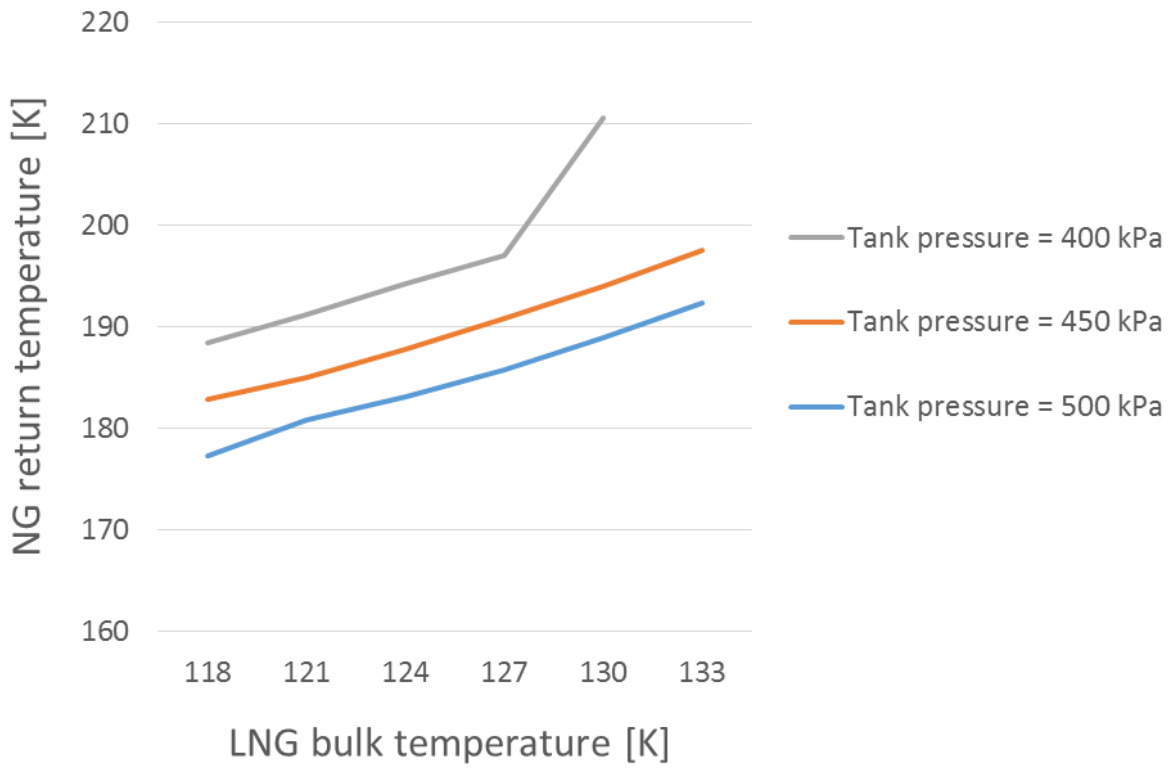

Figure 38 - NG return temperature for various LNG temperatures with different high P_{tank} (filling ratio = 0.9 and reference design)

LNG bulk temperatures from -137.15 °C (136 K) and above will demand higher operational pressures than used on KV Bergen. Raising the operation pressure from 4.0 - 5.0 bar to 6.0 - 7.0 bar will not be difficult, but will require some modification of the LNG evaporation

system. The fuel tank is classified to handle up to 9.0 barg (Table 4) and the GRU will reduce the pressure before the NG enters the engines. As the figures presented in Chapter 5 show, the $\dot{m}_{PBU}$ increases for higher P_{tank}, independent of PBU geometry or system modifications. Thus, with more heat required for heating the additional LNG, the thermal capacity of the PBU must be increased. This can be done through combining the different parameters discussed in this thesis. A possible combination is increasing the overall PBU size through the coil height together with a thermal governed PID-controller securing $T_{return} > T_{target}$.

As the evaporation capacity increases with higher P_{tank} and larger $\dot{m}_{PBU}$, the condensation rate does also become higher. The explanation is that $T_{sat,\,liq}$ increases for higher P_{tank}, and that the condensation rate is proportional to the difference between $T_{sat,\,liq}$ and T_{bulk} (Equation 4.72 in Chapter 4.9). Thus, for higher P_{tank}, $\dot{m}_{con}$ increases somewhat which the PBU must compensate for. In return, any drop in pressure below $P_{de\text{-}loading}$ will take longer time as more vapor must condense.

It must be stated that when bunkering LNG with a temperature close to the saturation temperatures for the desired operational tank pressure, T_{bulk} might after a long time increase above the saturation temperature. This can happen both due to the heat added by the PBU and due to the heat in-leakages to the tank (which are not included in this work), resulting in evaporation of the LNG and an undesired natural pressurization of the tank. If P_{tank} rises to high, the excess vapor must be vented off, which represents both a loss in fuel and thereby money, and increased emissions.

6.3 Assisted pumping

For the NG Engines the pressure inside the fuel tank does not matter as long as the pressure at the GRU inlet is high enough. By inserting a cryogenic pump, it is possible to avoid the requirement of a minimum pressure inside the tank when using the NG Engines. The pump lifts the pressure of the LNG before use; consequently the challenge with sudden rapid drops in pressure and de-loading of the NG Engines can be completely avoided. Locating the pump between the fuel tank and the fuel vaporizer, the PVU, the LNG will always enter the PVU with minimum $P_{de\text{-}loading}$ = 3.6 bar, or a higher preferred operating pressure. The pump can either be used in addition to the conventional PBU-system, by operating the pump in parallel whenever the tank pressure is too low, or as the sole pressure builder in the entire system. Both are discussed below.

The capacity of a cryogenic pump supplying the PVU with LNG to the NG Engines does not need to be large. The PVU is designed for a maximum LNG flow rate of 0.45 kg/s (Cryo AB 2012), and an 88 % engine load on KV Bergen (2200 kW) demands 0.159 kg/s of LNG (Hernes 2014). With an LNG temperature of 121 K and P_{tank} = 4.60 bar, the fuel density from the tank is 427.3 kg/m^3, resulting in a volumetric flow rate of 0.371 L/s through the pump. Similarly, for the PVU's maximum capacity of 0.45 kg/s, the volumetric flow rate is 1.053 L/s. Thus, the required pump capacity for lifting 1 L/s a few bars does not a provide any difficulties.

Applying pumps is reported by two sources, one of them (Cryomar 2015), and it was installed on at least one vessel by a Norwegian supplier. The main disadvantage of applying a pump is that it contains rotating machinery, which adds to the maintenance, both man hours and other costs. Lower operating hours per year will reduce maintenance costs for the pump. This can be achieved by only using the pump when the PBU is not able to secure the required operating pressure. However, this requires a parallel piping system between the fuel tank and the PVU, which results in higher investments. It could be possible to reduce the PBU size and capacity somewhat due to the security of the pump, but this would again lead to more operational and maintenance (O&M) costs of the system securing the required pressure.

By operating the pump as the sole pressurizer, the PBU could be omitted. This would reduce the investment costs, but increase O&M costs as the pump is operating whenever the NG Engines are running. Due to the lower availability of a pump than the PBU, a second pump working in parallel must be considered. This would lower the potential reduction in investment cost compared to the design used on KV Bergen.

The equipment will be bulky and increase the already large footprint of the LNG system, which is a disadvantage compared to conventional fuel systems. (Cryomar 2015) stated that it is possible to avoid NG Engine de-loading by installing a pump between the fuel tank and the PVU, but did not recommend the solution due to higher investment and O&M costs and lower availability than other “de-loading preventers”.

6.4 Reducing the NG Engine load

Actually, the de-loading pressure is not a fixed value for a given LNG fuel and engine system. The stated de-loading pressure in (DiRenzo 2014a) of 3.6 bar, is correct for a full engine trial. Thus, if at least one of the four NG Engines are running with 100 % load, P_{tank} must be above 3.6 bar. (Cryomar 2015) stated that for lower loads, the required pressure at the GRU inlet is reduced. Under normal NG Engine operation, the total load will be divided between the available engines and thus the $P_{de\text{-}loading}$ will be somewhat lower.

If the tank pressure is observed to start falling rapidly during operation, the total load on the NG Engines can be reduced and thus lowering $P_{de\text{-}loading}$. This procedure will at least give the crew more time to stabilize the P_{tank} before it drops below $P_{de\text{-}loading}$.

As presented in Chapter 6.2, the minimum pressure in the tank is linked to the LNG bulk temperature through the liquid saturation pressure. Depending on how much the engine load can be reduced, with the corresponding $P_{de\text{-}loading}$ and the T_{bulk}, it is possible that the $P_{de\text{-}loading}$ becomes lower than $P_{sat,\,liq}$. This means that by reducing the engine load, a de-loading event can be avoided, both due to the extra time provided for the crew to stabilize P_{tank} and if the T_{bulk} is sufficiently high, that $P_{sat.\,liq} > P_{de\text{-}loading}$. The liquid saturation pressures given in Table 30 in Chapter 6.2 indicate that T_{bulk} should be above 127 K if the $P_{de\text{-}loading}$ can be reduced down to 3.1 bar for low loads. This is only an estimated value. Neither the Engine producer (Mitsubishi Heavy Industries 2014) nor the LNG system provider (Cryo AB 2012) outlines the required pressure at the GRU inlet for reduced NG Engine loads.

Reducing engine loads may contribute to avoiding de-loading events, but the method is not recommended lacking sufficient knowledge of the required pressures for all NG Engine loads. Only when coupling an engine load directly to the de-loading pressure in the fuel tank, the target of significantly reducing the engine de-loading risk can possibly be met. Nevertheless, the concept still depends on a sufficiently high liquid bulk temperature in the fuel tank.

7 Results and discussion – pressure development

The research presented in Chapter 5 and Chapter 6 was not conducted in order to find the $\dot{m}_{PBU}$, the NG return temperature and the pressurization rate for their sole purposes, but to integrate them with the pressure development model outlined in Chapter 4. The focus for the pressure development simulations is to prevent P_{tank} from dropping below the de-loading pressure of the NG Engines. Thus, the objective of this chapter is to evaluate the results from the sensitivity analysis and describe how the pressure develops in the fuel tank on KV Bergen for different tank conditions and sloshing regimes. This deduction leads towards the conclusions in Chapter 9.

7.1 Pressure build-up capacity of the PBU

When including an active PBU in the pressure developments in order to compensate for the condensation, a PBU geometry and system design that is capable of delivering dry NG above T_{target} to the tank, must be chosen. Comparing the resulting $\dot{m}_{PBU}$ and NG return temperature for the parameter changes described in Chapter 5, only those that returned dry vapor above T_{target} for filling ratio = 0.9 and P_{tank} = 500 kPa have been included in Figure 39 and in Figure 40, together with the reference design. Departing from the parameters suitable for modifications listed in Table 18, the following design variations from the reference design achieved $T_{return} \geq 227$ K: $d_{tube,\,i}$ = 0.04 m, z_{coil} = 0.60 m, $\dot{V}_{WG}$ = 120 m^3/h and $T_{WG,\,avg}$ = 52 °C. Neither decreasing the wall spacing nor switching to a dual-twinned coil design secured T_{return} above the desired NG return temperature. No combination of the parameter modifications has been evaluated at this point; only the effect of one parameter at the time.

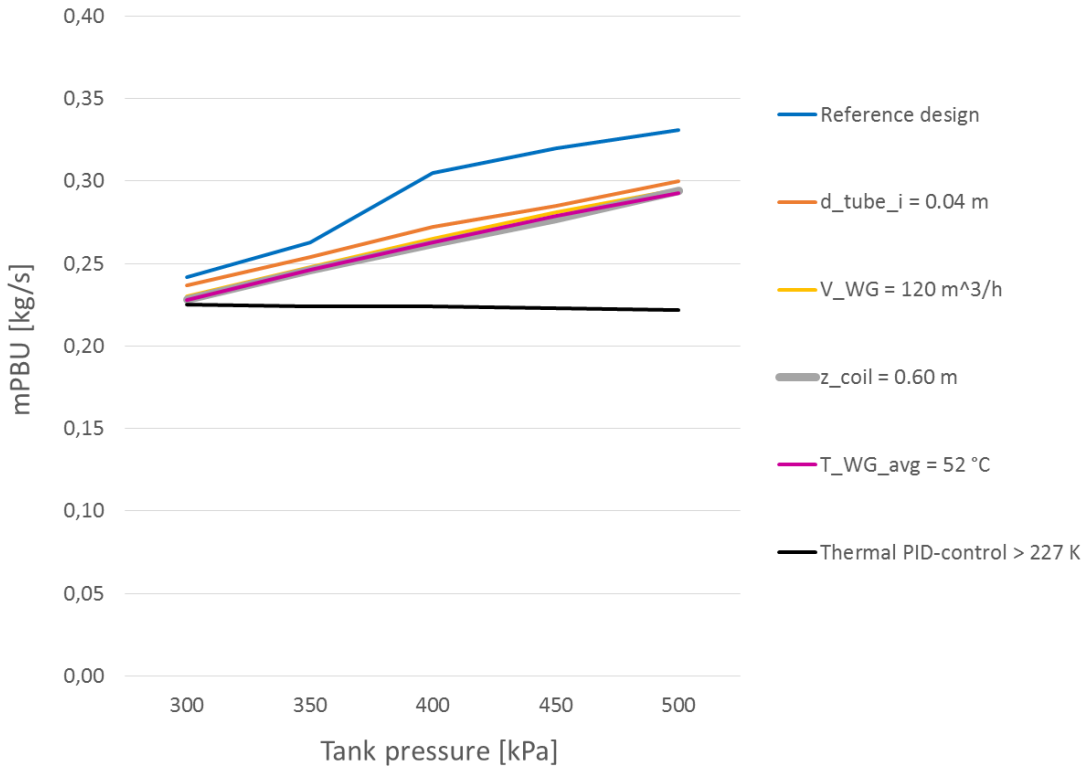

Figure 39 - $\dot{m}_{PBU}$ for selective parameters modified from the reference design (filling ratio = 0.9)

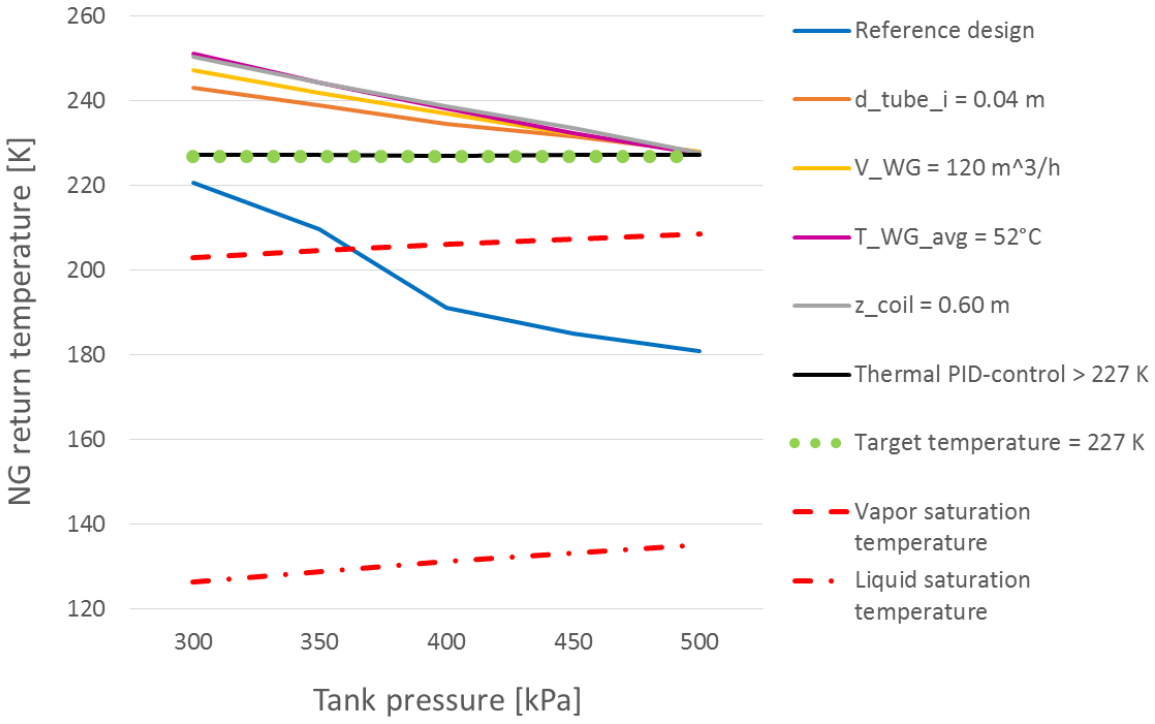

Figure 40 - Comparison of NG return temperatures for selective parameters modified from the reference design (filling ratio = 0.9)

As can be seen from the two figures, the four selected PBU designs and operational conditions result in similar curves, both with respect to the $\dot{m}_{PBU}$ and with respect to the NG return temperature. Neither of the modifications changes the pressure build-up capacity significantly from the others, thus from a thermodynamically perspective it does not really matter which of the configurations is used for the pressure development simulations. Avoiding the higher or lower curve for T_{return} in Figure 40, a system modification of $\dot{V}_{WG}$ = 120 m³/h has been chosen for the pressure development simulations. Economical, technical and practical differences were not considered in this process, but must be included when the best modifications shall be chosen for a vessel.

The LNG system is most vulnerable for de-loading events at the highest filling ratios (Chapter 1.3); therefore the resulting $\dot{m}_{PBU}$ and T_{return} for a filling ratio of 0.9 and different tank pressures are given in Table 31.

P_{tank} [kPa]	$\dot{m}_{PBU}$ [kg/s]	T_{return} [K]
300	0.230	247.38
350	0.248	242.02
400	0.265	236.94
450	0.281	232.22
500	0.295	227.97

Table 31 - $\dot{m}_{PBU}$ and T_{return} for relevant tank pressures with $\dot{V}_{WG}$ = 120 m³/h (filling ratio = 0.9 and reference design)

A second choice regarding the PBU and system design could have been implementing a thermal governed PID-controller and thereby secured the desired T_{return}. As discussed in Chapter 5.2.3, this solution does not increase the heat transfer in the PBU, but simply decreases the mass flow rate. The consequence is a lower pressurization capacity than for the other design modifications presented in Figure 39 and in Figure 40, in terms of both averaged lower $\dot{m}_{PBU}$ and T_{return}.

As drop in pressure is predominantly caused by some sort of sloshing inside the fuel tank, breaking up the thermal conductivity layer at the liquid-vapor interface. The pressure development for the fuel tank on KV Bergen will be investigated for varying sloshing with the different pressure drop compensation measures discussed in Chapter 5 and in Chapter 6. Before implementing sloshing into the model, Figure 41 shows the pressurization from 299 kPa to 495 kPa of the fuel tank on KV Bergen in calm sea for three different filling ratios. This contributes with knowledge of the pressure build-up capability of the system. In dashed lines are the corresponding pressurization capability with the thermal governed PID-controller.

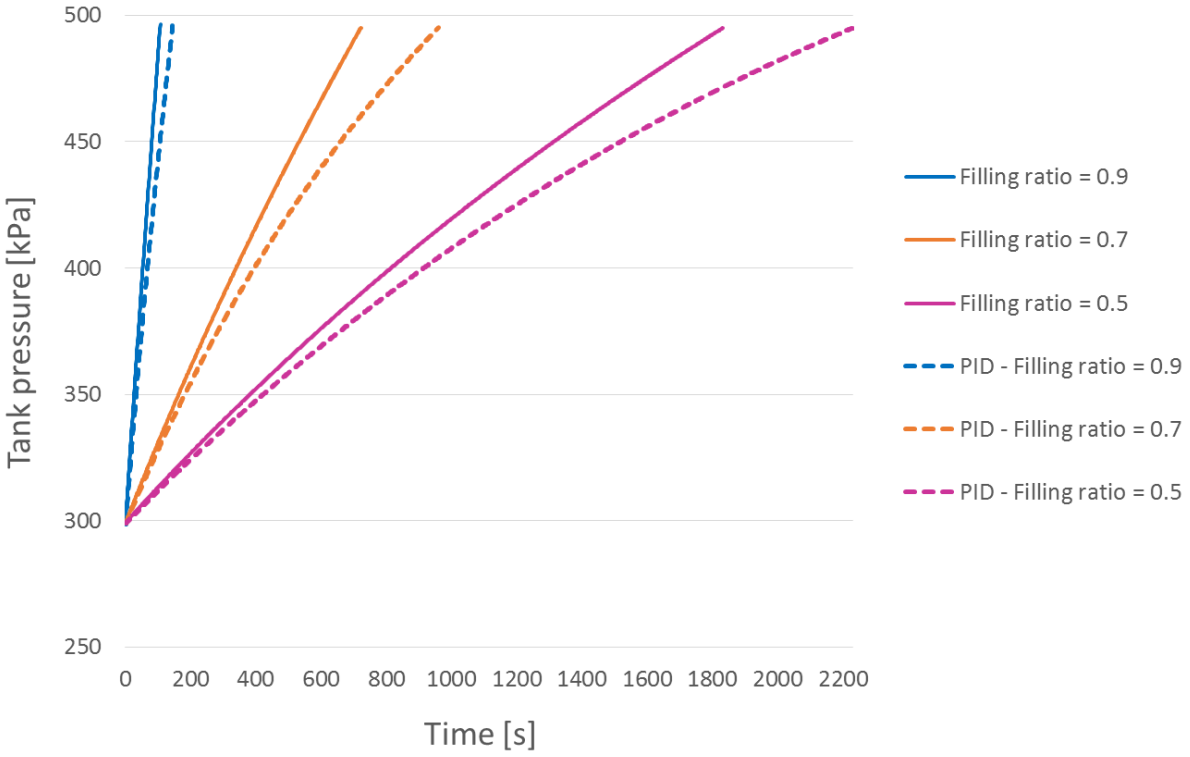

Figure 41 - Pressurization from 299 kPa to 495 kPa on KV Bergen in calm sea, comparing $\dot{V}_{WG}$ = 120 m^3/h with thermal PID-control for different filling ratios

The pressurization is highly sensitive to filling ratios from 107 s, at a filling ratio of 0.9 compared to 1832 s for a half full tank. This is the same trend as described in Figure 16 (Chapter 4.7) for the drop in pressure on KV Bergen for calm sea when the PBU was de-activated. The pressurization takes longer time at low filling ratios for three reasons, a larger vapor section to pressurize, a larger area where condensation occurs, and lower $\dot{m}_{PBU}$ due to the lower

hydrostatic “driving force” of the thermosyphon. The pressurization lines in the figure bends slightly as the pressurization becomes more demanding for higher P_{tank} with increased condensation rate with higher $T_{sat,\,liq}$.

Comparing the pressure build-up capacity when applying the thermal governed PID-controller contra boosting the heat transfer rate with higher $\dot{V}_{WG}$, it is obvious that the pressurization in Figure 41 takes longer time when the mass flow rate is reduced. As the filling ratio is lowered, the relative difference in pressurization time is reduced from 36 % for a filling ratio of 0.9 to 22 % for a half-full tank.

Unless otherwise stated, all pressure developments presented in this chapter are based on a filling ratio of 0.9, a condensation rate corresponding to $\chi_{conduction,\,eff}$ = 0.00123 m (Chapter 4.8) and with a PBU capacity given in Table 31 above.

7.2 Sloshing in the reference case

When introducing sloshing into the system, the partly destruction of the thermal conductivity layer at the liquid-vapor interface is included in the pressure development simulations. Combining the pressurization capacity presented in Figure 41 and with the sloshing factor (SF) and thus the destruction ratio (DR), both described in Chapter 4.9, the pressure development for a tank with an initial pressure of 500 kPa is shown in Figure 42.

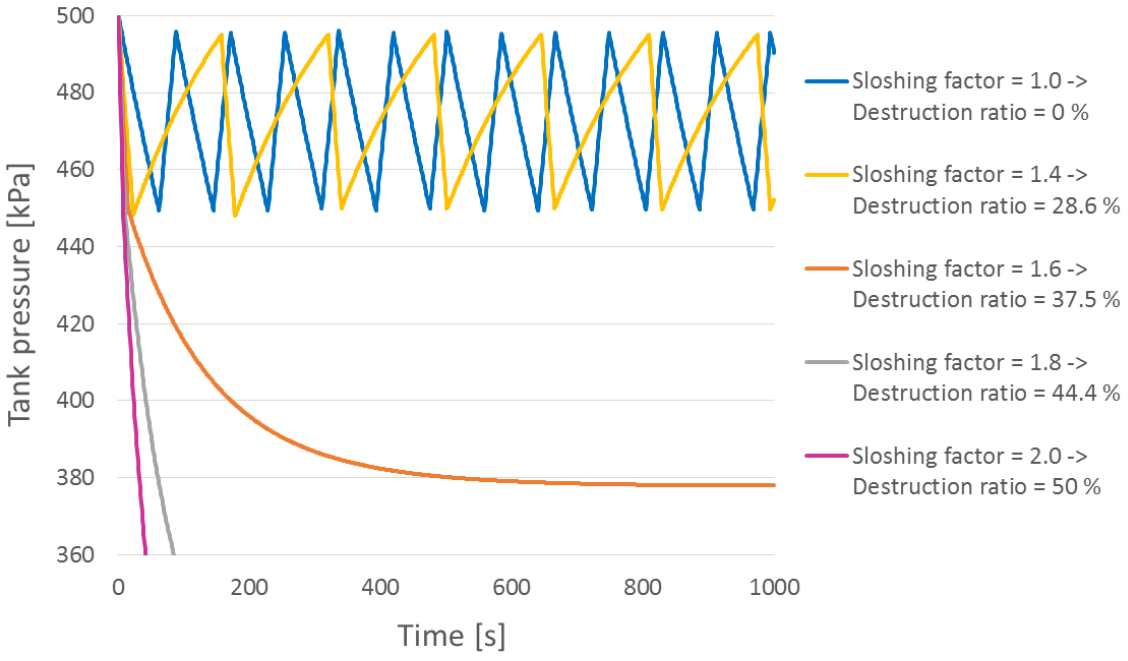

Figure 42 - Pressure development for varying sloshing factor (filling ratio = 0.9 and $\dot{V}_{WG}$ = 120 m³/h)

Figure 42 reveals that sloshing severely enhances the condensation rate and thus the pressure drop in the fuel tank. For small in-tank motions with low sloshing factors, the PBU is capable of fully compensating the condensation. The pressure fluctuates between 450 kPa and

495 kPa, the on-set respectively and off-set of the PBU, with increasing time span for the pressurization and decreasing time span for the pressure reduction with increasing SF. For high sloshing factors, the PBU is far from being capable of compensating for the condensation and prevent P_{tank} from dropping below $P_{de\text{-}loading}$. In between, there is a range of sloshing factors that results in condensation rates exactly matching the pressure build-up capacity of the PBU for specific tank pressures. Therefore, P_{tank} will be stabilized for a value higher than $P_{de\text{-}loading}$. Of particular interest is the sloshing factor that gives a stabilized P_{tank} as close as possible to $P_{de\text{-}loading}$. For the case presented above, the maximum fluid motion in the tank corresponds to a sloshing factor of 1.64, as illustrated in Figure 43. In other words, for sloshing ratio not exceeding 1.64, no de-loading of the NG Engines will occur for this specific case.

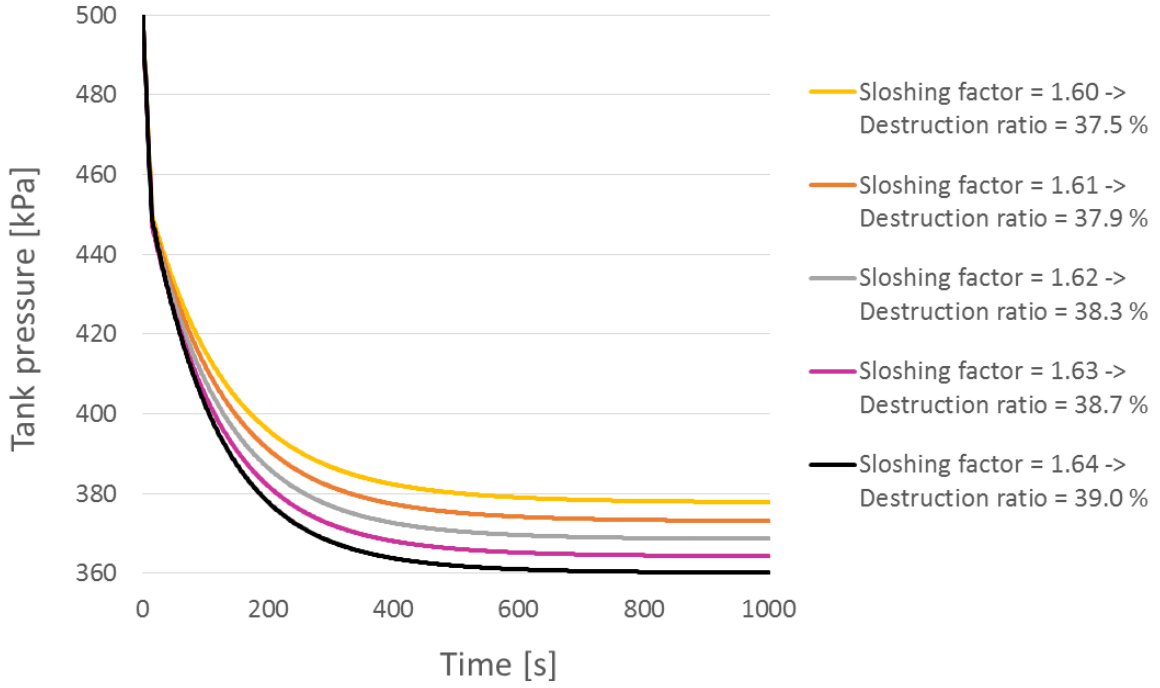

Figure 43 - Pressure development for varying sloshing factor – Balancing $P_{de\text{-}loading}$ with SF (filling ratio = 0.9 and $\dot{V}_{WG}$ = 120 m³/h)

If the effective thermal conductivity layer thickness $\chi_{conduction,\ eff}$, the sloshing factor or the destruction ratio is modeled otherwise than described in this thesis, a different sloshing factor would result in a stabilized $P_{tank} = P_{de\text{-}loadin}$ for the system conditions presented above based on the reference design and $\dot{V}_{WG}$ = 120 m³/h.

For simulations conducted with lower filling ratios, the same trends as presented in Figure 42 will be found.

7.3 Pressure development with warmer LNG

The stabilizing situation for P_{tank} described in the previous chapter is determined by the varying condensation rate, since the evaporation capacity is not affected by the sloshing. If the vessel operates in rougher sea, causing the sloshing factor to increase above 1.64, measures must be taken to prevent de-loading. The impact of warmer LNG on the pressure development, first addressed in Chapter 6.2 is further explored below.

The key finding was that if the bulk LNG kept a temperature of minimum 130 K, than the liquid saturation pressure would be higher than the de-loading pressure, 375 kPa versus 360 kPa. A de-loading will no longer be a threat for the operation of the ship in rough sea, since the minimum tank pressure is $P_{sat,\ liq}$. Figure 44 shows the pressure developments for a large range of potential bulk LNG temperatures without use of the PBU. Sloshing is not included in this simulation in order to illustrate the concept of minimum P_{tank} above $P_{de\text{-}loading}$ for increasing T_{bulk}. The only thing that sloshing would contribute with, is that the shape of the curves (for 118 K to 133 K) would be steeper, and thereby would the P_{tank} use less time to stabilize at the $P_{sat,\ liq}$ (130 K and 133 K). For the simulations with low T_{bulk}, de-loading of the NG Engines would occur more rapidly.

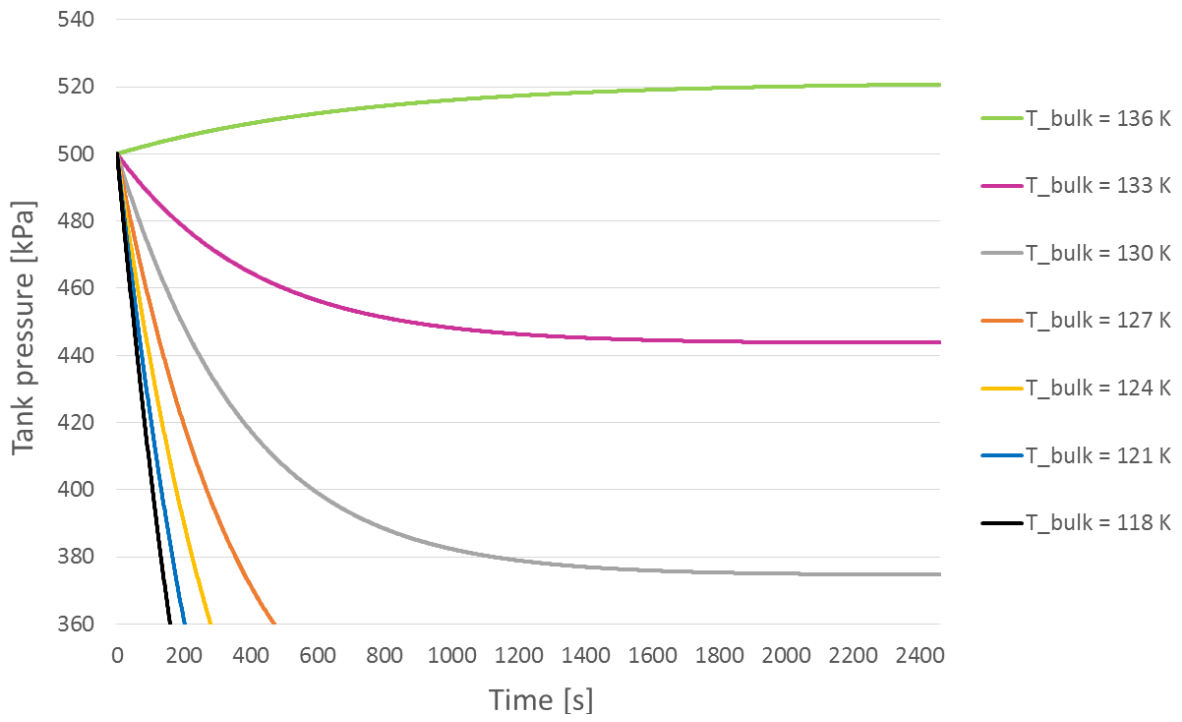

Figure 44 - Pressure development for different LNG bulk temperatures without use of the PBU (filling ratio = 0.9 and SF = 1)

For increasing LNG bulk temperatures, the drop in pressure from 500 kPa to 360 kPa takes longer time. For a rise in T_{bulk} from 121 K to 127 K, the necessary time for the drop in pressure increases with 132 % from 203 s to 471 s. The tank pressure evolves from the initial P_{tank} = 500 kPa to the liquid saturation pressure for the T_{bulk} above 130 K. This implies that P_{tank}

increases for bulk temperatures with $P_{sat,\ liq}$ above 500 kPa. In practice, P_{tank} would never be at 500 kPa with T_{bulk} = 136 K, and therefore not increase as indicated in the figure above. It would decrease from a higher pressure down to the saturation pressure of 521.6 kPa, quite similar to the P_{tank} for T_{bulk} = 130 and 133 K depicted in the figure above.

Figure 45 shows the modeled pressure development for T_{bulk} = 130 K when both sloshing and PBU are included. Utilizing that $P_{sat,\ liq}$ is above $P_{de\text{-}loading}$, it is intuitive that the pressure drops almost instantaneously for violent sloshing, but soon stabilizes on a P_{tank} somewhat above $P_{sat,\ liq}$ = 374.68 kPa.

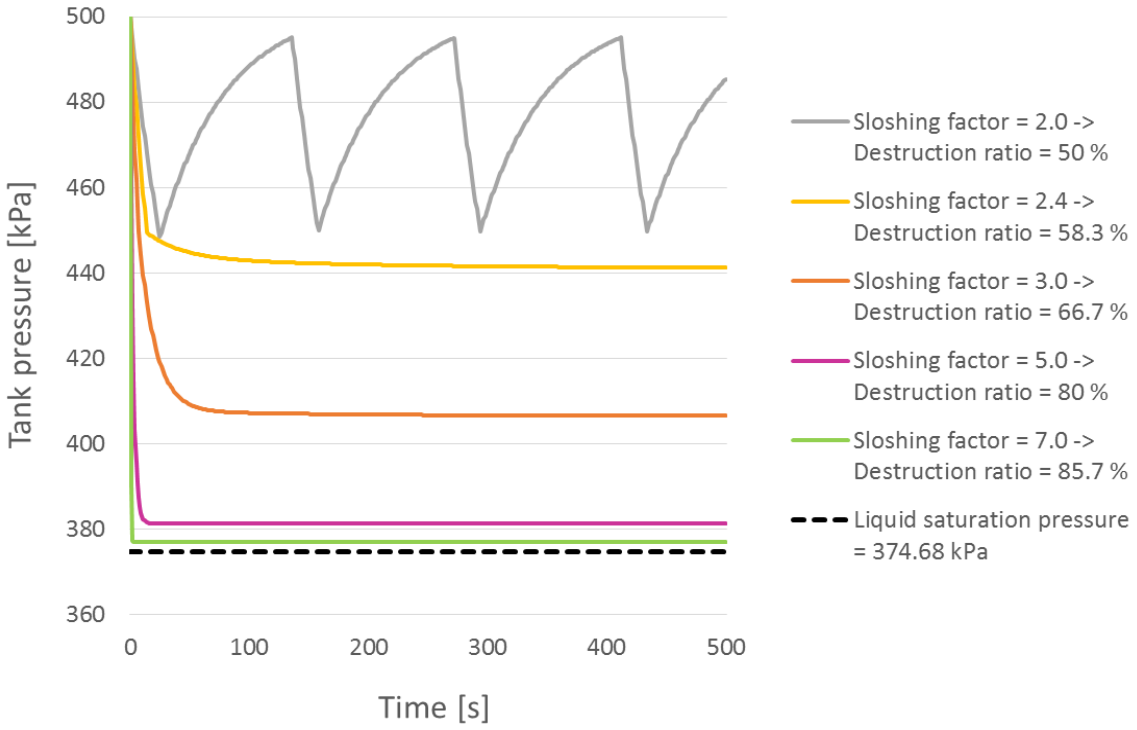

Figure 45 - Pressure development for varying sloshing factor for T_{bulk} = 130 K (filling ratio = 0.9)

The almost immediate stabilization of the pressure for the highest sloshing factors looks a bit artificial. One reason is that the system starts with a de-active PBU, which first is activated when P_{tank} drops below 450 kPa. Thus, for intense sloshing, the pressure can drop below $P_{de\text{-}loading}$ in the first second of the simulation. The NG Engines would not de-load instantaneously as the NG is flowing in the pipe through the PVU (the Product Vaporizer Unit) to the NG Engine, keeping a higher pressure. However, after some seconds the PBU is activated and raises the tank pressure to the stabilizing pressure above $P_{sat,\ liq}$.

When comparing the pressure development for a tank containing LNG at 121 K in Figure 42 with that for 130 K in the figure above, the differences are striking. Whereas the pressure drops below 360 kPa in only 42 s for T_{bulk} = 121 K and SF = 2.0, the PBU is fully capable to compensate for the condensation when T_{bulk} = 130 K. P_{tank} will then oscillate between the on-set and off-set pressures of the PBU – in the grey line both in Figure 45 and in Figure 46. Figure 46 depicts the pressure development with SF = 2 for different T_{bulk}.

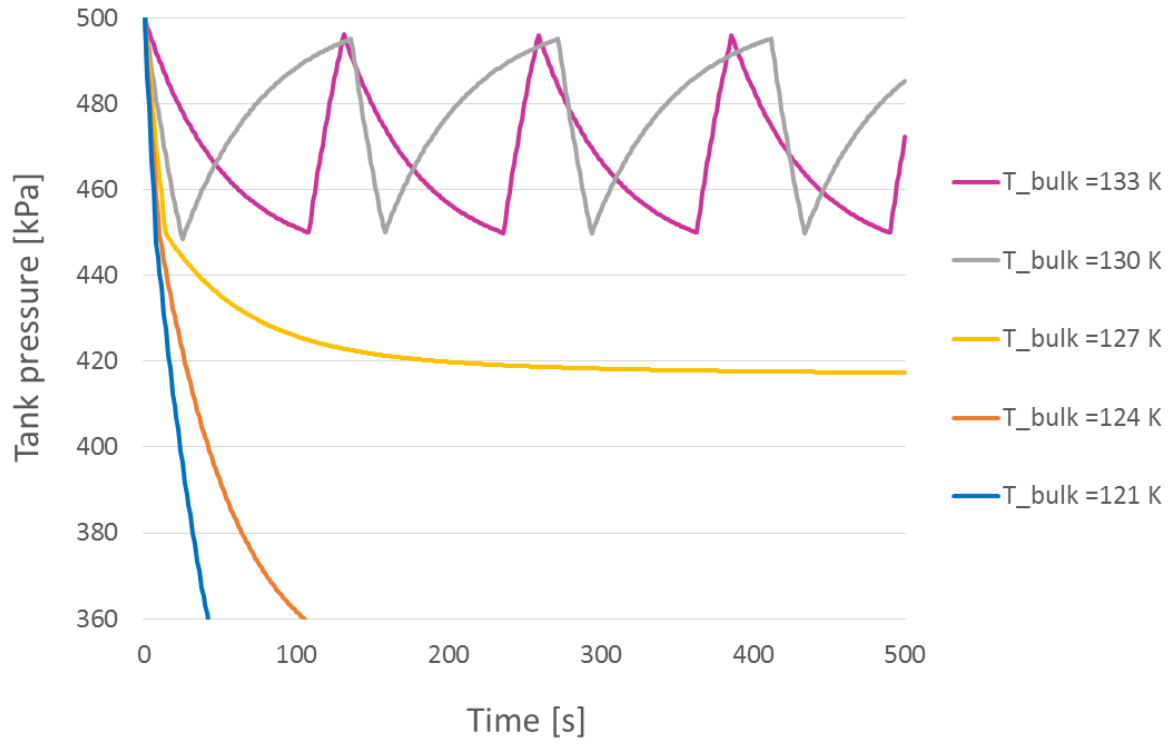

Figure 46 - Pressure development for different LNG bulk temperatures when using the PBU (filling ratio = 0.9, SF = 2)

Compared to Figure 44, the P_{tank} stabilizes on a higher pressure in the figure above where the PBU is included, even for a doubling of the sloshing factor. For the two highest T_{bulk}, the pressure is oscillating, while the simulation stabilizes at an intermediate pressure for T_{bulk} = 127 K. The importance of warmer LNG is evident as the sloshing is included.

7.4 Heating of LNG with PBU

If the temperature of the LNG at bunkering of the vessel is lower than desired, there exists three options for how the cold LNG can be heated. As the insulation of the fuel tank is good, the heat in-leakages are small and are thus not included in this analysis.

The first option relates to bunkering from a truck, and this is used for at least one vessel (Cryomar 2015). After bunkering, the (too) cold LNG is sent back to the truck, and then for a second time back to the fuel tank on the ship. The bunkering lines are not sufficiently insulated to prevent the temperature of the LNG to rise, and the circulation pump emits heat to the LNG as well. The rise in temperature will depend on the design and length of the bunkering line, together with the outside temperature. Thus bunkering from a truck, the LNG can be sent back and forth until the desired T_{bulk} is reached. This solution can probably not be used if the bunkering takes place at LNG production facilities, where the LNG is stored on large tanks. Then, an intermediate LNG storage tank must be installed onshore for

heating of the LNG, allowing for the LNG to be sent back and forth onto the ship as described above.

The second option is to submerge the bunkering line into the sea and exploiting the much higher heat transfer capacity of water than of air. This reduces the number of times that the LNG has to be sent back and forth in order to reach the desired T_{bulk}. It might even be possible to heat the LNG up to the desired temperature at the first bunkering, which then would allow this procedure to be used when bunkering (too) cold LNG directly from an LNG production plant.

The third option is to heat the LNG with the PBU as described in Chapter 6.2. Due to the large amount of LNG that needs to be heated, the PBU must operate for an extended period of time. If for example a ship is bunkering in the evening, the PBU could be active all night in order to ensure a sufficiently high LNG temperature to avoid de-loading when the ship is ready to sail the next morning. The modeling of the temperature development of the LNG is conducted in the same way as for the rise in temperature of the NG when the tank is pressurized, as described in Chapter 4.6. An internal energy balance as well as a mass balance for the LNG have to be incorporated with the equations derived in Chapter 4.6. The two additional equations are:

$$U_{LNG,\,\mathrm{tank}}(t+dt) = U_{LNG,\,\mathrm{tank}}(t) - \left[u_{LNG,\,\mathrm{tank}}(t)\cdot \dot{m}_{PBU}(t) - u_{con}(t)\cdot \dot{m}_{con}(t)\right]\mathrm{dt} \qquad (6.3)$$

$$m_{LNG,\,\mathrm{tank}}(t+dt) = m_{LNG,\,\mathrm{tank}}(t) - \left[\dot{m}_{PBU}(t) - \dot{m}_{con}(t)\right]\,\mathrm{dt} \qquad (6.4)$$

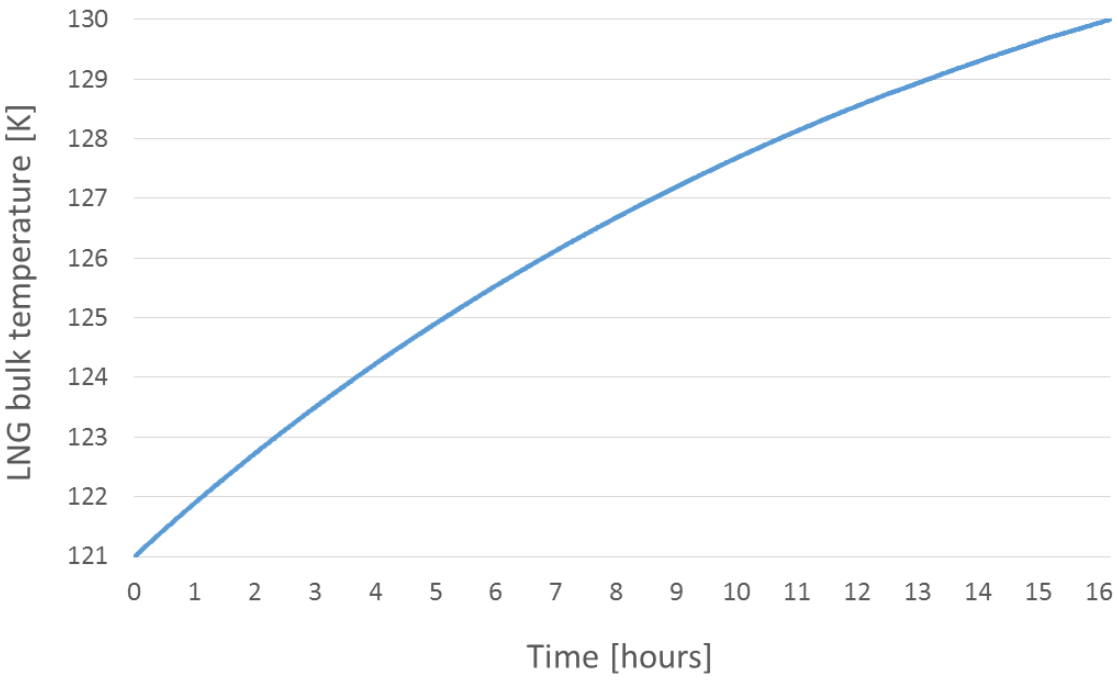

Figure 47 - Temperature development of LNG when heated by the PBU (filling ratio = 0.9)

Figure 47 shows the temperature development of the bulk LNG on KV Bergen with a filling ratio of 0.9 when heated by the PBU from 121 K to 130 K. The temperature is rising faster at the lower temperatures; the heat capacity of the LNG is slightly increasing at higher temperatures. Whereas the first degree Kelvin from 121 K to 122 K is achieved in 68 minutes, the last one from 129 K to 130 K takes 181 minutes. In total, the increase of the temperature takes 972 minutes, or more than 16 hours. These numbers are given in Table 32.

T_{bulk}	**Time before T_{bulk} reached**	**dt/dT – time for last K increase for T_{bulk}**
K	*min*	*min/K*
121	-	-
122	68	68
123	141	73
124	221	80
125	309	88
126	407	98
127	517	110
128	642	125
129	791	149
130	972	181

Table 32 - Temperature development of LNG when heated by the PBU

The time frame presented above, is in the same order of magnitude as (Cryomar 2015) reported for heating the LNG with the PBU on a vessel using their equipment. They stated that operating the PBU for 12-15 hours, the tank pressure was stable even when the vessel was exposed to rough sea. As the temperatures development of the LNG for this case is not known, it is hard to compare the numbers directly, but 16.21 hours for a 9 K rise in temperature of an almost full LNG tank appears plausible.

8 Suggestions for further work

The work on the behavior of marine LNG fuel systems in motion or the use of active and passive measures to maintain the pressure in fuel tanks has not been exhausted with this master thesis. Therefore, some suggestions for further work are given.

8.1 Improve the PBU model

It can be assumed that the PBU on KV Bergen is able to deliver dry vapor for all relevant filling ratios and tank pressure levels. Although it was possible to achieve a superheated NG returning to the fuel tank by modifying the PBU geometry and the system configurations relative to the reference design (Table 11), the impression is that the heat transfer correlations used are underestimating the heat transfer in the PBU. A second possibility is that the pressure losses through the PBU cycle actually are larger than modelled, resulting in a too large mass flow rate passed through the PBU. If one or both of these two factors should be correct, fewer and smaller modifications of geometry or system configurations would be required in order to achieve the desired T_{return}.

8.2 Enhanced understanding of in-tank motions and their correlation to the model

In-tank motions are in this work modeled in the terms of sloshing factor (SF) and the destruction ratio (DR), as described in Chapter 4.9. The connection between waves and sloshing regime can be made more sophisticated than this, for example addressing the relation between SF and DR with a different correlation. A detailed evaluation of the impact on the pressure development of the SF-DR relation should be performed.

If possible, different sloshing regimes should be analysed, as in the experiment described in the Literature Study (Chapter 3), using liquid Nitrogen pressurized with gaseous Nitrogen, performed by (Ludwig, Dreyer et al. 2013). A laboratory test should be conducted with a small-scale tank containing LNG allowing simulations for all the relevant temperatures, pressures and filling ratios described in this thesis.

8.5 Enhanced heat transfer rates with finned tubes

Given the reference design for KV Bergen, the PBU is not able to deliver enough heat to the LNG to exclude sudden drops in pressure. Other options for increasing the heat transfer than those discussed in this document should be investigated. One solution could be to modify the tubes in order to obtain higher heat transfer coefficients. This can both be conducted for the outside and for the inside of the tubes. One suggestion is to implement fins on the tubes, either serrated fins or complete disks.

Fins should be installed on the outer surface of the tubes. The explanation is that the outer heat transfer coefficient is significant lower than the inner heat transfer coefficient, and that the difference in the tube surface areas A_i and A_o is not large enough to compen-

sate for these differences. Also, fins on the inside of the tubes will cause large friction induced pressure drops for the NG, and thus reduce the mass flow rate and pressure build-up capacity.

The enhanced risk for ice formations caused by all the small new corners may exceed the gain achieved from larger heat transfer rates, and must thus be considered.

8.6 Effect of reduced pressure drop in return pipe

A last suggestion for further work is to study the impact of modifying the return pipe from the PBU to the fuel tank. In this thesis it is found that the pressure loss through the return pipe contributes with the majority of the losses through the PBU cycle. A larger pipe diameter would reduces these losses, enable a higher mass flow rate, but correspondingly lower the NG return temperature unless the heat transfer rate is enhanced.

9 Conclusions

Both de-loading events on KV Bergen occurred shortly after bunkering, indicating that the fuel tank was almost full with cold LNG. As presented in Figure 16 (Chapter 4.8), the drop in pressure occurs faster at high filling ratios than at lower ratios due to a smaller vapor volume. Combined with the higher condensation rate for cold LNG than for warm, illustrated with the pressure development in Figure 44 (Chapter 7.3), the conditions of the tank may have been the worst possible to prevent a de-loading of the NG Engines.

The tank pressure in marine LNG fuel systems can be maintained, or at least stabilized above the de-loading pressure by utilizing the principles of thermodynamics. The results from this master thesis strongly suggest that the best solution to prevent de-loading of the NG Engines is to raise the LNG bulk temperature sufficiently in order to obtain a higher liquid saturation pressure than the required inlet pressure of the Gas Ramp Unit. For KV Bergen, with an estimated de-loading pressure of 360 kPa, an LNG bulk temperature of 130 K with corresponding $P_{sat,\ liq}$ = 374.68 kPa is sufficient to prevent further de-loading events, regardless of sea conditions and the intensity of the in-tank sloshing (Chapter 6.2). This is illustrated below for a sloshing factor of 2 for various T_{bulk} with Figure 46 (Chapter 7.2).

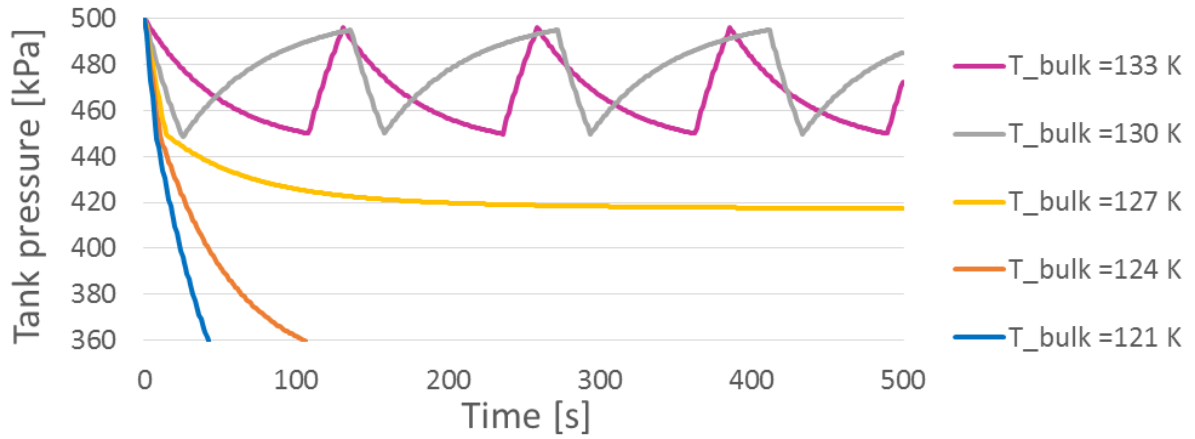

Figure 48 – Development of P_{tank} for different T_{bulk} when using the PBU (filling ratio = 0.9, SF = 2)

This finding suggests that the capacity of the PBU could be down-scaled in future fuel system designs although not excluded altogether. If the main purpose of the PBU no longer is to maintain the pressure, it could still be used to raise the LNG bulk temperature if necessary.

A thermal governed PID-controller should be installed in the PBU, ensuring that the LNG is completely evaporated and sufficiently superheated before returned to the fuel tank.

A further option for LNG fuel systems with well-designed PBUs is to use gaseous Nitrogen as a back-up pressurant. The most critical time for de-loading is at high filling ratios, but a 12 bottle battery (á 50 L and 200 kPa) is sufficient to pressurize a 90 % full fuel tank on KV Bergen from 3.8 bar to 5.5 bar not less than almost four times. The use of Nitrogen as an emergency pressurant will not materially impact the quality of the fuel; the added Nitrogen from one or more pressurization is negligible compared to the Nitrogen in the LNG fuel.

References

Acciaro, M. (2014). "Real option analysis for environmental compliance: LNG and emission control areas." Transportation Research Part D: Transport and Environment **28**(0): 41-50.

Burel, F., et al. (2013). "Improving sustainability of maritime transport through utilization of Liquefied Natural Gas (LNG) for propulsion." Energy **57**(0): 412-420.

Cengel, Y. A. and J. M. Cimbala (2006). Fluid Mechanics Fundamentals and Applications. Singapore, McGraw-Hill.

Code Consultants Inc (2010). "Antifreeze Solutions in Home Fire Sprinkler Systems." 3-11.

Coyle, D. d. l. V., F. F.; Durr, C. (2007). "Natural Gas Specification Challenges in the LNG Industry." KBR.

Cryo AB - Components (2005). "Component manual Kystvakt - Barents class."

Cryo AB - KV Bergen (2009). "User operation manual - KV Bergen."

Cryo AB (2007). PID, Process and Instrument Diagram - B600104682-07. MF Korsfjord.

Cryo AB (2010). "Manual for Natural Gas Propulsion System_KV Bergen."

Cryo AB (2012). Manual for Myklebust Verft , Yard building No. 49 - CH4/natural gas fuel Propellant System. Project Kystvakten.

Cryomar (2015). Meeting between Cryomar (Anders Jetlund, Reidar Slettestøl) and master candidate Hugo Eugen Hernes with Supervisor Petter Nekså. Trondheim, Norway.

Cullinane, K. and R. Bergqvist (2014). "Emission control areas and their impact on maritime transport." Transportation Research Part D: Transport and Environment **28**(0): 1-5.

DiRenzo, J. (2014a). Investigation of an LNG fuel system for a Norwegian coast guard ship. Trondheim, NTNU. **Master thesis**.

DiRenzo, J., et al. (2014b). Analysis of Natural Gas Engine De-Loading on LNG Fuelled Vessels. 3rd Trondheim Gas Tecnology Conference. TGTC-3. Trondheim, Elsevier Ltd.

Dorao, C. A. (2012). Separation Equipment - TEP 08. Trondheim, NTNU.

Espeland, J. A. (2012). Black Out Report October 2012. KV Bergen, Norwegian Coastal Guard.

Fernández-Seara, J. P.-P., C.; Dopazo, J. A. (2013). "On the performance of a vertical helical coil heat exchanger. Numerical model and experimental validation." Science Direct Applied Thermal Engineering.

Flachbart, R. H., et al. (2008). "Thermodynamic vent system performance testing with subcooled liquid methane and gaseous helium pressurant." Cryogenics **48**(5-6): 217-222.

Gassnor (2012). Composition of LNG delivered to KV Bergen 18. Oct 12. DVSYS.42_AE-2201-N2/Al1/PV.F_CV.

Hernes, H. (2014). Investigation of LNG fuel systems for ships in movement. Energy and Process Department. Trondheim, NTNU.

Incropera, F. P., et al. (2013). Principles of Heat and Mass Transfer, John Wiley & Sons, Inc.

Kern, D. Q. (1950). Process Heat Transfer. Singapore, McGraw-Hill Book Company.

Linde Cryo AB (2006). Assembly LNG Vaporizer - KV Bergen. B600083494-0.

Linde Cryo AB (2008). LNG fuel system Flow Diagram 1250-HSCP-10-DNV. MF Korsfjord System Drawings.

Ludwig, C., et al. (2013). "Pressure variations in a cryogenic liquid storage tank subjected to periodic excitations." International Journal of Heat and Mass Transfer **66**: 223-234.

M. Conde Engineering (2011). "Thermophysical Properties of Brines - Models." Properties of Working Fluids - Brines. from http://www.mrc-eng.com/Downloads/Brine%20Properties.pdf.

Mitsubishi Heavy Industries (2014). "GS16R-PTK Gas Engine set rating." Energy Products. Retrieved 11th October, 2014, from https://www.mhi-global.com/products/expand/product_explanation_gas_01.html.

Myklebust Verft AS B49/B52 (2009). Systemtegning gass, 676kW/1500rpm Mitsubishi GS12R. M1059GDWG.

Naterer, G. F. (2003). Heat Transfer in Single and Multiphase Systems - Gas Liquid Systems, CRC PRESS LLC.

Norwegian Maritime Authority (2013). "Norwegian Ship Register." 2014, from http://www.sjofartsdir.no/shipsearch/.

Næss, E. L., Martin (1990). Varmeovergang ved koking. Kompendium i TEP - 07 Industriell Varmeteknikk. Trondheim, Norway, NTNU, Institutt for energi- og prosessteknikk.

Scurlock, R. G. (2006). Low-Loss Storage and Handling of Cryogenic Liquids: The Application of Cryogenic Fluid Dynamics, Kryos Publications.

Serth, R. W. (2007). "Process Heat Transfer: Principles and Applications - Ch. 10 - Reboilers."

The Norwegian Coast Guard (2013). "A Presentation of the Norwegian Coast Guard".

Transport Canada (1984). Standard for Inert Gas Systems. Function and Design Considerations.

Whalley, P. B. (1976). HTFS DR43: Single and two phase flow in helical coils. Oxfordshire, Thermodynamics Division, AERE Harwell.

Whalley, P. B. (1984). Vertical Thermosyphon Reboilers Part 2: Analysis of the system. Oxford, Department of Engineering Science, University of Oxford

Zhang, S. Y., Yeli (2005). "Energy and momentum dissipation through wave breaking." Journal of Geophysical Research 110(C9).